2020

DYNAMIC TESTING: AN EXPERIMENTAL APPROACH TO DEFECT IDENTIFICATION IN ADDITIVE MANUFACTURED PARTS

Aimee Allen
Michigan Technological University, amallen@mtu.edu

DYNAMIC TESTING: AN EXPERIMENTAL APPROACH TO DEFECT IDENTIFICATION IN ADDITIVE MANUFACTURED PARTS

By

Aimee M. Allen

A THESIS

Submitted in partial fulfillment of the requirements for the degree of

MASTER OF SCIENCE

In Mechanical Engineering

MICHIGAN TECHNOLOGICAL UNIVERSITY

2020

This thesis has been approved in partial fulfillment of the requirements for the Degree of MASTER OF SCIENCE in Mechanical Engineering.

Department of Mechanical Engineering-Engineering Mechanics

Thesis Co-Advisor:	*Jason. R. Blough*
Thesis Co-Advisor:	*Andrew R. Barnard*
Committee Member:	*James P. DeClerck*
Department Chair:	*William W. Predebon*

Table of Contents

List of figures

List of tables

Preface

This research was conducted at Michigan Technological University. This project supports research performed at Missouri University of Science and Technology. Kevin Johnson, a PhD student working on this project, performed previous research on this project and provided the Finite Element results for many of the comparisons. Some of the methods and results were included in conference papers presented at 2019 SFF in Austin, TX [1] and 2020 IMAC in Houston, TX [2]. This work was funded by the Department of Energy's Kansas City National Security Campus which is operated and managed by Honeywell Federal Manufacturing Technologies, LLC under contract number DE-NA0002839.

Acknowledgements

I would like to thank Ben Brown at Honeywell Federal Manufacturing and Technologies for providing this research opportunity. I would also like to thank my advisors, Dr. Jason Blough and Dr. Andrew Barnard for encouraging me to pursue this opportunity and for their continued support and guidance throughout the project. I would like to thank Dr. James DeClerck for always having his door open for questions. I would like to thank Kevin Johnson for research assistance and the Finite Element Analysis results. I also want to thank MS&T for their assistance and partnership with this research. Lastly, I would like to thank my family and friends for not letting me through in the towel when I wanted to give up.

List of abbreviations

DIC: Digital Image Correlation

ECD: Eddy Current Detection

FEA: Finite Element Analysis

FRAC: Frequency Response Assurance Criterion

FRF: Frequency Response Function

NDE: Nondestructive evaluation

PBF: powder-bed fusion

PSD: power spectral density

PZT: Lead Zirconate Titanate; a piezoelectric ceramic material

SLDV: Scanning Laser Doppler Vibrometer

SLM: Selective Laser Melting

UT: Ultrasonic Testing

XCT: X-ray Computed Tomography

Abstract

Today's additive manufacturing (AM) industry produces specialized parts at low volume or with complex geometries. Traditional testing methods are effective, but costly and time consuming to perform. The AM industry lacks an optimized testing method for identifying internal defects that occur in parts. The evaluation of multiple parts printed on the same build plate for internal defects using various nondestructive (dynamic) testing techniques is presented. From these experiments, perspective was gained on when and how dynamic testing can be used to find defects. Insight gained from these experiments can help the industry in future testing for internal defects.

1 Introduction

Additive manufacturing is becoming more popular in industry due to its ability to surpass traditional casting methods by producing specialized parts at low volume or with complex geometries [3, 4]. AM is a 3D printing process that occurs from stacked layers of material formed to create parts. AM has been commercially available for nearly 30 years, but the concept of AM may have started as early as the late 1960's. Commercial AM started in 1987 by 3D Systems, Inc with stereolithography, a type of polymer resin printing, [4, 5, 6, 7] AM has continued to grow since its beginning in polymer printing to encompass various printing processes and materials.

There are seven categories of printing processes in today's industry that include photopolymerization, jetting, extrusion, lamination, and fusion processes [7]. In 2002, Polymer printing expanded to include biomaterial printing. While the first 3D printing metal machine was debuted around 2011. ASTM Committee F42 was formed in 2009 to begin establishing standards in AM [7]. As AM has grown, manufacturers have become more interested in process control for dimensional and geometrical accuracy. End users have been interested in the quality of products and industry is shifting to evaluate the best method for finding part flaws. Since medical and aerospace applications have strict guidelines for part functionality, non-destructive evaluation of AM parts is of paramount interest in these industries.

The ability to assess part quality is the major reason why AM is not more widely adopted in industry [8, 9]. Surface defects can be identified with the naked eye or with imaging software. Internal defects are more difficult to identify since they cannot be tested for visually. The most common method for detecting internal defects is x-ray computed tomography (XCT). While this method is effective in finding defects, it is costly and time consuming to perform [10]. Currently, the industry needs an optimized testing method for identifying internal defects. Some alternative methods being investigated include eddy current detection (ECD), ultrasonic technology (UT), and impedance-based non-destructive evaluation (NDE).

Dynamic testing is another option for optimizing AM for identifying critical flaws. Dynamic testing is both cheaper and faster than XCT. The goal of this research focuses on determining whether dynamic testing techniques are viable methods for assessing internal part integrity.

1.1 Background

1.1.1 Summary Non-Destructive Testing Techniques in AM

The most common method for detecting internal defects is x-ray computed tomography (XCT). This method is currently being used for most AM part integrity analysis, but due

to its limitations other methods are being investigated. The following methods are explained in detail in this section: XCT, ECD, UT, and Impedance-Based NDE.

XCT is the most common method used to find internal defects in AM parts due to its ability to assess dimensional inaccuracies as well as internal defects. XCT technology consists of taking numerous x-ray images of the part around an axis of rotation and using computer-aided technology to recreate a 3D model [10].While XCT is effective, there are significant disadvantages to this technique. The drawbacks of XCT include a significant amount of time involved for taking each x-ray slice as well as a high cost for the radiation needed to take the slices. The resolution of the XCT measurement is dependent on how far the x-ray image penetrates the object [10]. Because of this, XCT is not particularly well suited for large AM parts nor parts with high densities. Crack detection is also unreliable with XCT, since cracks perpendicular to the scan beam will not be identified [11].

ECD is used in industry to assess defects in metal components on the surface and subsurface of thin materials. Since ECD is used to detect surface flaws, it can be used in-situ in addition to post-processing to detect defects. The ECD method produces an eddy current, or a varying magnetic field, at specified excitation frequencies. When the part is scanned, defects will appear as magnetic irregularities [12]. A disadvantage to this method is that defects can only be found in conductive materials. ECD's ability to find defects is dependent on surface finish. Poor surface finish increases the noise floor above where defects can be detected [11].

UT is performed with an ultrasound testing machine which uses an ultrasound probe to emit sound waves through a part. Defects are detected by the speed at which sound waves are reflected to the probe. Traditionally, UT uses a couplant (liquid) between the probe and the test part. The introduction of the couplant introduces special test considerations since the part will be placed in a liquid [13]. UT can be combined with special equipment in which the couplant is not required, such as laser ultrasonic testing (LUT). LUT uses a laser to provide and measure the signal in a part [9]. LUT is under development in AM but has potential as a novel NDE technique since it does not require a couplant and is noncontact. Similar to ECD, good surface finish is needed for LUT to reduce noise in the measurements.

Similar to dynamic evaluation, impedance-based NDE is cheaper and less time consuming than XCT. This method was briefly investigated in addition to dynamic evaluation in the research presented. Impedance-Based NDE is performed with piezoelectric materials, such as lead zirconate titanate (PZT). The PZT is adhered to the structure via a patch. This method of testing consists of sending a signal to the adhered PZT which both excites the structure and measures its response [14]. The part's mechanical impedance is directly related to and can be separated from the impedance of the transducer. According to one study, this method has potential in finding dimensional and positional inaccuracies but may not be as suitable for finding internal porosity [15]. Another issue with this testing is that the PZT is permanently adhered to the structure.

There are a few problems with XCT and the alternative testing techniques. In general, there is a limited amount of research published into optimizing NDE testing in AM. For the testing performed, only LUT and impedance-based NDE show promise in holistic part integrity. Considering these NDE methods, dynamic evaluation has the potential to be a novel testing technique in future AM internal defect analysis.

1.1.2 Introduction to Dynamic Evaluation

Dynamic evaluation consists of exciting a structure and measuring the response often in the form of a Frequency Response Function (FRF). A frequency response function shows the natural frequencies of the structure. Natural frequencies of the structure are displayed as peaks in the FRF. Natural frequencies are structural properties defined by mass, stiffness, and boundary conditions [16]. Internal defects are detected by peak shifts in the FRF when compared to nominal parts. Dynamic evaluation is versatile, in that many different types of transducers can be used to measure the response.

1.1.3 Description of AM Builds

Selective Laser Melting (SLM) is one type of 3D metal printing used in AM. The SLM is a powder-bed fusion (PBF) process. The PBF process laser sinters layers of metal powder to form parts on a build plate [17]. The parts presented were created from 304L steel powder. Some parts were built with support material. Support material aids in the printing process by providing a structure for the laser to sinter for parts difficult geometries such as overhangs or ledges. The support material is removed in post-processing. Since all metal parts were tested prior to removal from the build plate, the parts presented were tested with support material.

Ideally, the parts would be tested free-free, but removing parts from the build plate costs additional time and expense. One of the goals of this research is to determine if defects in parts can be detected while still attached to the build plate. Therefore, all parts were tested with a fixed boundary condition.

Incomplete fusion holes also known as voids are one type of internal defect in that occurs in SLM. Voids are created when the laser poorly sinters or misses sintering the layer of powder [18]. Voids affect part integrity by changing structural properties of a part. A large portion of the presented research is aimed at determining void location and size.

1.1.4 Dynamic Evaluation on AM Builds

Dynamic testing traditionally uses impact and/or shaker testing often with accelerometers or microphones. All builds were first tested using one (or both) of these techniques. Unfortunately, impact and shaker testing have a limited dynamic range which is targeted for lower frequency ranges – up to 8,000 – 10,000 Hz. Some shakers are rated for higher dynamic ranges, but these require small payloads – less than 2 lb. [19, 20]. Creative tests

were introduced to reach higher frequencies. These tests included using speakers for acoustic excitation, a BB-gun for high velocity/short duration impacts, and piezoelectric excitation. Impedance-based measurements were also performed.

A Scanning Laser Doppler Vibrometer (SLDV) was used in conjunction with accelerometers or microphone(s) to record the response from dynamic excitation. The SLDV utilizes the Doppler Effect and optical interferometry to measure velocity and/or displacement of a vibrating object [21]. Doppler shifts are created when the laser sends a signal to the part and the signal is reflected back. These signals combine constructively or destructively. An optical interferometry is used to determine the sign of the Doppler shift. The sign determines the direction of the part's motion. The signal is then demodulated to provide the user with velocity and/or displacement [21].

Finite Element Analysis (FEA) was used to find natural frequencies and modes shapes for each of the builds. The boundary conditions and testing locations from the FEA models were created to be representative of the experimental tests performed. Only the pertinent information and results from FEA are presented, since the research is focused on experimental testing.

Frequency Response Assurance Criterion (FRAC) was used to assess how correlated an FRF or sets of FRFs are from one another. FRAC is often used to determine how close a simulated FRF is from the experimental FRF. The following research uses FRAC to determine how correlated nominal parts tested experimentally are from one another. The equation for FRAC is shown in ([22], Eq. 1). The FRF, X_a, is the theoretical FRF and the FRF, X_e, is the FRF that is being correlated. The results are correlated on a scale from 0 to 1, with 0 being no correlation and 1 being completely correlated.

$$FRAC = \frac{X_a^T X_e}{\sqrt{X_a^T X_a}\sqrt{X_e^T X_e}} \quad (1)$$

X_a = theoretical FRF
X_e = correlated FRF

1.2 Results from Previous Testing

Previously two different types of builds were tested on this project. Two builds with 5 chimneys and a build with 5 brackets shown in ([23], Fig. 1). Chimney Build 1 the only build printed with support material at the base of the part. These parts were dynamically tested with an impact hammer and shaker in correlation with LDV or Digital Image Correlation (DIC). One intentional defect was planted in the chimney build and two intentional defects were printed in the bracket build sent from MS&T. MTU was tasked with finding which parts had these defects.

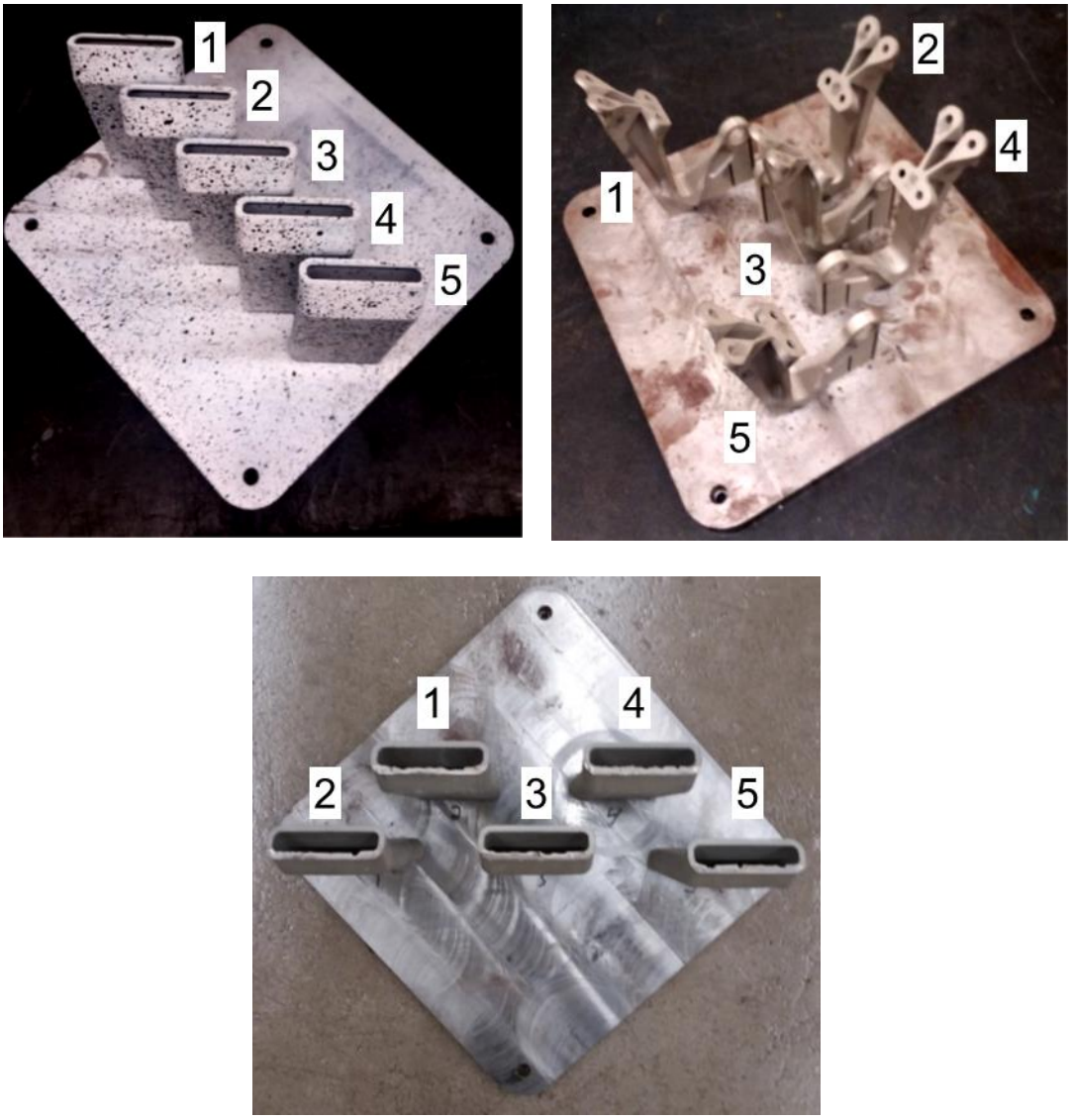

Fig. 1: Chimney Build 1 (Left), Bracket Build 1 (Right), Chimney Build 2 (bottom)

The defects in all builds were found from impact and shaker testing. Chimney Build 1 had a difference in hatch spacing on Chimney 4 causing it to be denser. Brackets 2 and 5 on the bracket build and Chimney 2 on Chimney Build 2 were built with smaller hatch spacing than the surrounding parts.

From analyzing these builds, it was found that the support material breaks down the more the parts are tested. The breakdown of support material changes the structural response of the part.

Higher frequency modes are less affected by support material and sympathetic resonance. Sympathetic resonance occurs when a part that is not excited exhibits a response to a part with similar natural frequencies that is excited [23]. This phenomenon is often

demonstrated with tuning forks tuned to the same frequency. One tuning fork is excited, yet both tuning forks will exhibit a response. The testing presented focuses on assessing these higher frequency modes.

1.3 Goals

The goal of this research was to determine if dynamic evaluation can improve the validation process for additively manufactured metals. Improving the validation process is based on distinguishing the limits for identifying defect size and location. Using this knowledge, parts can be optimized for better part integrity and defect detection. Various experimental tests were performed to analyze this goal. Finite Element Analysis was used to support the experimental results. Based on these experiments, insight was gained on which dynamic testing methods future research should focus on for determining part integrity.

2 Methods

2.1 Forest Tensile Bar Builds

Two Forest Tensile Bar Builds were analyzed. The first build shipped to MTU was printed with defects. The second build consisted of only nominal parts. Both builds were identical in part size and part location on the plate.

The CAD model of the build with defects is shown in ([2], Fig. 2). There are nine groups of five bars for a total of 45 bars. The bars were placed randomly on the build, so that no groups were clustered together.

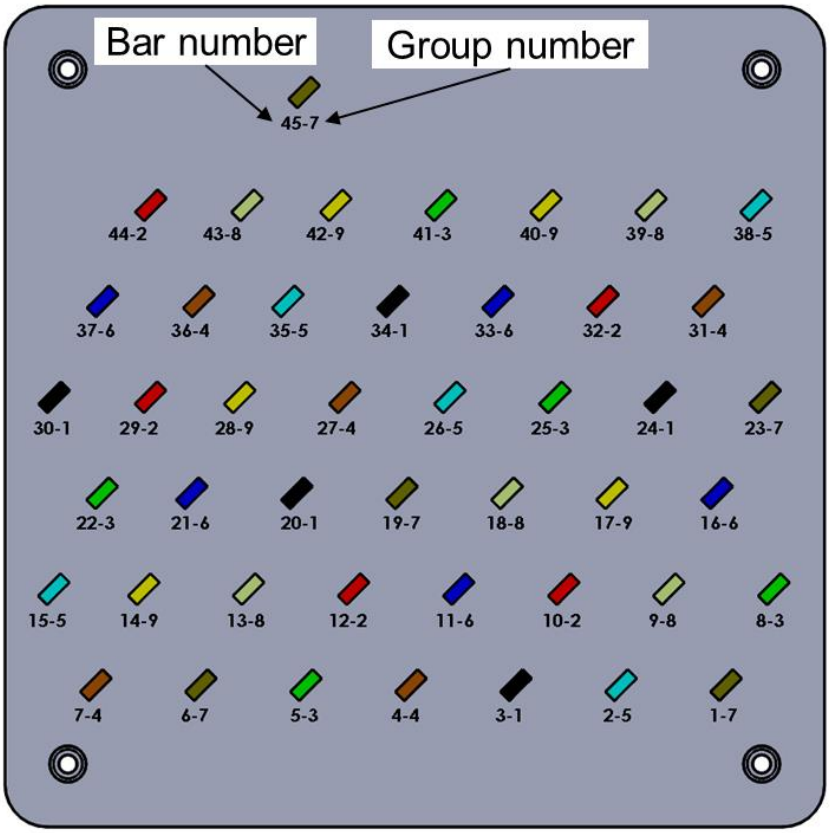

Fig. 2: CAD model of tensile bar build with bar and group numbers labeled

The first group was built nominal with the subsequent groups having defects. The voids varied from 50-400 μm and increased by 50 μm increments starting with Group 2 and ending with Group 9 ([2], Table 1).

Table 1: Tensile Forest Build defect description by group number

Group	1	2	3	4	5	6	7	8	9
Defect size (µm)	0	50	100	150	200	250	300	350	400

The physical build and void description are shown in (Fig. 3). The height of each of the tensile bars is 4.7 in. The defect is located 1.75 in from the base of the part. The base of the defect is the same for all groups at a length of 0.21 in [2].The defect increases in height with increasing group number.

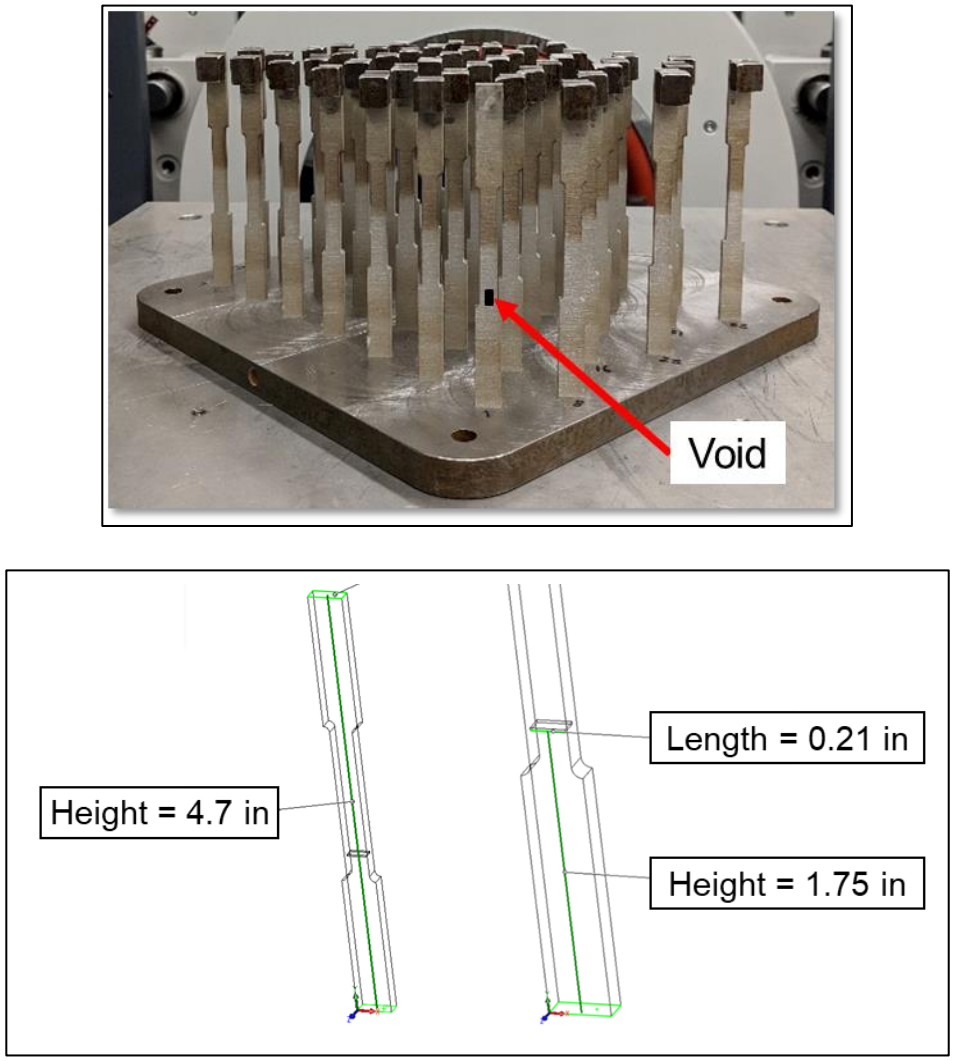

Fig. 3: Physical tensile build (top) and defect location (bottom)

2.1.1 Shaker Testing

The build with defects was tested on the Dongling GT500-240-1 shaker. The build plate was bolted to a square aluminum adapter plate with dimensions of 19.75 x 19.75 x 1.5 inches (Fig. 4). The adapter plate was bolted to the slip table on the shaker. The slip table that the adapter plate attaches to has the dimensions of 19.75 x 19.75 x 1.1875 inches (Fig. 4). The adapter plate was created so that the build could be bolted at different angles to the shaker table.

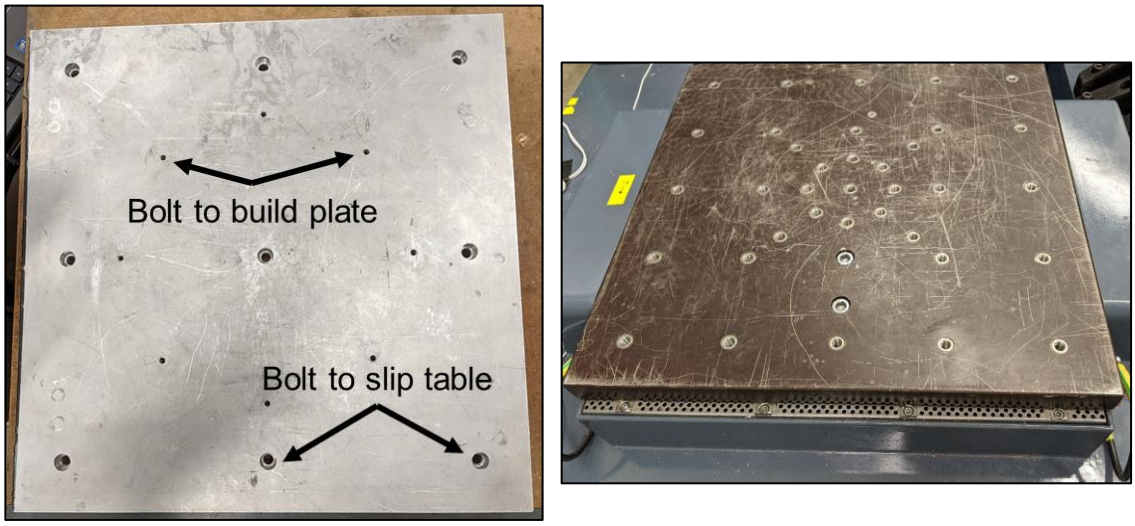

Fig. 4: Adapter plate (left) and slip table (right)

The build was shaken to excite the bending modes in the X – direction with a periodic chirp from 0-5120 Hz (Fig. 5). The SLDV recorded the response at the top of each bar.

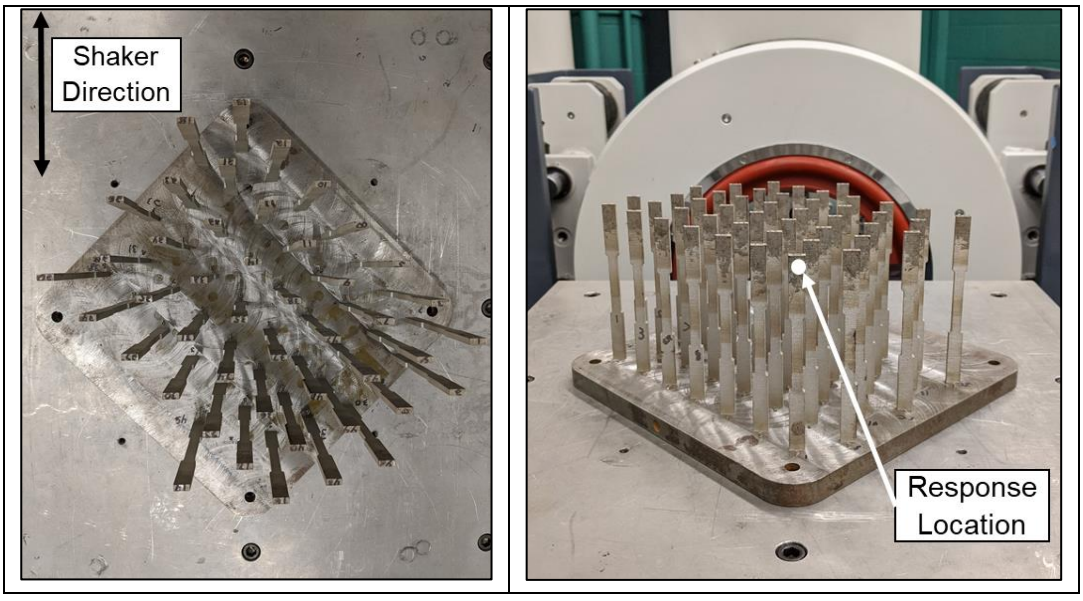

Fig. 5: Top view with shaker direction labeled (right) and shaker testing setup (left)

2.1.2 Impact Testing

Following shaker testing on the build with defects, both forest builds were impact tested to determine if the defect groups could be distinguished from one another. The boundary condition for the plate was the same as shaker testing i.e. bolted to the shaker slip table. Weights were added to the top of the bars with wax to reduce the effect of sympathetic frequencies influencing the result of the bar of interest. The weights and testing setup are shown in (Fig. 6). A modal impact hammer (PCB Model: 086E80) hammer impacted the back side of each bar with the response measured by the SLDV on the front side of the bar.

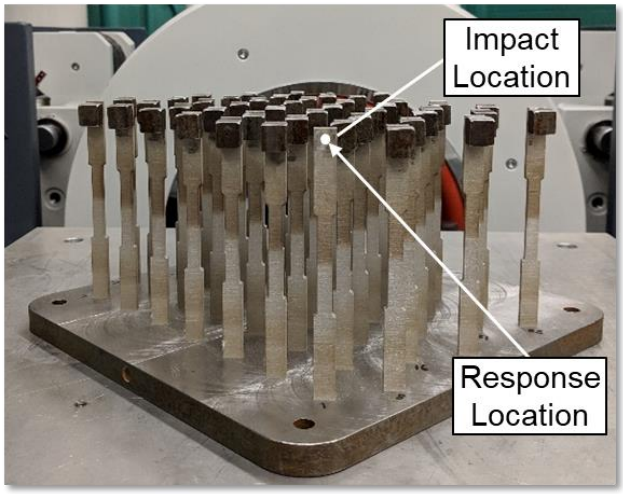

Fig. 6: Tensile bar build impact testing setup

2.1.3 Damping Values

The damping values for both the build with defects and the nominal build were calculated as another method to determine differences between the two builds. The damping values were calculated using the 3 dB down or half power method [24]. This method uses the FRF plotted in dB to find the natural frequency (ω_n). From the natural frequency peak, the frequency values 3 dB down are selected. An example of the points taken from the FRF is shown in (Fig. 7). The natural frequencies, f_1, f_n, and f_2 in Hertz, can be converted to radians to obtain ω_1, ω_n, and ω_2.

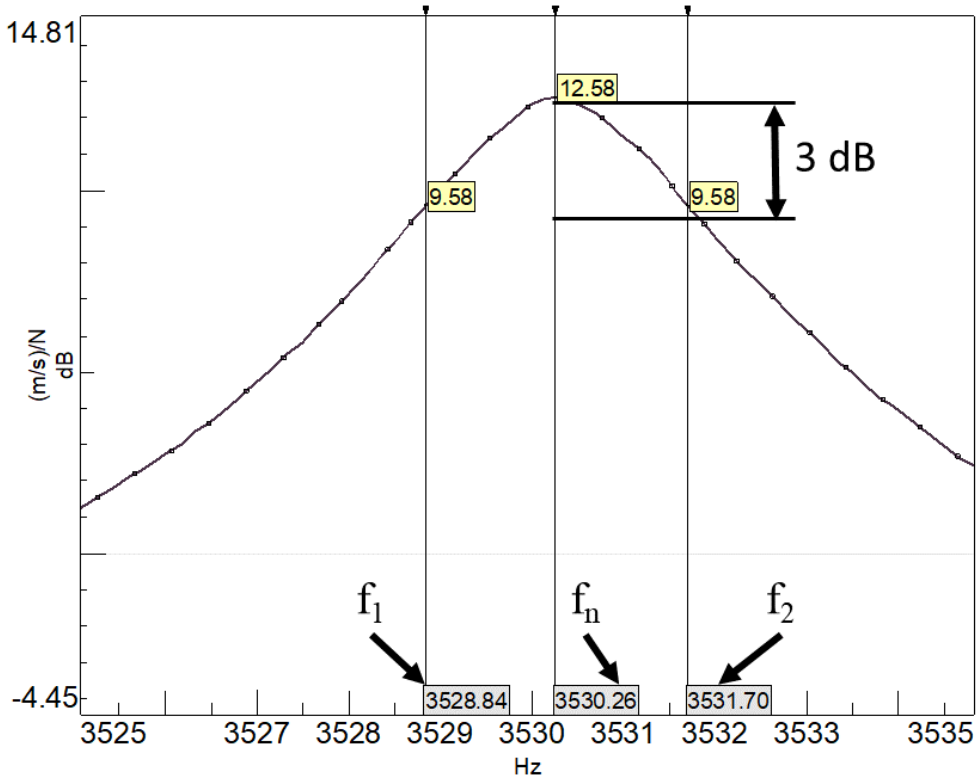

Fig. 7: Bar 26 from impact testing on nominal build example of the 3 dB down method

The damping ratio (ζ) is calculated using the equation for determining the Q factor ([24], Eq. 2). The Q factor or quality factor was not used in the results, but is another property of the system.

$$Q = \frac{1}{2\zeta} = \frac{\omega_n}{\omega_2 - \omega_1} \quad or \quad \zeta = \frac{\omega_2 - \omega_1}{2\omega_n} \tag{2}$$

Q = Q factor
ζ = damping ratio
ω_n = natural frequency
ω_2 = 3 dB frequency above ω_n
ω_1 = 3 dB frequency below ω_n

2.1.4 FEA

FEA was performed for these builds for one bar in each defect group. The natural frequencies and mode shapes are shown in (Fig. 8). The percent difference from the largest defect (400 μm) to nominal is also shown in the figure. The bars were modeled with a fixed boundary condition at the base of the part. The results from impact testing were compared to FEA. From this comparison, acoustic testing was proposed, focused on finding the first axial mode at 9,755 Hz. This mode showed the largest difference between nominal and a defective part, proposing the highest likelihood of detecting the defect.

Mode:	1	2	3	4	5	6	7	8	9
Freq. (Hz)	203	432	1292	2522	3530	4073	6921	6972	9755
% difference (400 µm)	0.39	1.25	0.10	0.10	0.27	0.42	0.88	0.07	2.22
Shape:		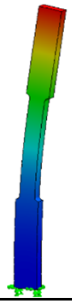		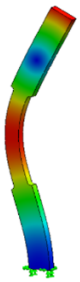	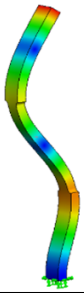	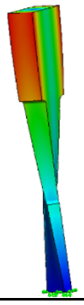	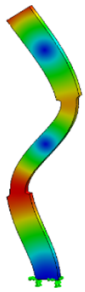	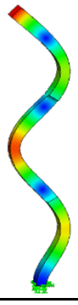	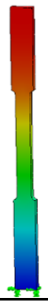
Mode Shape	cantilever x-axis	cantilever y-axis	2nd bending x-axis	2nd bending y-axis	3rd bending x-axis	1st torsional	3rd bending y-axis	4th bending x-axis	1st axial

Fig. 8: FEA of tensile bars with defects up to the 1st axial mode

2.1.5 Acoustic Testing

2.1.5.1 Acoustic Test 1

The first acoustic test consisted of a B&C DE1085TN speaker with a B&C Speakers M60 acoustic horn. The build plate was bolted to a rigid plate with the speaker and horn bolted on the reverse side (Fig. 9). A periodic chirp signal from 1,000-12,800 Hz was used to excite the base of the plate with 20 averages taken per bar. The SLDV measured the bar responses at the top of each bar.

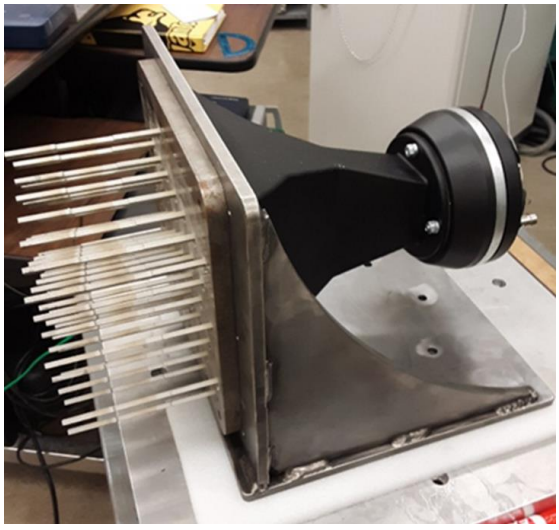

Fig. 9: Test 1 setup for acoustic testing

2.1.5.2 Acoustic Test 2

The first test did not provide enough excitation to the bars for the SLDV to record the axial mode. The second acoustic test consisted of two speakers mounted on an adapter plate, built by Kevin (Fig. 10). The adapter plate replaced the acoustic horn for this testing.

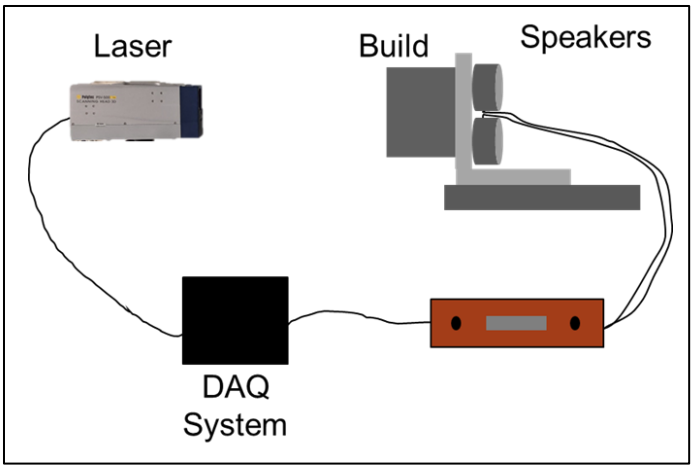

Fig. 10: Model setup of second acoustic testing performed on forest build plates

The adapter plate had a 0.69-inch spacing between the speakers and the build plate to provide an acoustic reverberant chamber. This spacing was calculated from the wavelength equation shown in ([25], Eq. 3). A half-wavelength ($\lambda/2$) was calculated instead of a whole wavelength (λ) for the axial mode at 9755 Hz. A half-wavelength was used to reduce the amount of material needed to create the chamber.

$$\lambda = \frac{c}{f} \tag{3}$$

λ = wavelength
c = speed of sound
f = natural frequency

The adapter plate with the 0.69-inch spacing is displayed in (Fig. 11). The same signal parameters were used for this testing as the previous test.

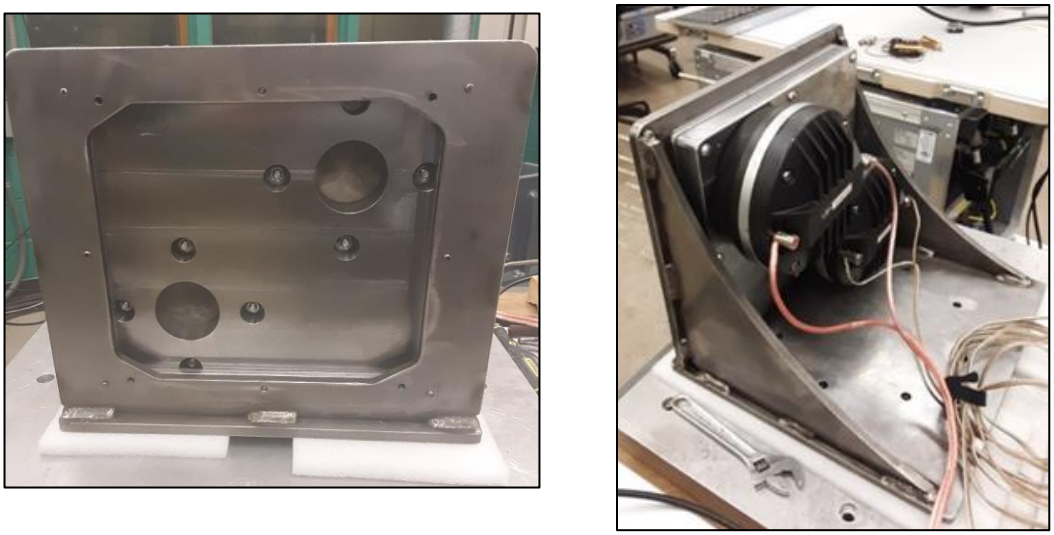

Fig. 11: Spacing between speakers/build plate (left) and physical setup for Test 2 (right)

In addition to taking the response at each of the bars, a grid of points 17 down by 18 across was taken on the base plate for a total of 280 points. Twenty-six points were removed since they fell directly on top of a bar and are displayed as white boxes in (Fig. 12). The base plate response was used to compare to the bar response to see how much the base plate modes affect the bar response.

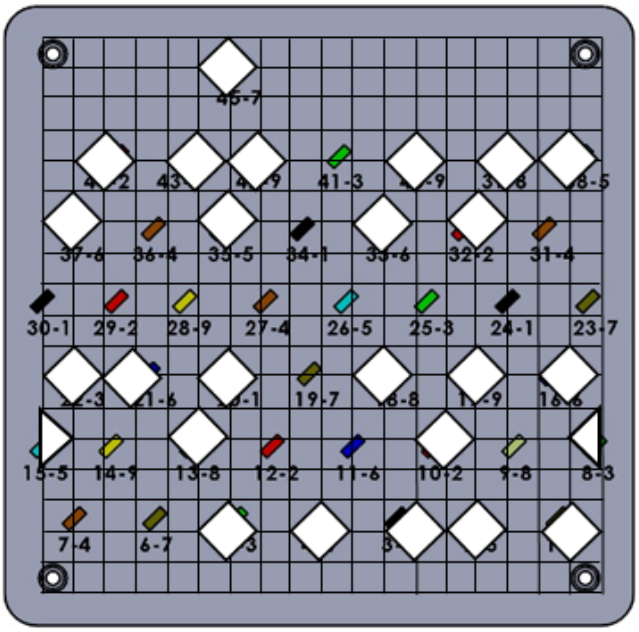

Fig. 12: Grid of points taken on forest build plate for acoustic testing

2.1.5.3 Acoustic Test 3

The third acoustic test consisted of changing the orientation of the plate from vertical to horizontal (Fig. 13). The horizontal position allowed sand to be added to the plate to reduce the contribution of plate modes. The other testing conditions remained the same as the second test.

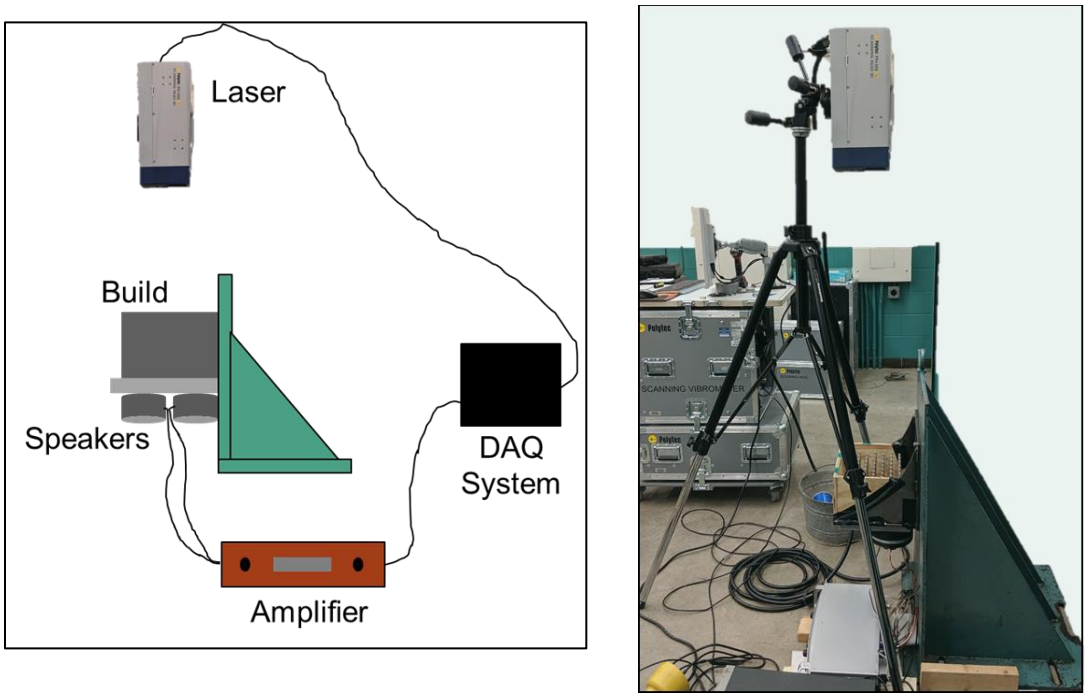

Fig. 13: Test 3 setup model (left) and Test 3 physical setup (right)

A close-up of using sand on the plate is shown in (Fig. 14). The plate was tested nominal, with 0.5-inches of sand, and with 1.5-inches of sand. There was one test performed from 8,000-16,000 Hz to observe the range of the speaker excitation. Only the nominal plate was tested in this configuration, since some of the bars continued to show no axial mode at 9755 Hz due to the plate modes around this frequency.

Fig. 14: Close-up of build plate with sand

2.1.6 Piezoelectric Excitation

Piezoelectric excitation was investigated after previous testing did not distinguish the defect groups. Two lasers were used for this testing, since accelerometers were difficult to attach between the bars. The second laser, a Polytec OFV 353, was a single point laser (not scanning). The OFV is a helium neon laser which requires reflective tape to be placed on the part to record the response. The OFV laser was used as the reference with the SLDV as the response (Fig. 15).

The first amplifier used was the Leipei® LP-2020TI stereo amplifier, since the PZT amplifier took a few months to order and receive. This amplifier had a maximum voltage output of 5V. The signal to the amplifier was a periodic chirp from 5000-12800 Hz. The nominal build was tested free on a piece of foam. The PZT patch was superglued to the build plate (Fig. 15).

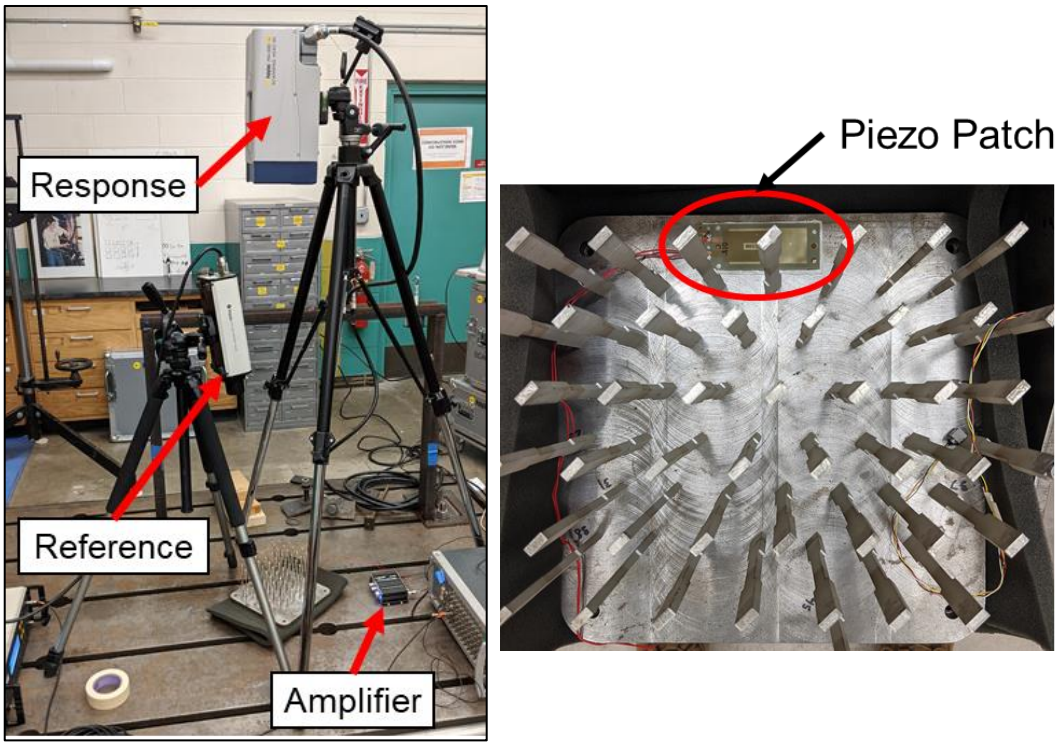

Fig. 15: Piezoelectric Excitation setup (left) and PZT attachment (right)

The first experiment consisted of testing Bars 1, 2 ,6, 7, 13, 14, 21, 24, 25, 28, 32, 36, 39, and 42 (Fig. 16). These bars were selected based on the base plate modes from FEA between 9000-10000 Hz (Fig. 16). The location on the plate for these bars should be excited by plate modes and display the axial mode of interest. The plate has the most motion at the red areas and the least motion at the blue areas. The bars selected should be close to the areas that display the most motion.

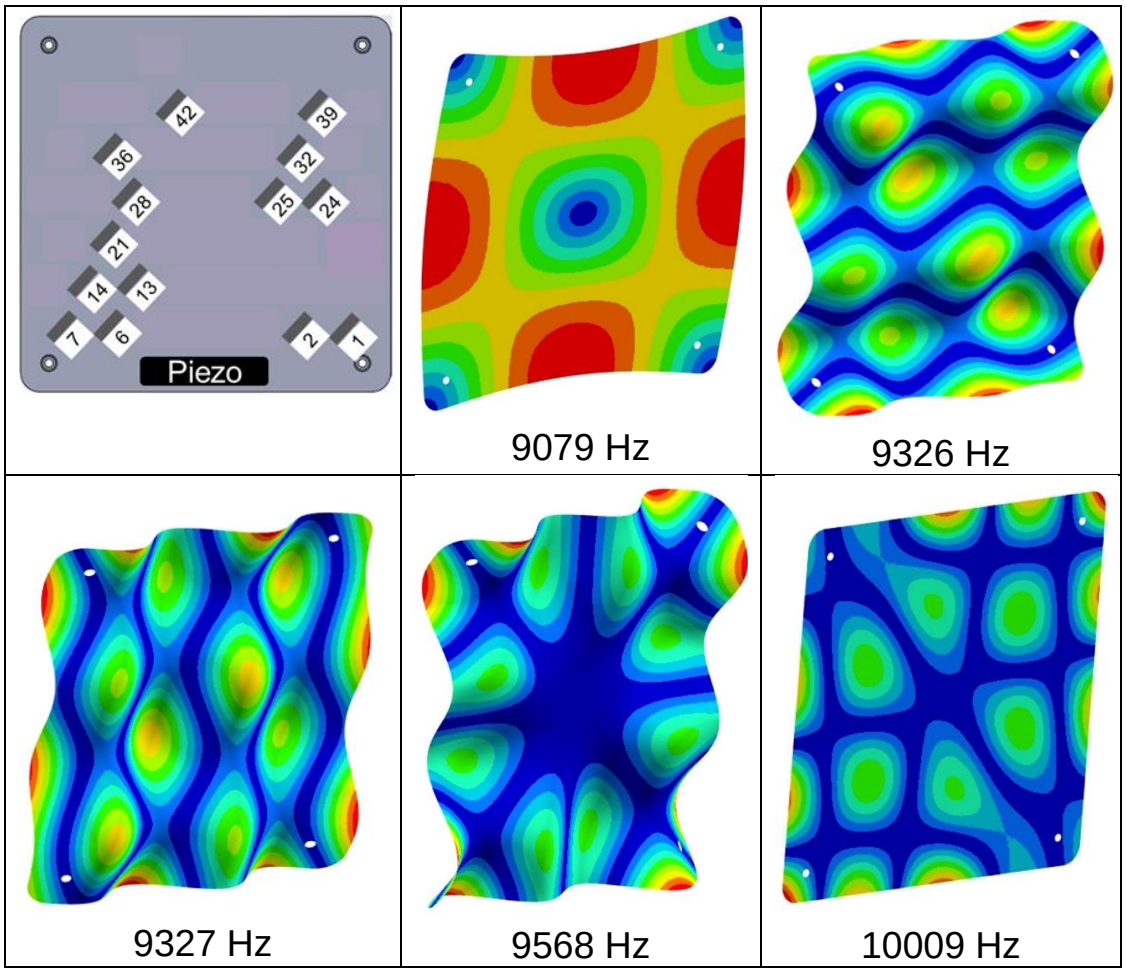

Fig. 16: Bars tested with PZT (top left) and base plate modes between 9000-10000 Hz

The second round of testing with the PZT consisted of using the piezoelectric amp – Model: PZD350A from Trek®. This amplifier can provide the high voltages and low current that the PZT requires. The same testing conditions were used as the previous test except that the voltage was changed to 10 V in amplitude (double of the stereo amplifier). The results from this testing were compared to the previous amplifier.

2.2 Topology Optimized Brackets

The topology optimized build consisted of three brackets also known as the GE Challenge brackets. All the brackets were nominal on the build and printed with support material (Fig. 17). The plan in testing these parts was to find the natural frequencies and compare them to FEA. All testing performed on this build consisted of impacting the "ears" (Fig. 17).

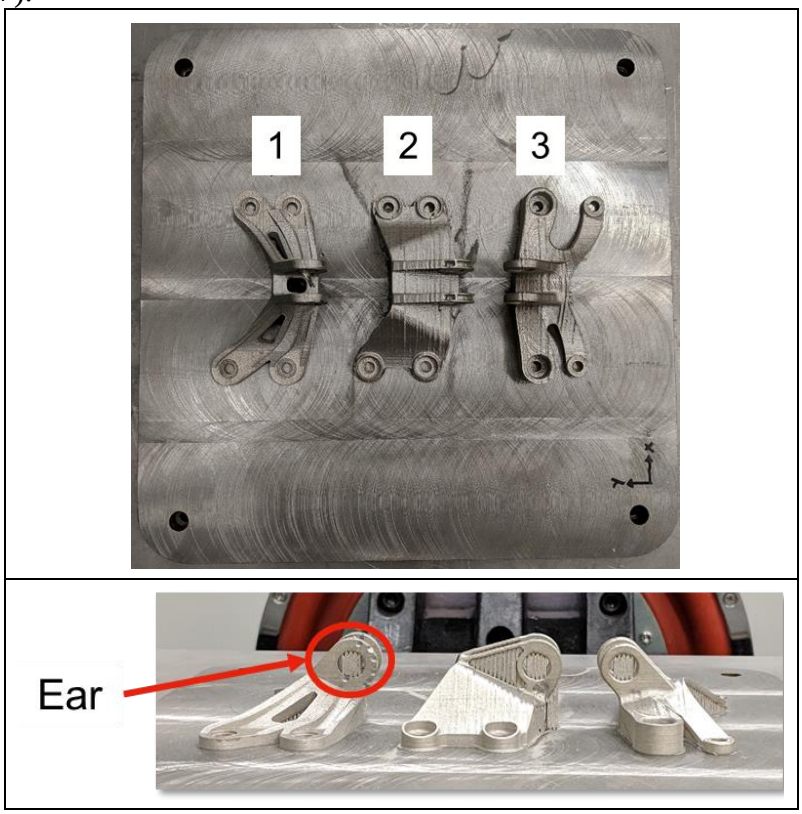

Fig. 17: Topology Optimized Brackets with brackets labeled (top) and side view (bottom)

2.2.1 FEA

The FEA for these parts was performed by MS&T. The first mode was at 5,536 Hz with the last mode of interest at 8,324 Hz (Fig. 18**)**. The FEA model consisted of the brackets fixed to the plate without the support material. All significant modes appeared to be in the ears of the brackets. Bracket 1 and Bracket 3 have similar natural frequencies and motion for modes 5 and 8.

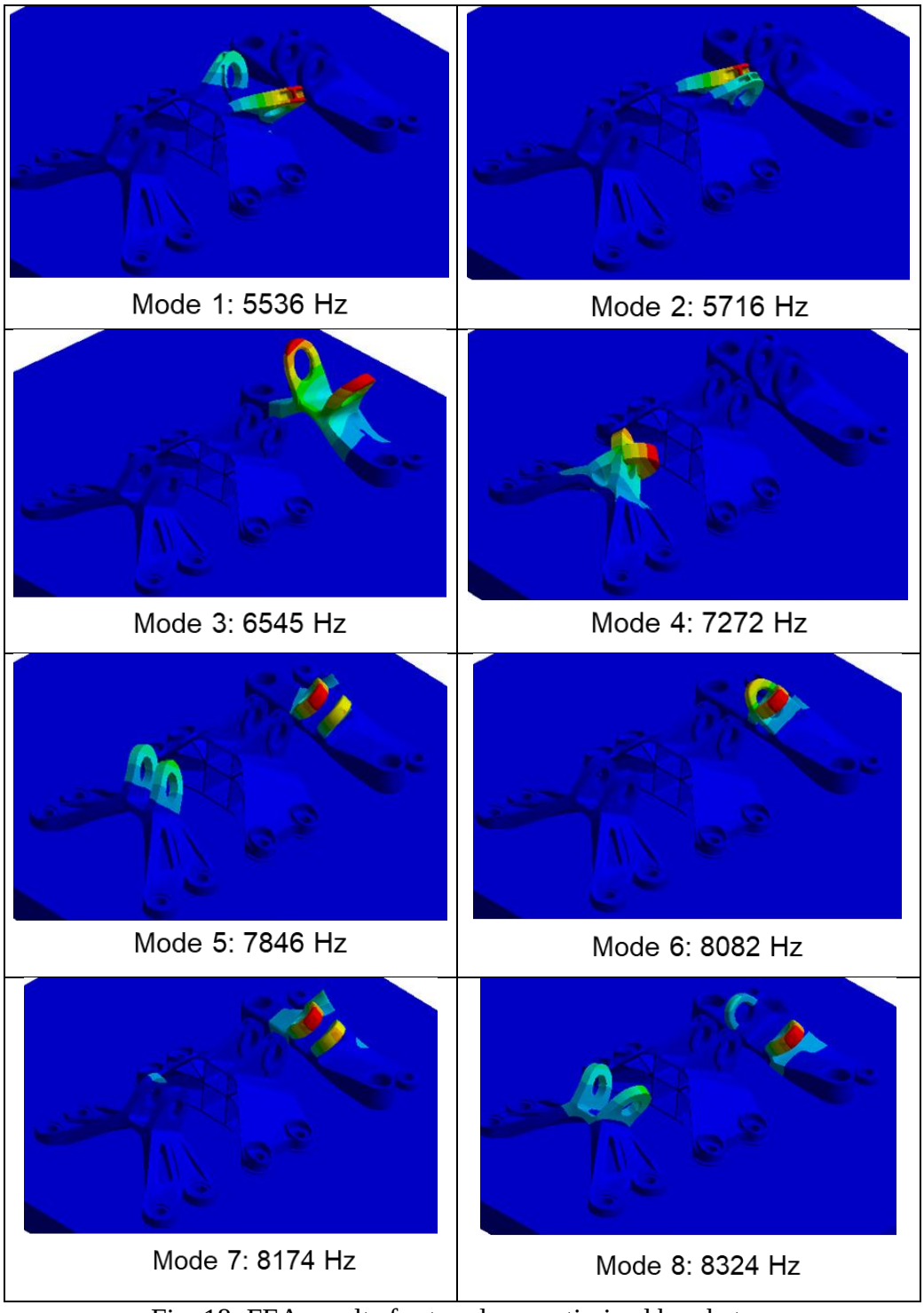

Fig. 18: FEA results for topology optimized brackets

2.2.2 Impact Testing

The brackets were first impact tested in the ears, since the ears provided a flat surface to impact. The proposed points for testing these brackets are shown in (Fig. 19). The small impact hammer (PCB Model: 086E80) impacted the back side of the ear with the response recorded on the other ear with the SLDV.

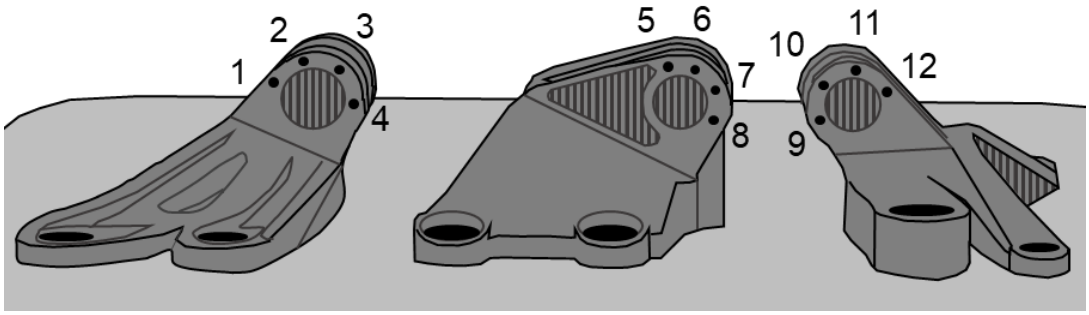

Fig. 19: Topology optimized brackets testing point locations

The small impact hammer was exchanged for the larger impact hammer (PCB Model: 086C04) when there was not enough excitation in the response.

2.2.3 BB-gun Testing

Since the topology optimized brackets did not get enough excitation from the impact hammer and a shaker was not practical in testing these brackets, testing with a BB-gun was proposed. The BB-gun used in this testing is a semi-auto P10 BB Pistol by Crosman®. The BB-gun expels steel BB's and uses CO_2 cartridges to fire.

The setup for BB-gun testing is shown in (Fig. 20). The test was contained within two plastic totes lined with sheet metal in between. A hole was cut in the top for a light and microphone. Another hole was cut into the side of the tote in order to site the BB-gun at the brackets. Foam was placed over the build plate to reduce the effect of ricochets. A microphone with a windscreen was used to record the response. The first test used a PCB 130D21 microphone. The preliminary tests caused the microphone to overload. A different microphone was tried, PCB 426A05, but this microphone also overloaded.

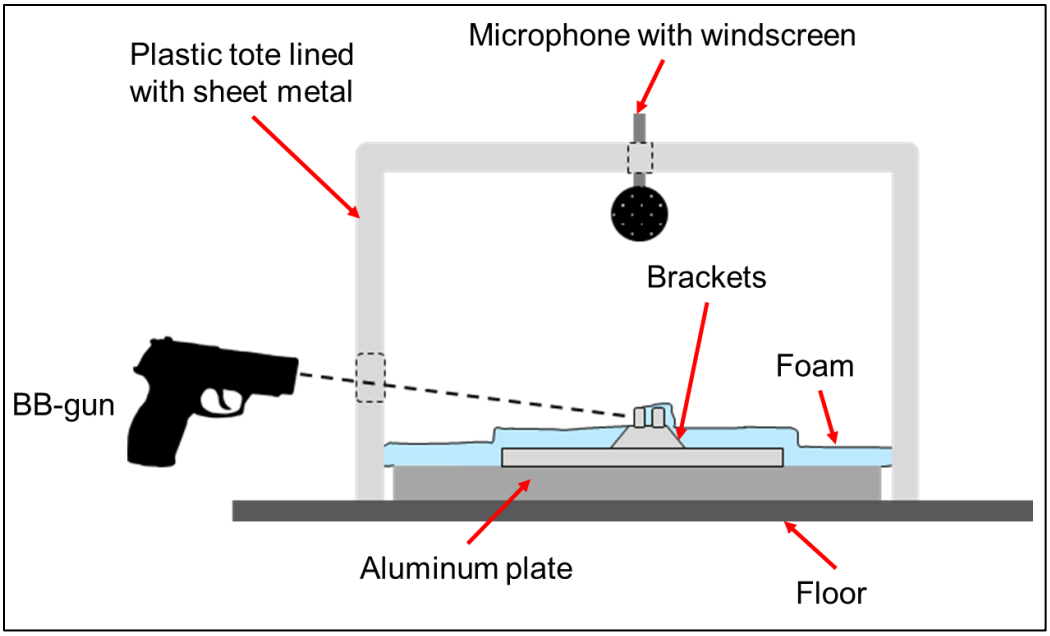

Fig. 20: Model of BB-gun testing (top) and physical test setup (bottom)

In order to reduce the microphone overload, a muffler was added to the BB-gun. The muffler consisted of a 3D printed plastic adapter piece connected to PVC pipe (Fig. 21). The adapter piece was epoxied to the PVC pipe.

Fig. 21: BB-gun with muffler adapter

The PVC Pipe had foam glued to the inside and holes cut in the exterior (Fig. 22). The foam and holes allow the gases to spread out before entering the testing container which reduces the sound transferred into the test chamber. A PVC cap was placed over the end of the muffler with a hole cut into the top of it to allow the pellet to exit.


Fig. 22: Muffler adapter piece (left), foam added inside muffler (right), PVC end cap (bottom)

Neither microphone overloaded with the addition of the muffler. The first microphone (PCB Model: 130D21) was used in the results. The plate was tested both free on foam and fixed to the aluminum adapter plate (Fig. 22). The plate was tested in both configurations to determine where build plate modes were affecting the results.

2.3 Airbus Builds

The Airbus builds were all printed nominal parts to simulate a production run. A total of seven builds were printed and tested. Two brackets were printed on each plate along with four tensile bars (Fig. 23). After testing was completed, the four tensile specimens were removed from the build plate and pulled for yield strength by MS&T.

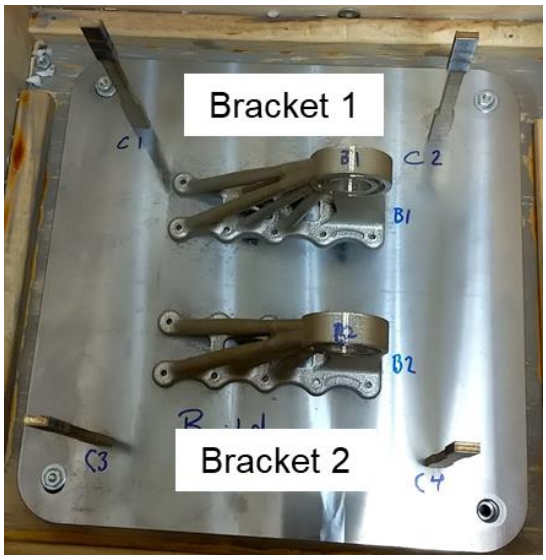

Fig. 23: Physical Airbus build printed with four tensile bar specimens

2.3.1 FEA

The FEA for these brackets was performed by MS&T. The following eleven mode shapes were used for comparison in the results (Fig. 24). The first couple modes appear to have bending/torsion in the top of the bracket. The later modes appear to be mostly bending/twisting in the legs of the brackets.

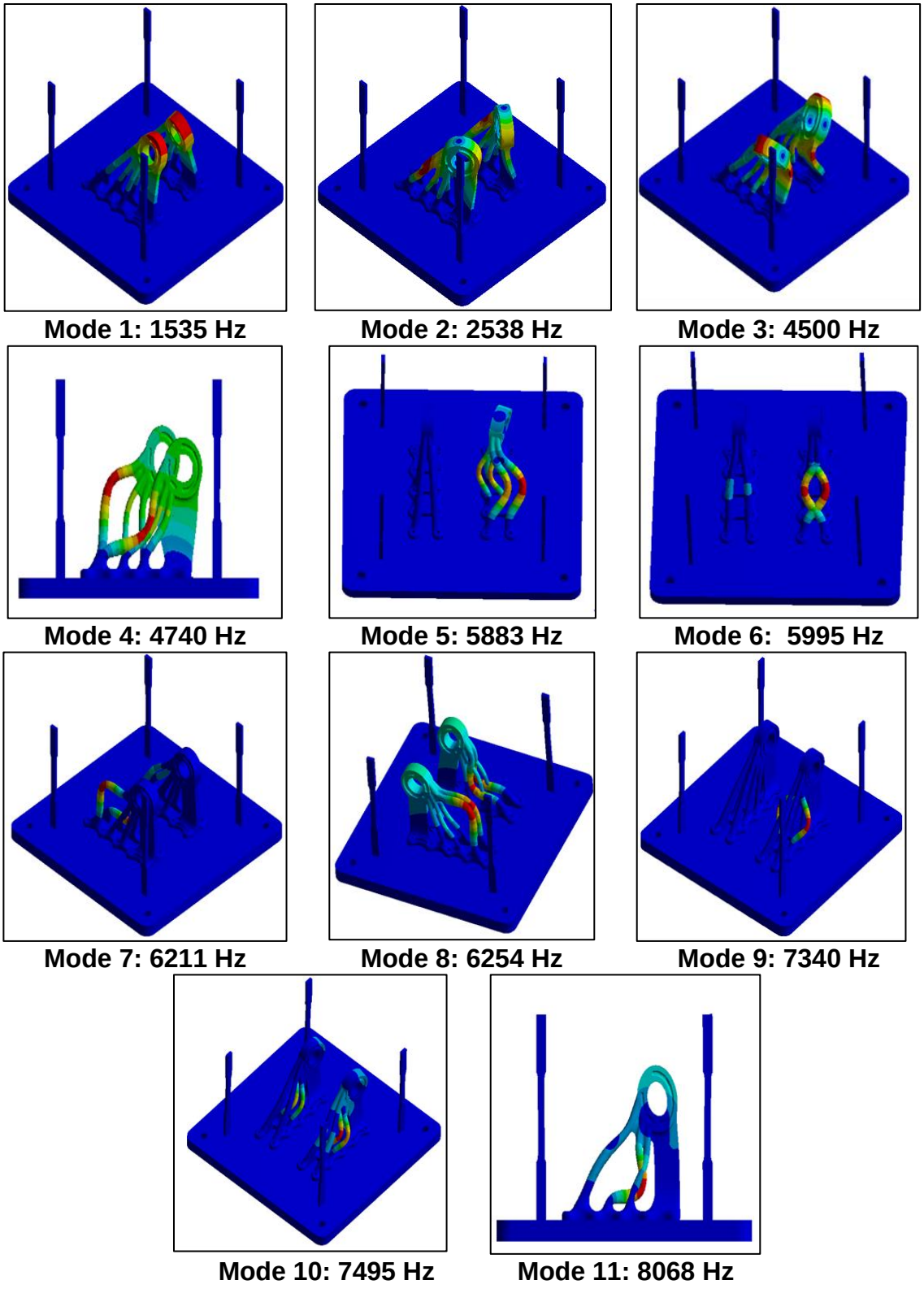

Fig. 24: FEA modes for Airbus brackets

2.3.2 Shaker Testing

The first five builds were shaker tested to compare to FEA modes. The plates were fixed to the adapter plate on the shaker table. The signal sent to the shaker was a periodic chirp from 0 to 6250 Hz. Two configurations were tested to get results on both brackets with the SLDV measuring the response. The first configuration bolted the plate at 90º looking at Bracket 1 (Fig. 25). The second test configuration bolted the plate at 45º looking at Bracket 2 (Fig. 25). Operating deflection shapes were taken for these configurations in addition to finding the natural frequencies.

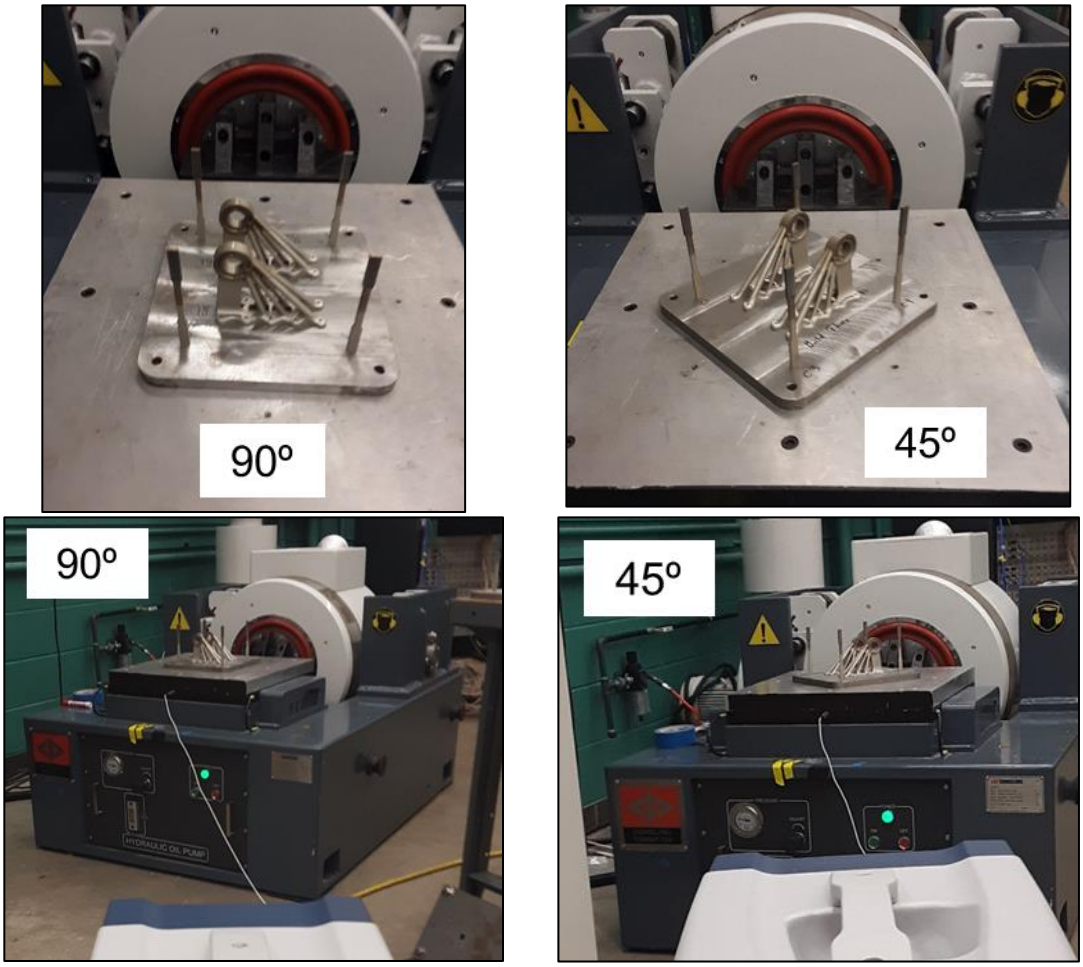

Fig. 25: Airbus shaker testing at 90º (left) and shaker testing at 45º (right)

2.3.3 Impact Testing

The brackets were tested with three boundary conditions – semi-fixed, fixed, and free. Three boundary conditions were tested for two reasons. The first was that the semi-fixed boundary condition did not provide consistent results due to possible table modes. The

second two boundary conditions were tested to determine if there were any significant changes between fixed and free testing.

For all boundary conditions, the same equipment and points were tested. The small impact hammer (PCB Model: 086E80) applied the impact and the response was measured with SLDV. Since the SLDV could not measure in between the brackets, the measurement points on Bracket 1 were taken on the opposite side in comparison to Bracket 2. The points tested are shown in (Fig. 26). Eight points were tested per bracket for a total of 16 points per build.

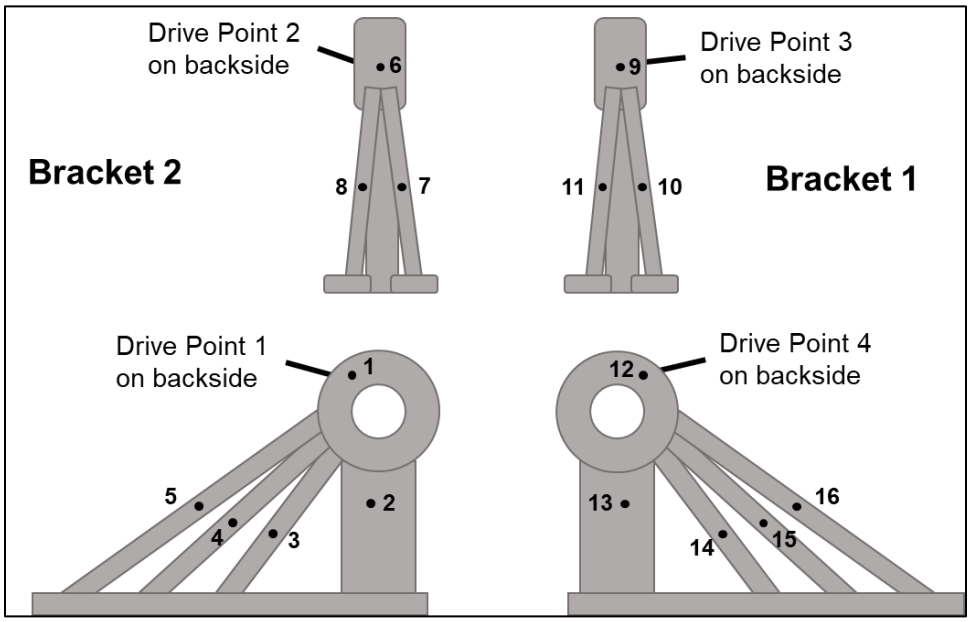

Fig. 26: Points tested with impact hammer on Airbus brackets

2.3.3.1 Semi-Fixed Boundary Condition

The first test consisted of fixing (bolting) the brackets to the aluminum adapter plate placed on a table (Fig. 27). The aluminum plate was not fixed to the table and the table was not fixed to the floor. Since the aluminum plate was not fixed to the table, this was a semi-fixed boundary condition. The first five builds were tested with this boundary condition.

Fig. 27: Semi-fixed boundary condition for testing Airbus builds on table

2.3.3.2 Fixed Boundary Condition

The second boundary condition tested consisted of fixing (bolting) the build to the fixture used for acoustic testing (Fig. 28). After comparing the first five builds with free-free testing, there was no reason to test the last two builds fixed. The results from both tests yielded similar results, except that free-free testing gave cleaner FRFs.

Fig. 28: Airbus build fixed (bolted) to speaker test fixture

2.3.3.3 Free Boundary Condition

All seven builds were tested free on a piece of foam (Fig. 29). The plate and foam were placed on top of the test fixture used for acoustic testing. After all builds were tested free, the tensile bars were removed from each plate and sent to MS&T to be tensile tested.

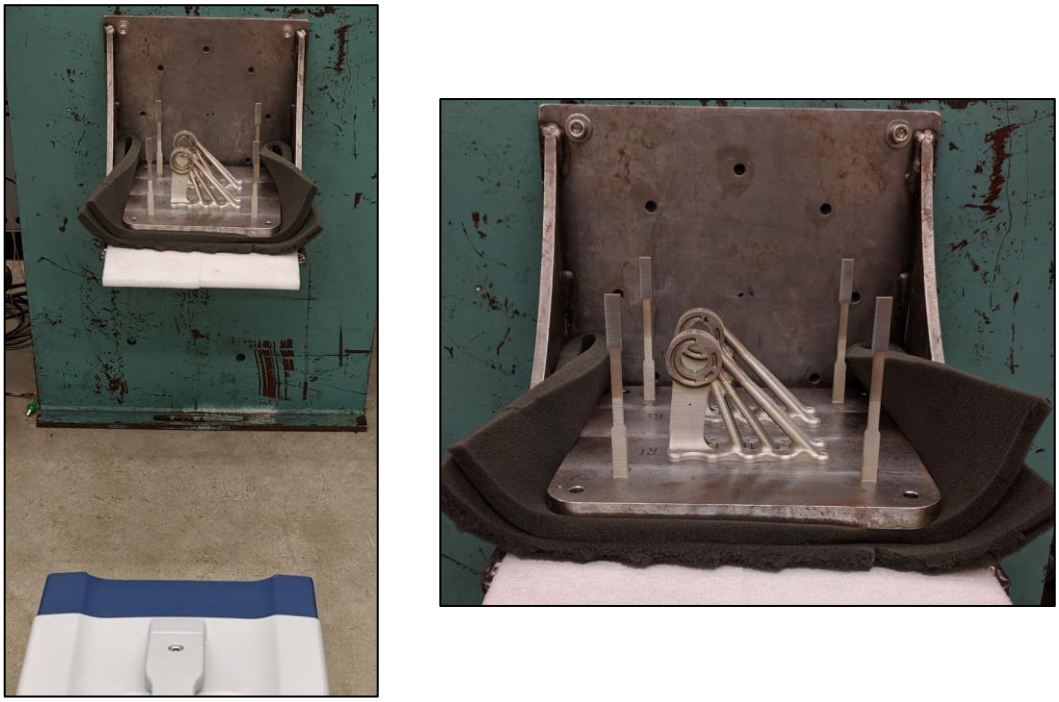

Fig. 29: Airbus build testing free-free setup (left) and close-up of build plate (right)

2.3.4 FRAC

FRAC was applied to the Airbus builds to determine the correlation between every FRF on each build. A MATLAB program was created to apply FRAC (Appendix A). Since all builds were nominal, any of them could be chosen as the simulated FRF. The simulated FRF in this case was chosen to be Build 7. The experimental FRFs were taken from all other builds. The FRAC analysis was computed for Points 1-5 and 12-16 for a total of 10 points. Points 6-11 were not included since they were not tested on all builds.

The FRF of every point on Build 7 was compared to the same points on all other builds. For example, Point 1 on Build 7 was compared to Point 1 on Builds 1-6. Then the same was done for Points 2-5 and 12-16. An average of all the builds was taken to obtain the correlation of each build to the simulated build (Build 7).

3 Results

The results section is organized by the three build types tested: Forest Tensile Builds, Topology Optimized Brackets, and Airbus Builds. Each experimental test performed is a subsection under the three build types. The main conclusions from each build are summarized at the beginning of each section.

3.1 Forest Tensile Bar Builds

3.1.1 Summary of Forest Build Results

The forest tensile builds were physically tested four different ways: shaker testing, impact testing, acoustic testing, and piezoelectric testing.

Shaker testing was performed first as it is the simplest experiment to perform. When the results of this testing showed noisy FRFs, impact testing was performed.

The results from impact testing obtained the first four bending modes in the x-direction of the structure. Impact testing provided the best analysis on this build and further statistical analysis was performed. The damping values were also determined for this build as some of the bars showed damped peaks.

After the defect groups could not be determined from impact testing, some analysis on natural frequencies and bar locations was performed. The statistical and damping ratio analysis showed trends in these builds. These trends indicated that the location of a bar on the plate affected the results more than the current defects that were put into these builds. Cover gas flow in the printing process is presumably the cause of the variation, giving directionality to the bars printed on the plate. The trends associated with location were discovered after all the testing on these builds was performed. Without this knowledge, the following tests were based on the assumption that determining the natural frequencies for the axial mode would have the highest likelihood of distinguishing the defect groups.

The acoustic tests focused on exciting this axial mode through the bottom of the plate. Three different tests were performed on this build. The first test did not provide enough excitation to the plate and the second test was largely driven by base plate modes. The third acoustic test aimed at reducing the effect of the base plate modes by adding sand to the plate. The sand reduced some of the base plate response, but bars that were located on a plate mode with low response did not receive excitation. The FRFs were difficult to analyze from this testing as the plate response gave indistinct peaks. The defect build was not tested after the nominal build failed to display the axial mode in some of the bar responses on the nominal build.

The last test performed on these plates aimed for capturing the axial mode as the acoustic testing was unable to provide the response required to analyze this mode. The PZT

testing excited the plate, with the bar response measured by the SLDV. The PZT testing had very similar results to the acoustic testing – some FRFs did not have distinct peaks. Additionally, some bars were not excited due to the base plate modes.

3.1.2 Shaker Testing

Only the defect build was shaker tested, as the nominal build was built and sent to MTU after the results were analyzed for this test. The shaker testing was performed with a periodic chirp and recorded with the SLDV at the top of each bar. This testing aimed at exciting the x-bending modes. The x-bending direction is bending in the front and back of the bar and the y-bending direction is side-to-side bending in the bar (Fig. 30).

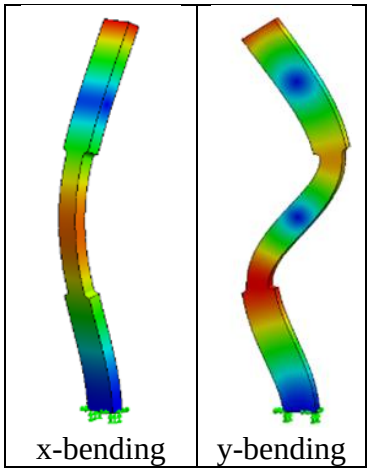

Fig. 30: X-bending direction (left) and y-bending direction (right) in tensile bar

The results from the FRF relationship between the generated signal to the shaker and the response recorded from the SLDV are shown in (Fig. 31). The FRFs appeared to have noise between natural frequencies. This noise is probably due to the whole plate being excited at once with all 45 bars attached. From the entire spectrum, it is difficult to see individual bar peaks.

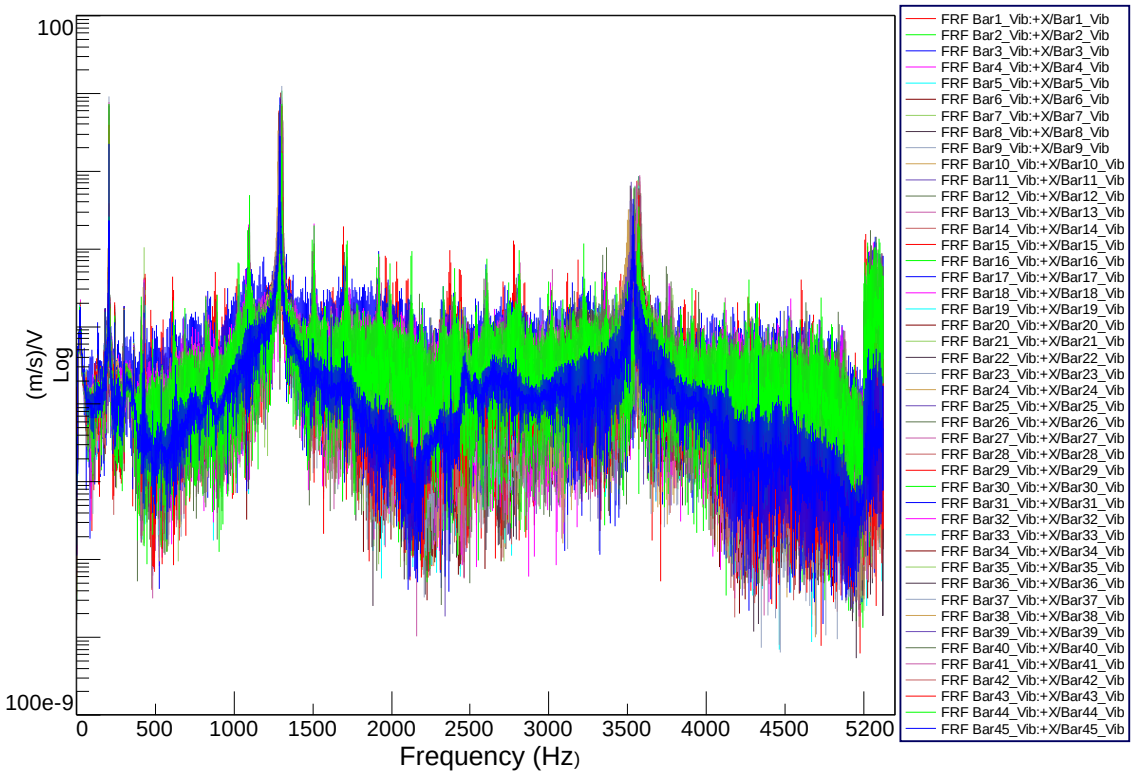

Fig. 31: FRF for shaker testing results of all 45 tensile bars on the build with defects

Zooming in on the first natural frequency for all 45 bars, the individual bar peaks can be seen (Fig. 32). Unfortunately, these natural frequency peaks have noise despite a high frequency resolution of 0.078 Hz. After analyzing these results, impact testing was suggested to obtain cleaner FRFs with more distinct natural frequency peaks.

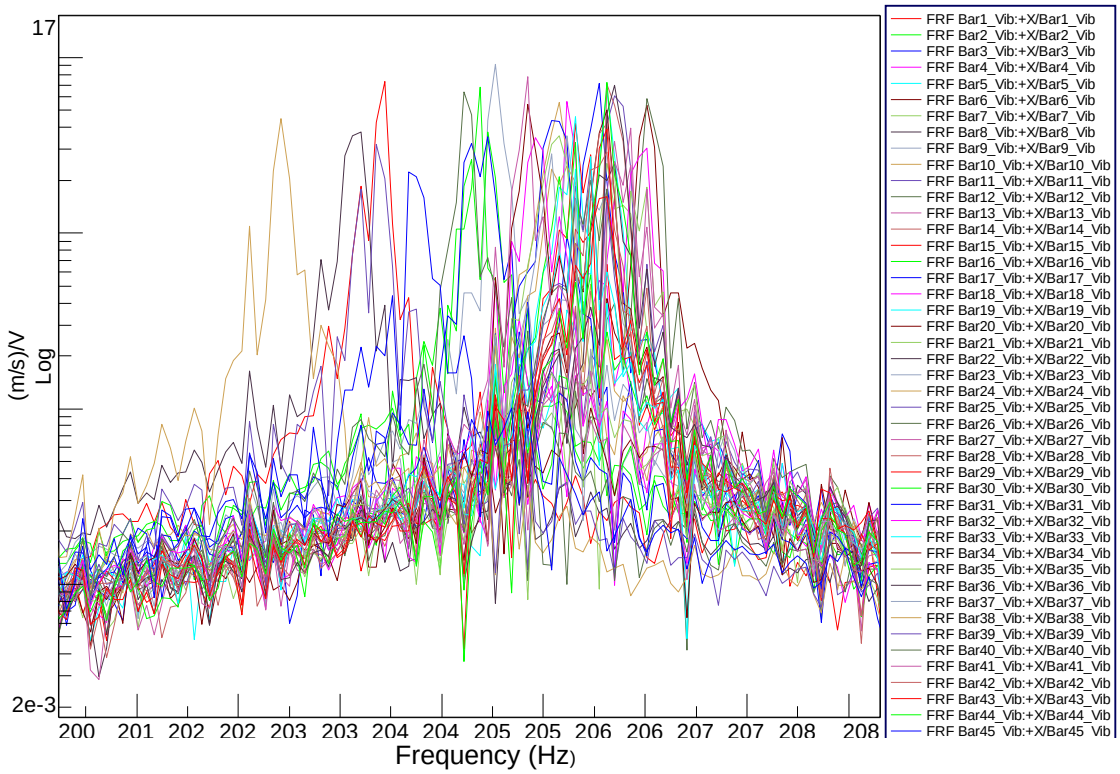

Fig. 32: Shaker testing on build with defects at Mode 1

3.1.3 Impact Testing

The goals of impact testing were to distinguish the defect groups on the defect build and compare the differences with the nominal build. The impact testing performed aimed at exciting the same x-bending modes as shaker testing. The bars were impacted from the same reference direction as the shaker with the SLDV. The same points being measured on each bar as the shaker testing. Both the nominal and defect build were impact tested using the same setup.

3.1.3.1 Build with Defects

Impact testing provided a greater dynamic range and cleaner FRFs than shaker testing. The FRFs between the impact hammer input and the SLDV response of each bar are shown in (Fig. 33). The first four x-direction bending modes were distinguishable in the FRF and are boxed in red. Modes 2, 4, and 7 are y-bending modes. Mode 6 is a torsional mode. These other four modes are lower in amplitude as most of the energy should be in the x-direction. These modes probably appear due to the SLDV measurement or impact force being slightly angled or off-center.

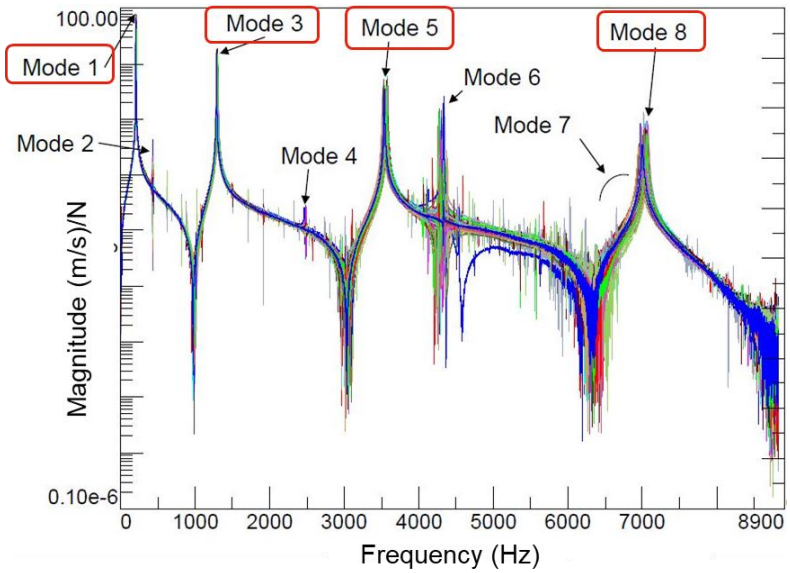

Fig. 33: Impact testing results display the first four bending modes (red)

There were no distinguishable differences between the defect groups from analyzing the FRFs. If the impact results are sensitive to the defects, the FRFs between the groups should be shifted from one another. Unfortunately, none of the x-direction modes appeared to show any defect groupings. Focusing on Mode 1, the FRFs of each of the bar groups appear to overlap one another (Fig. 34).

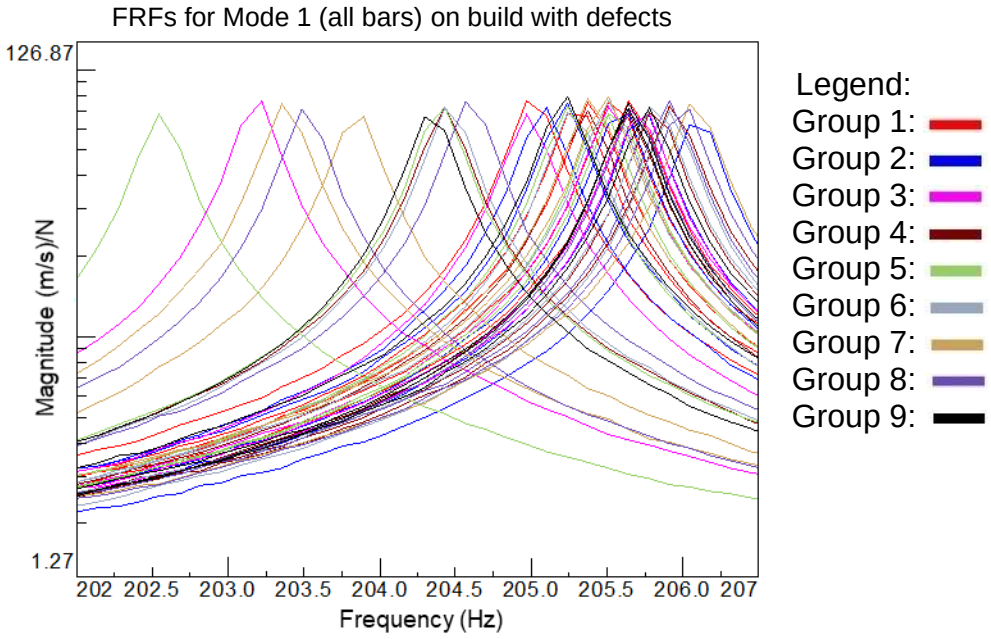

Fig. 34: FRFs for Mode 1 for all 45 bars on the build with defects

The fourth x-bending mode or Mode 8 displayed the same phenomena as Mode 1 (Fig. 35). There were no groups of defects congregated together. Since this mode is higher in

frequency the span of natural frequencies is larger than the first mode. Interestingly, the amplitude and damping differences are more apparent in this mode. These differences prompted determining the damping values associated with each mode from impact testing.

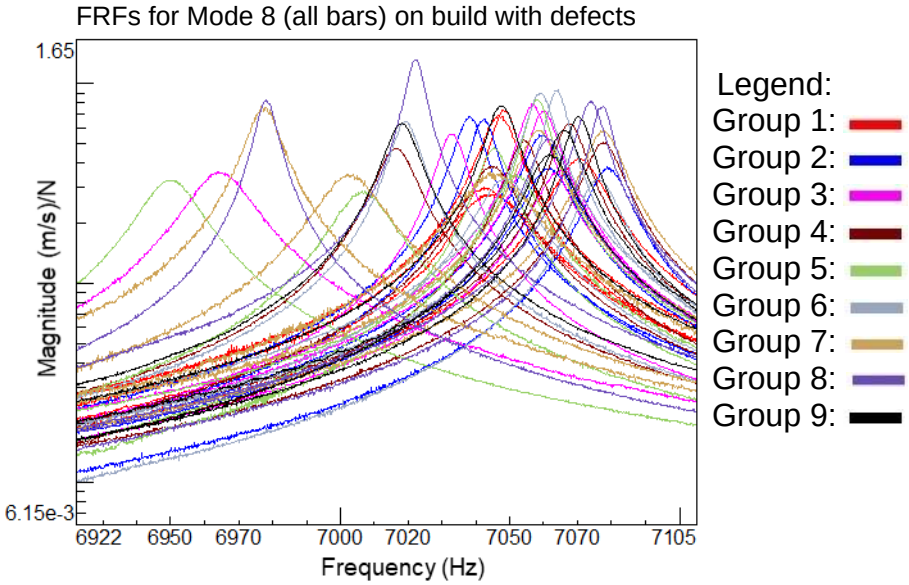

Fig. 35: FRFs for the build with defects at Mode 8

3.1.3.2 Nominal Build

The nominal build results were used as a comparison to the build with defects. For comparison, the nominal build bars are categorized by group number associated with the build with defects (Fig. 36). Interesting, the four lowest bars in frequency (circled in red) are in the same groups as Modes 1 and 8 on the defect build. There is no apparent reason for this to be, as those bars are from different groups on the defect build. The nominal bars should have no group association. Another difference between the builds is that the mean for this mode is shifted approximately 2 Hz or 1% lower than the defect build.

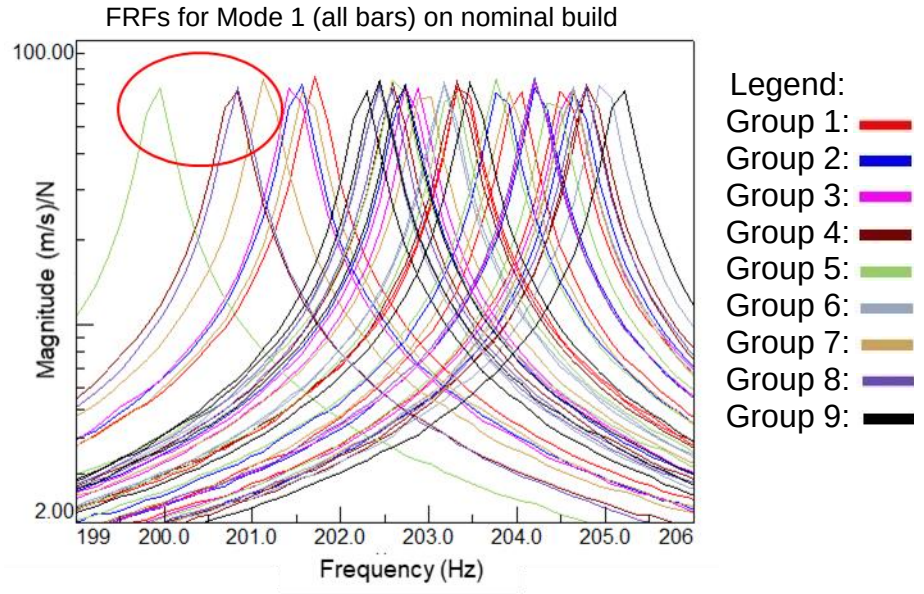

Fig. 36: FRFs for Mode 1 on the nominal build for all 45 bars

Comparing the nominal build Mode 8 with the defect build, the differences and amplitude and damping are similar (Fig. 37). The group location anomaly found in both nominal Mode 1 and the defect build is the same for this mode as well (circled in red). The mean for this mode is also shifted lower by approximately 1% or 77.5 Hz in comparison to the defect build. The shifts in mean are investigated further in the statistical analysis.

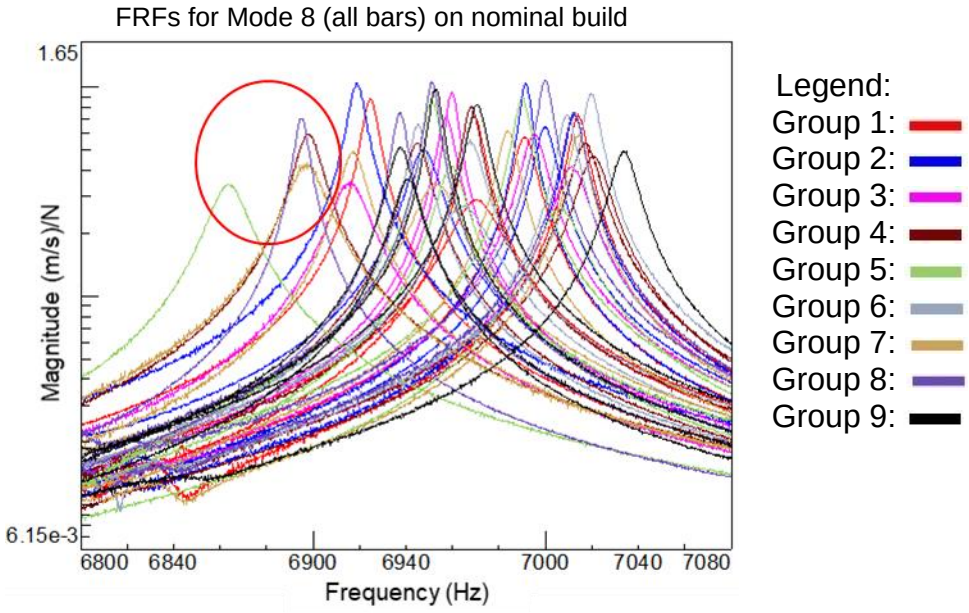

Fig. 37: FRFs for Mode 8 on the nominal build with similarity to defect builds circled

There appeared to be some possible patterns from the nominal build compared to the defect build. There may be some similarity between bar location on the plate as the groups were identical for the first four bar frequencies for both builds. There also appears to be a mean shift between the two builds. Both of these irregularities are further investigated in the statistical analysis.

3.1.4 Statistical Analysis

Analyzing the results from impact testing, the statistical analysis evaluates the mean, variance, and standard deviation. The analysis extends to investigate further findings in frequency compared to bar number and column number.

The nominal build natural frequencies for the first four x-bending modes were tabulated to find the mean, range, and variance (Table 2). Comparing the two builds, the defect build has a higher mean, a smaller variation, and a smaller range than does the nominal build (indicated in red). The nominal build should have a smaller variance. The mean and variance is investigated further in the following sections to determine why this occurred.

Table 2: Mean, Variance, and range for tensile bar builds

Mean, Variance, and Range for Tensile builds								
Mode Number	Mode 1		Mode 3		Mode 5		Mode 8	
Build Type	Nominal	Defect	Nominal	Defect	Nominal	Defect	Nominal	Defect
Mean (Hz)	203.2	205.2	1284.5	1300.2	3519.3	3562.6	6966.7	7044.2
Variance (Hz^2)	1.6	0.7	60.8	33.3	365.6	304.2	1578.4	932.2
Range (Hz)	5.3	3.5	33.3	25.8	78.4	78.1	170.1	129.1

3.1.4.1 Mean Shift

The higher mean value for the defect build is investigated by calculating the mean shift for each group on the defect build (Table 3). For the build with defects, the mean was shifted on average 1.1% higher. If the defect was being detected, the mean value for each group should increase in mean shift for increasing defect. This does not appear to be the case as the highest defect group, Group 9, has approximately the same amount of shift as the nominal group, Group 1. This indicates that the x-bending modes are not sensitive to the defects printed in the defect build.

Table 3: Percent mean shift for the build with defects compared the mean value of the nominal build

		% mean shift								
X-bending Mode Number	Nominal Mean Value (Hz)	Group 1	Group 2	Group 3	Group 4	Group 5	Group 6	Group 7	Group 8	Group 9
1	203.2	1.06	1.17	0.90	1.10	0.72	1.07	0.81	0.96	1.05
2	1284.5	1.33	1.42	1.13	1.34	0.90	1.33	0.99	1.21	1.35
3	3519.3	1.31	1.44	1.13	1.33	0.87	1.42	0.98	1.24	1.37
4	6966.7	1.21	1.28	1.00	1.23	0.80	1.25	0.94	1.09	1.23

3.1.4.2 Standard Deviation

In addition to the mean shift, the standard deviation analysis indicates that that the x-bending modes are not detecting the defects in the defect build. The mean value for each defect group was compared to the standard deviation of the nominal build (Fig. 38). The average for each mode on the defect build is shown by a red triangle. All groups were between 1.1 and 2.7 standard deviations higher than the mean value on the nominal build. The groups follow a pattern for each mode in where Group 5 is closest to nominal, Group 8 is on the average for the defect build, and Group 2 is the farthest from nominal.

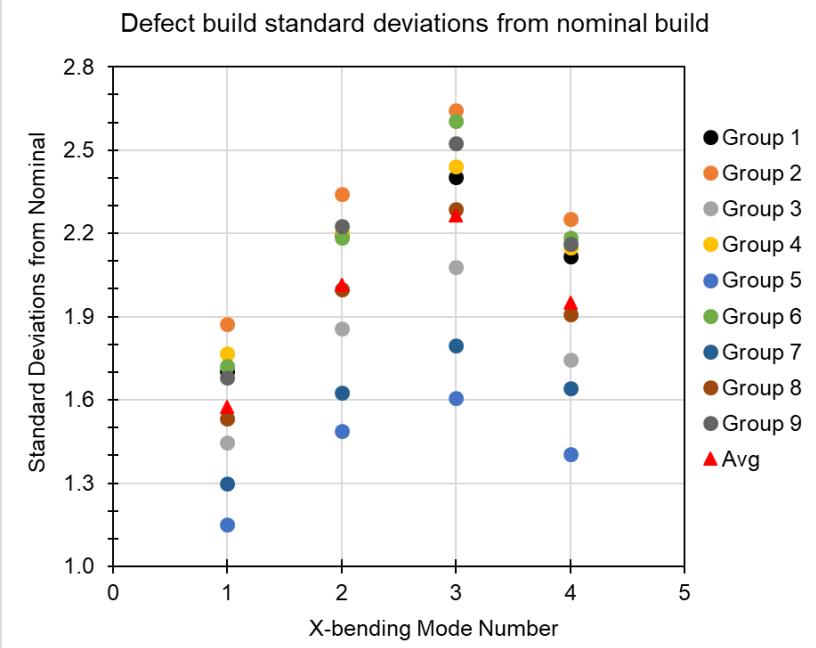

Fig. 38: Defect build compared to the standard devation from the nominal build

If the defects were detected, Group 9 should be farthest from the mean value and Group 1 should be nearest to the mean value. The standard deviation analysis shows that this is not the case.

3.1.4.3 Natural Frequency by Bar Number

The natural frequency was plotted against bar number to determine if any patterns appear between the two builds. A trend does appear in the data as the first bending mode demonstrates. The first bending mode shows that from the right to the left side of the plate the frequency increases until it hits the middle and then decreases to the other edge (Fig. 39). The pattern then starts over with the next row. The nominal build displays a decrease in frequency in the rows from the bottom to the top of the plate (Fig. 39). The decrease in frequency with increasing row number is not as prominent in the defect build. The x-bending Modes 2-4 follow the same trends as first x-bending mode (Appendix B.1).

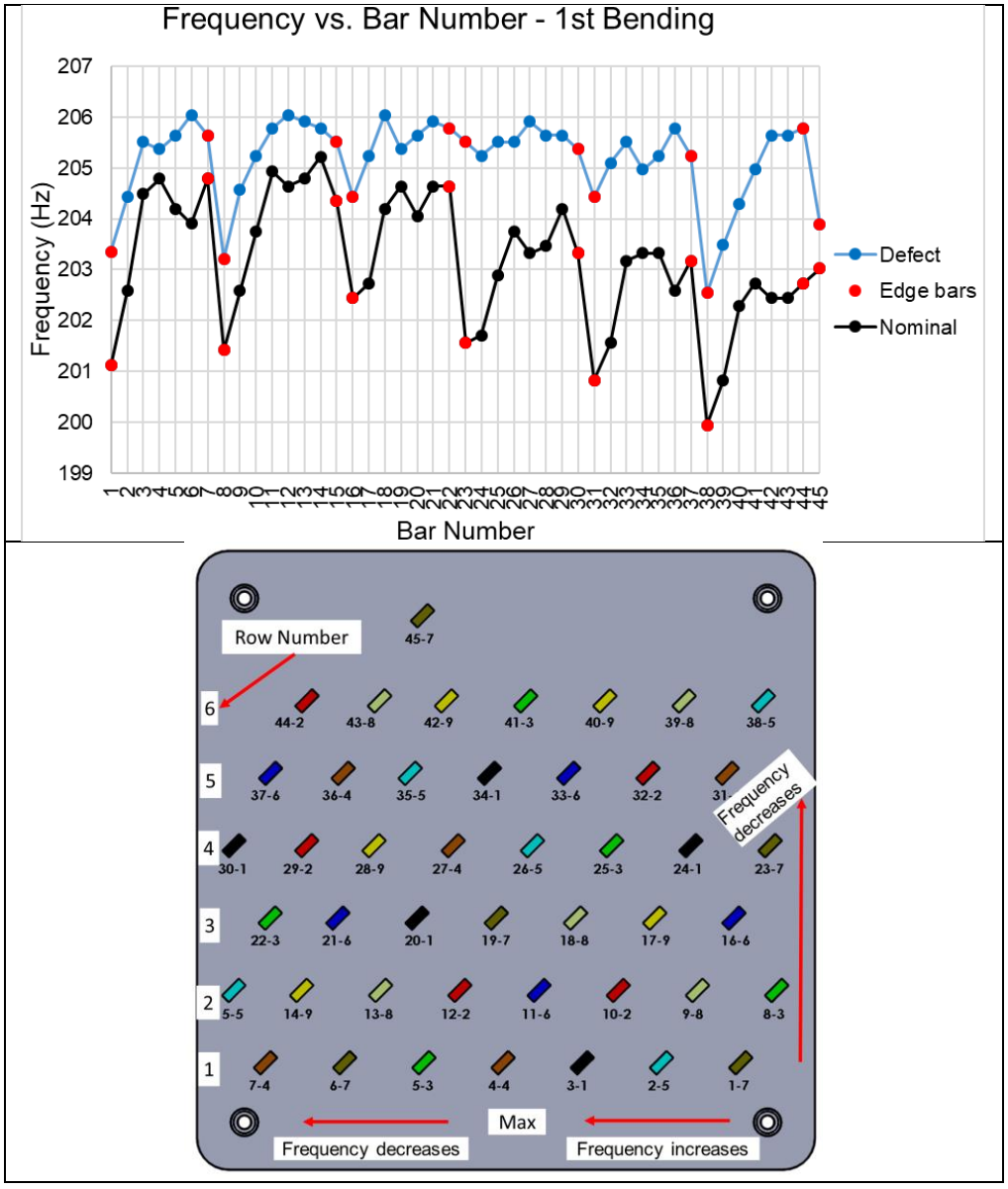

Fig. 39: Frequency vs bar number (top) and trends appearing on the build (bottom)

3.1.4.4 Natural Frequency by Column Number

The patterns from right left on the plate, prompted an investigation into the columns of the bars. The plate was split into seven columns (Fig. 40). Splitting the bars into columns was done to verify that part location on the plate has more of an effect than the defects placed in the bars.

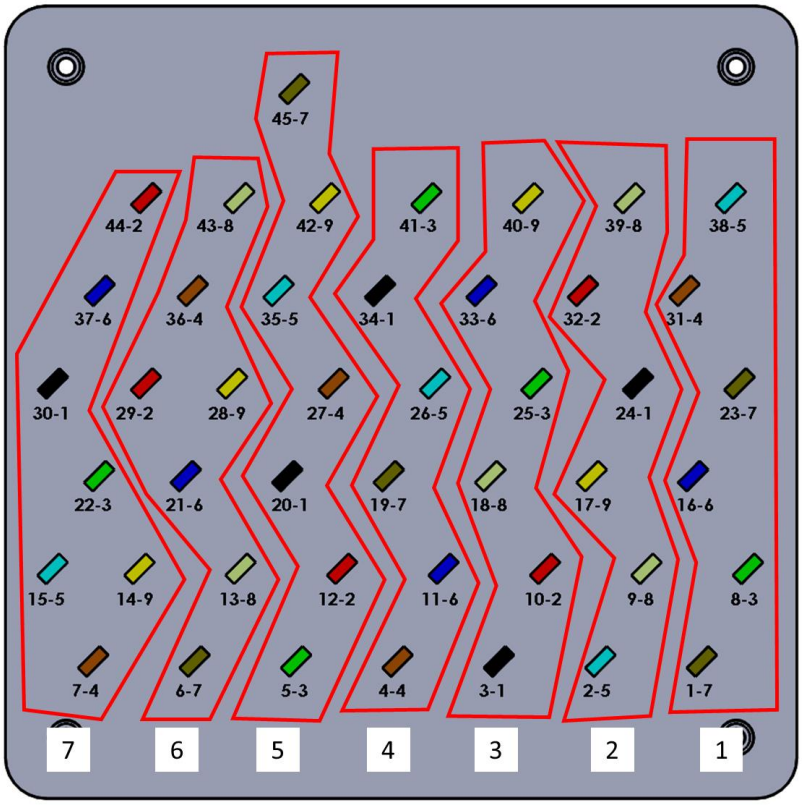

Fig. 40: Columns on builds (top) and columns versus frequency for Mode 1 (bottom)

The columns were plotted against frequency (Fig. 41). The defect build shows a general decrease in variation from Column 1 to Column 7. Bar 45 on the defect build appears as an outlier in Column 5. The frequency of Bar 45 is more associated with Column 1. The nominal build does not decrease in variation across the plate. The same trend is shown in in the second, third, and fourth x-bending modes which are shown in (Appendix B.2).

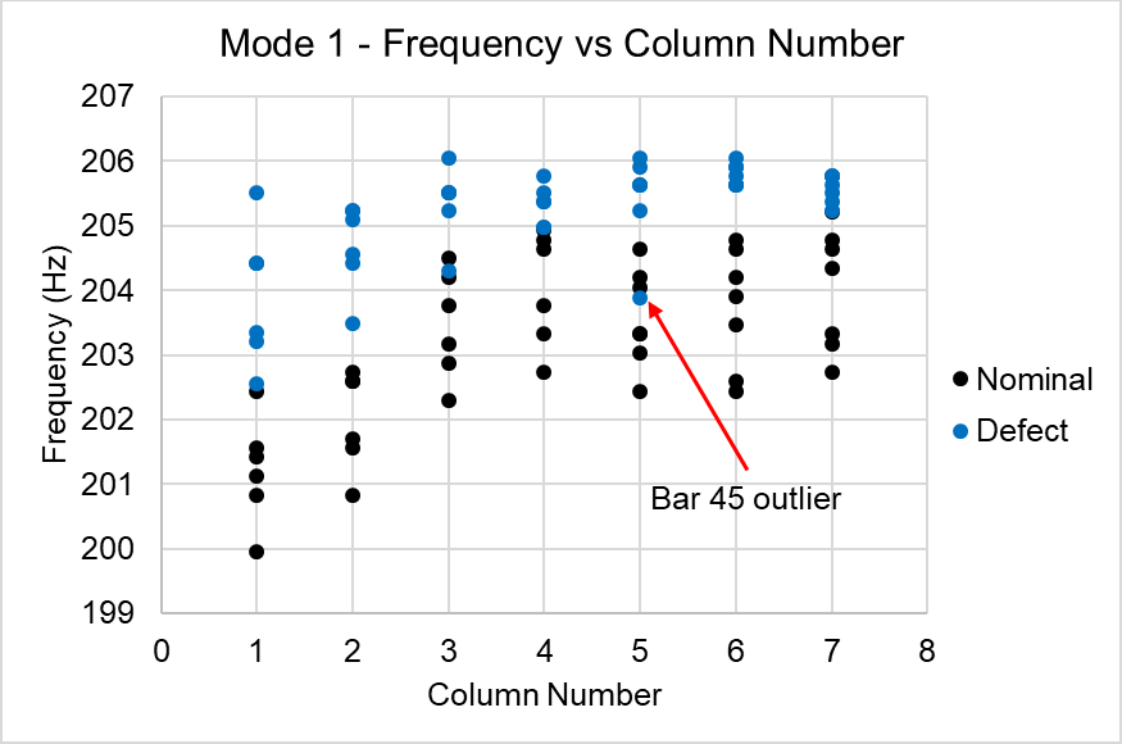

Fig. 41: Frequency versus column number for Mode 1 on the tensile forest builds

The column versus frequency analysis suggests that the bars on the right side of the plate are generally lower in frequency. Organizing the bars from lowest to highest in frequency, the nominal build had 8 bars on average in common (Fig. 42). These 8 bars are the lowest in frequency. They are all located on the right side of the plate. The bars were printed to be nominal on this build and the lower frequencies associated with location suggest a variation in the printing process.

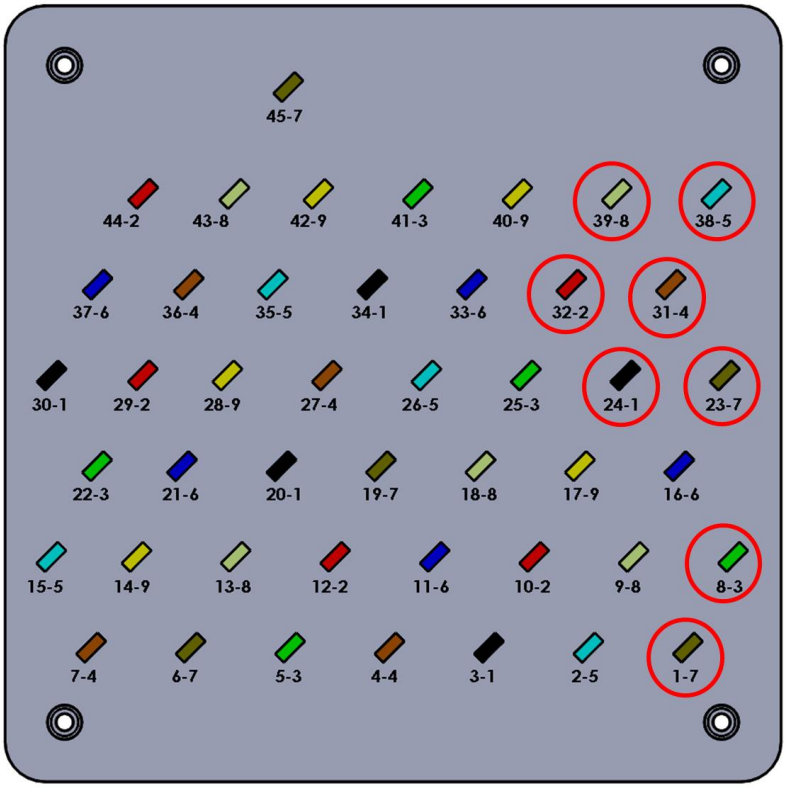

Fig. 42: Nominal build with the lowest bars in frequency circled in red

The trend on the nominal build is exacerbated in the defect build. The 10 bars shown in red were the lowest on average in frequency on this build (Fig. 43). The third x-bending mode had an additional bar lower in frequency associated with the right side of the plate. Interestingly, Bar 38 was the lowest in frequency for all modes on both the nominal and the defect build.

The bars being lower in frequency further suggests that the cause is associated with variation in the printing process. MS&T informed MTU that there is a cover gas flow from right to left across the plate while printing. This gas flow disrupts the material being printed, causing the trends that appear. MS&T has little control over how the gas flows in the print chamber. The variability will continue to occur until the flow can be more normalized across the build.

Unfortunately, the defects created in these bars are less sensitive to dynamic testing than the natural variability associated with printing the build. Unless the defects are larger (or more sensitive) than the print variability the ability to determine them from dynamic testing will be difficult.

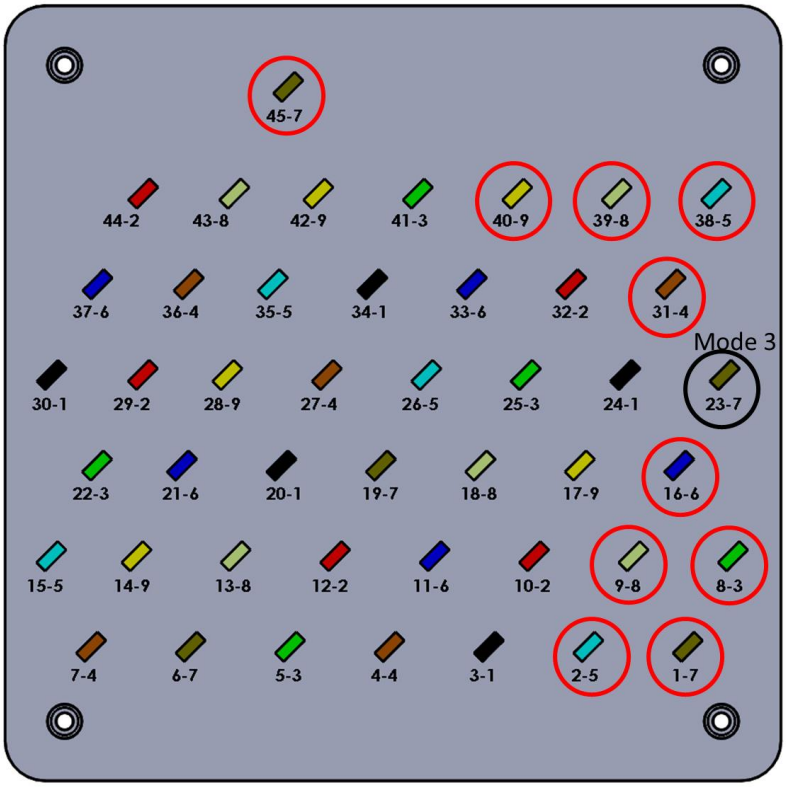

Fig. 43: Defect build with the lowest bars in frequency circled in red

3.1.5 Damping Ratios

The damping ratios were investigated since some of the FRFs appeared to have differences in damping. Using the 3 dB down method, the damping ratios were calculated for the x-bending modes on both the nominal and defect build. The average damping ratios for both the nominal and defect build are shown in (Table 4). The damping values ranged from 0.00042 to 0.00092 in the nominal build and from 0.00051 to 0.00080 in the build with defects.

Table 4: Average damping ratios for tensile forest builds x-bending modes

	Mean Damping Ratios	
X-bending Mode No.	Nominal	Defect
1	0.00072	0.00068
2	0.00042	0.00051
3	0.00092	0.00076
4	0.00072	0.00080

The nominal build displayed a pattern across the plate from one side to the other for the third and fourth x-bending modes. The edge bars appeared to have higher damping

values. The plate with the edge bars marked in red is shown in (Fig. 44). This pattern was not as prevalent on the first and second x-bending modes.

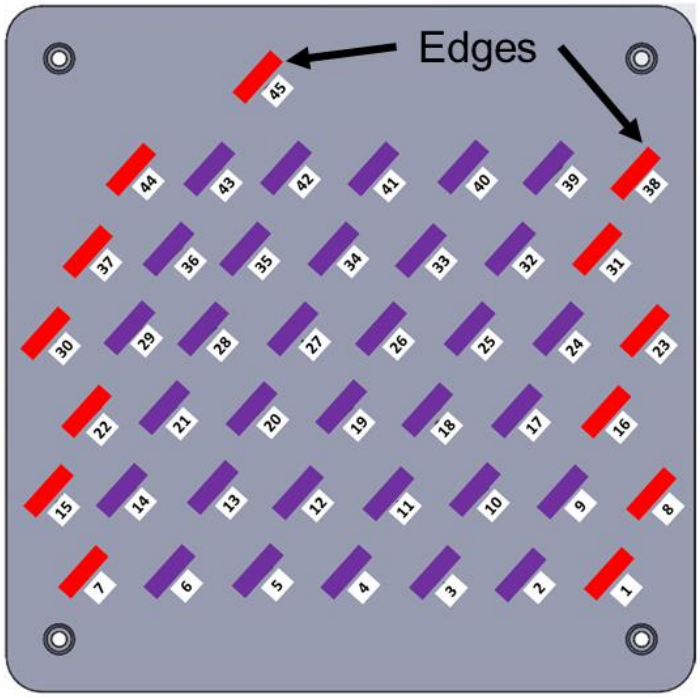

Fig. 44: Build plate with edge bars marked in red

The damping ratios for the first x-bending mode on both builds are shown in (Fig. 45). The bars on the edges of the plate are displayed by red dots in the figure on the nominal build. The mean and ± 3 standard deviations from the nominal build are displayed for each mode. All the bars on both builds were between three standard deviations from the mean with no apparent patterns appearing in this mode.

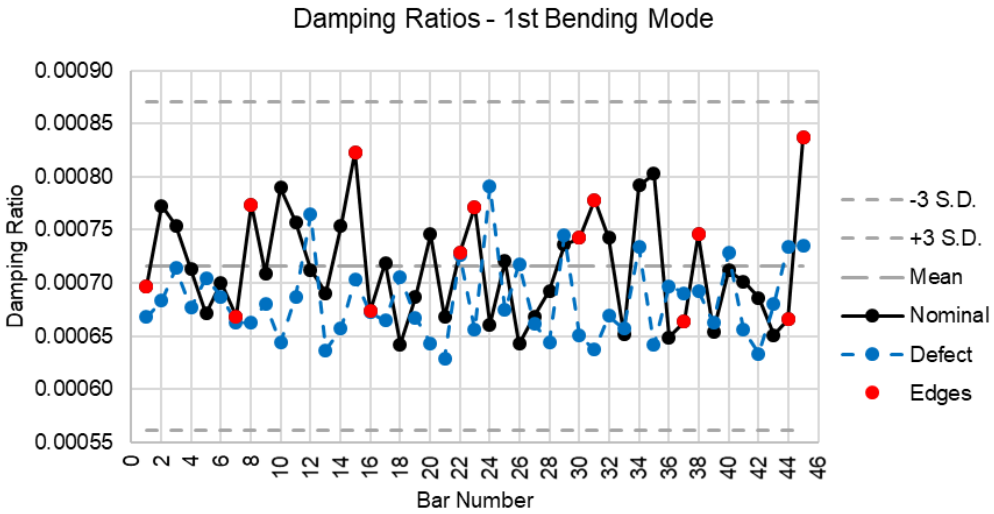

Fig. 45: Damping ratios for first x-bending mode

The second x-bending mode has the biggest difference between the nominal and defect build (Fig. 46). The build with defects has ten bars beyond 3 standard deviations from the mean. Nine of these bars are more than 6 standard deviations from the mean. Interestingly, one bar, Bar 40, was nearly 18 standard deviations from the mean value.

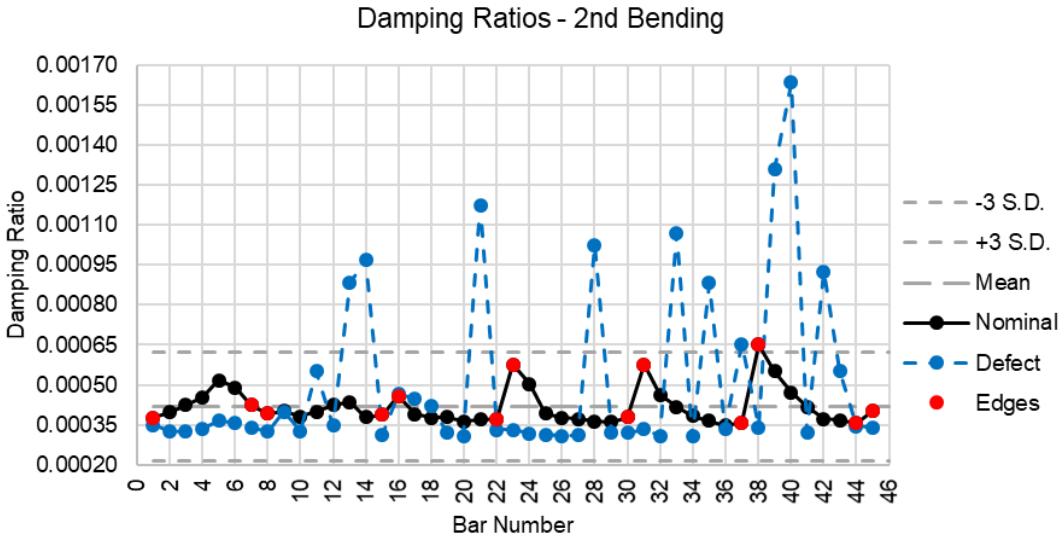

Fig. 46: Damping ratios for the second x-bending mode

The bars outside of ± 6 standard deviation are sorted by group number in (Table 5). Groups 8 and 9 have 66.7% of these bars. Forty-four percent are from Group 9 alone, the group with the largest defect. Interestingly, Group 6 had two of these bars, equating to 22% of the group. Group 7 did not have any of the bars, although this group was created to have a larger defect than Groups 5 and 6.

Table 5: Number of bars outside 6 SD on the build with defects related to group number

Group Number	Number of bars outside ± 6 SD
5	1
6	2
8	2
9	4

Further investigating the 2nd x-bending mode, the damping ratio versus group number was plotted with the FEA of this mode shown as a reference (Fig. 47). The second and third x-bending modes will be most affected by the defect due to the location of the defect being on the section that experiences the most stress. The plot assists in visualizing which groups are showing the largest variation in damping ratio. Groups 1, 2, 3, 4, and 7 appear to have low variation in damping ratio while 5, 6, 8, and 9 appear to have high variation. There is no apparent reason why Group 7 is lower in variation and not more similar to Groups 6 or 8.

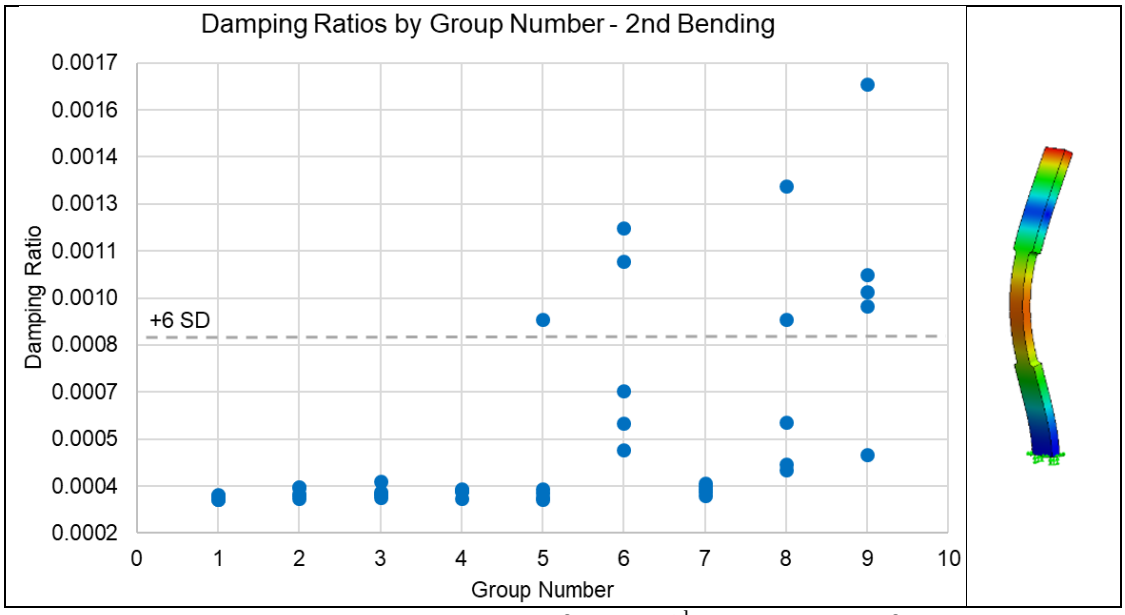

Fig. 47: Damping ratios by group number (left) and 2nd bending mode from FEA (right)

The damping ratios for the third x-bending mode are shown in (Fig. 48). The higher damping values on the edge bars are displayed in this mode for the nominal build. The edges of the plate appear to have the highest damping values followed by lower damping values from one side to the other. The build with defects did not appear to follow this trend. The defective build probably did not follow this trend due to the presence of defects also affecting the damping values. Oddly, the nominal build has a larger variation in damping ratios than the defect build. The presence of defects should cause the defect build to have higher variation.

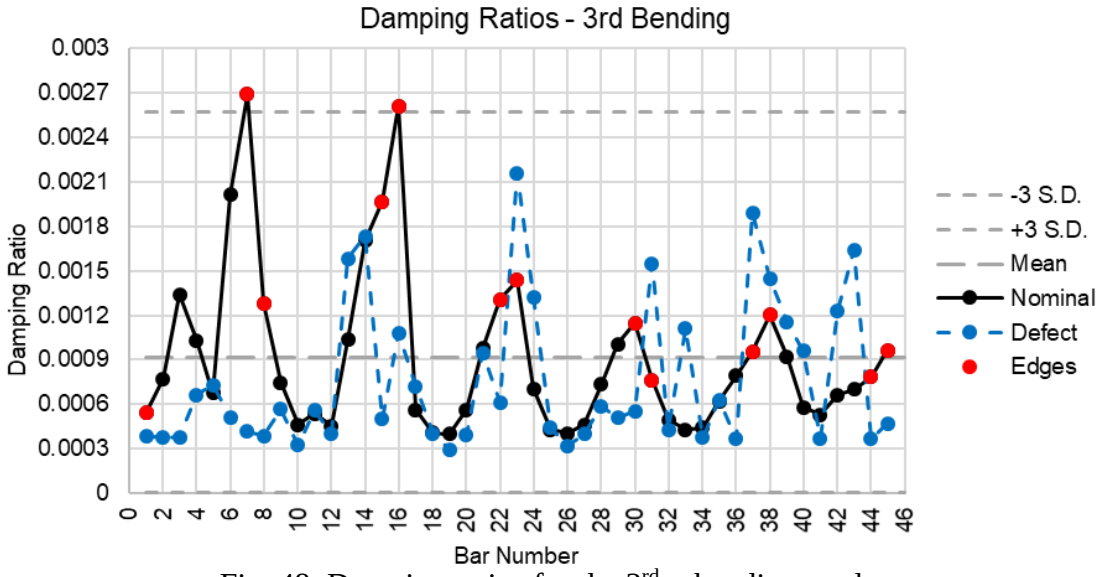

Fig. 48: Damping ratios for the 3rd x-bending mode

The damping ratios for the fourth bending mode display a similar trend to the third x-bending mode (Fig. 49). Higher damping values appear on the nominal build for the bars on the right and left sides of the plate. Unlike the third x-bending mode, both the defect and nominal build are within three standard deviations.

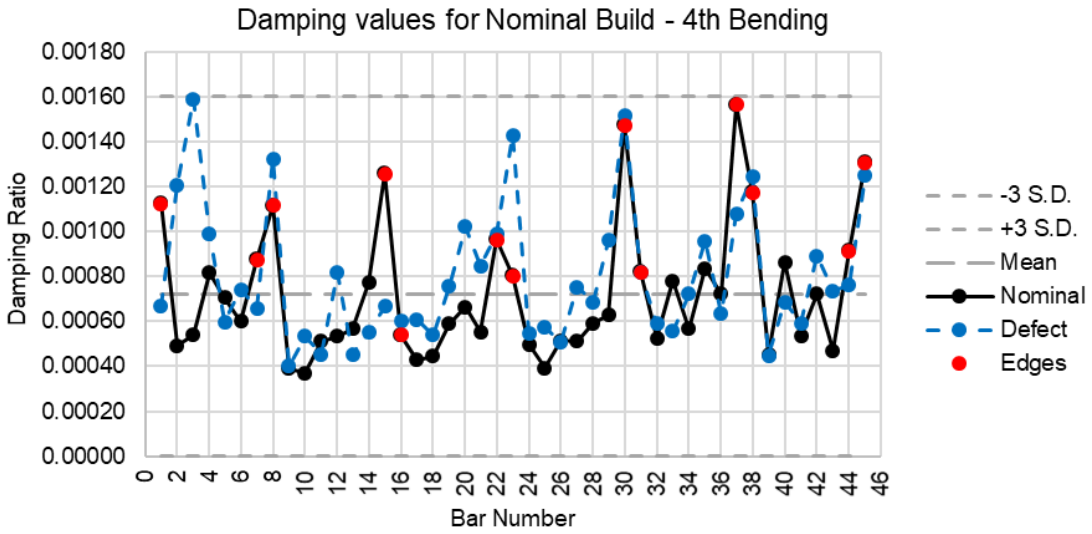

Fig. 49: Damping ratios for the fourth x-bending mode

Comparing the damping values to the results from natural frequency versus bar number, the trend is the same. Larger damping ratios on the edge bars appear to be associated with lower natural frequencies. Further following this trend, the bars in the middle of the plate have the smallest damping values. Overall, the damping ratios support the theory that the cover gas flow in the chamber is affecting the material properties more than the defects themselves.

3.1.6 Acoustic Testing

The acoustic testing between the speaker signal and SLDV response was aimed at exciting the axial mode after shaker, impact, and the statistical analysis failed to distinguish the defect groups. The first axial mode, Mode 9, was chosen for testing based on the FEA results. The axial mode has the highest likelihood of determining the defect, since this mode stresses the defect the most in relation to Modes 1 through 8.

3.1.6.1 Acoustic Test 1

The first acoustic test consisted of testing with one speaker using the acoustic horn. The plate did not receive enough excitation for the laser to pick up the response. Since there was not enough excitation for the first acoustic test, there were no results to display. The results are only displayed for Acoustic Test 2 and Acoustic Test 3.

3.1.6.2 Acoustic Test 2

The results from the second acoustic test with two speakers mounted to the adapter plate provided better excitation than Acoustic Test 1. The excitation was sufficient to measure the bar and base plate responses. The FRF for Bar 27, a bar in the middle of the plate, on the nominal build is shown in (Fig. 50). The FRF does not to appear to have "clean" peaks, making it difficult to detect the axial mode of interest. The frequency at which this mode should appear is shown by a black vertical line in the figure.

Comparing the bar response to the node on the plate, the plate appears to drive the bar response. The two FRFs are nearly identical in shape, except that Bar 27 is higher in amplitude. Therefore, the plate mode is overpowering the response in the bar so that it is indiscernible from the plate response.

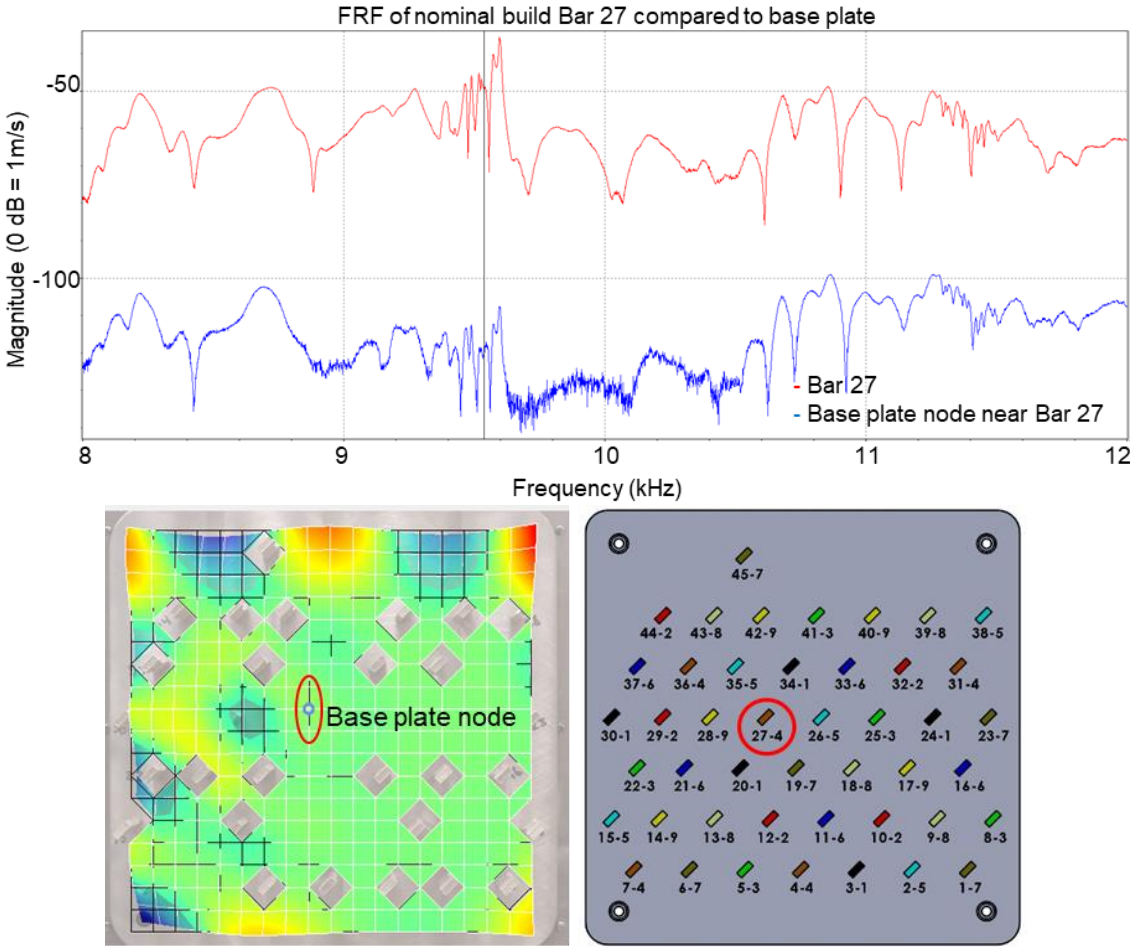

Fig. 50: FRF from nominal build and base plate (top), base plate node location (bottom left) and bar locations (bottom right)

A similar response occurs on Bar 11 for both the nominal and defect build (Fig. 51). The nominal build's bar and base plate node response are similar to the results from Bar 27.

The base plate appears to be driving the response in this bar as well. Interestingly, the defect build displays a peak at the axial mode, while the nominal build does not show this peak.

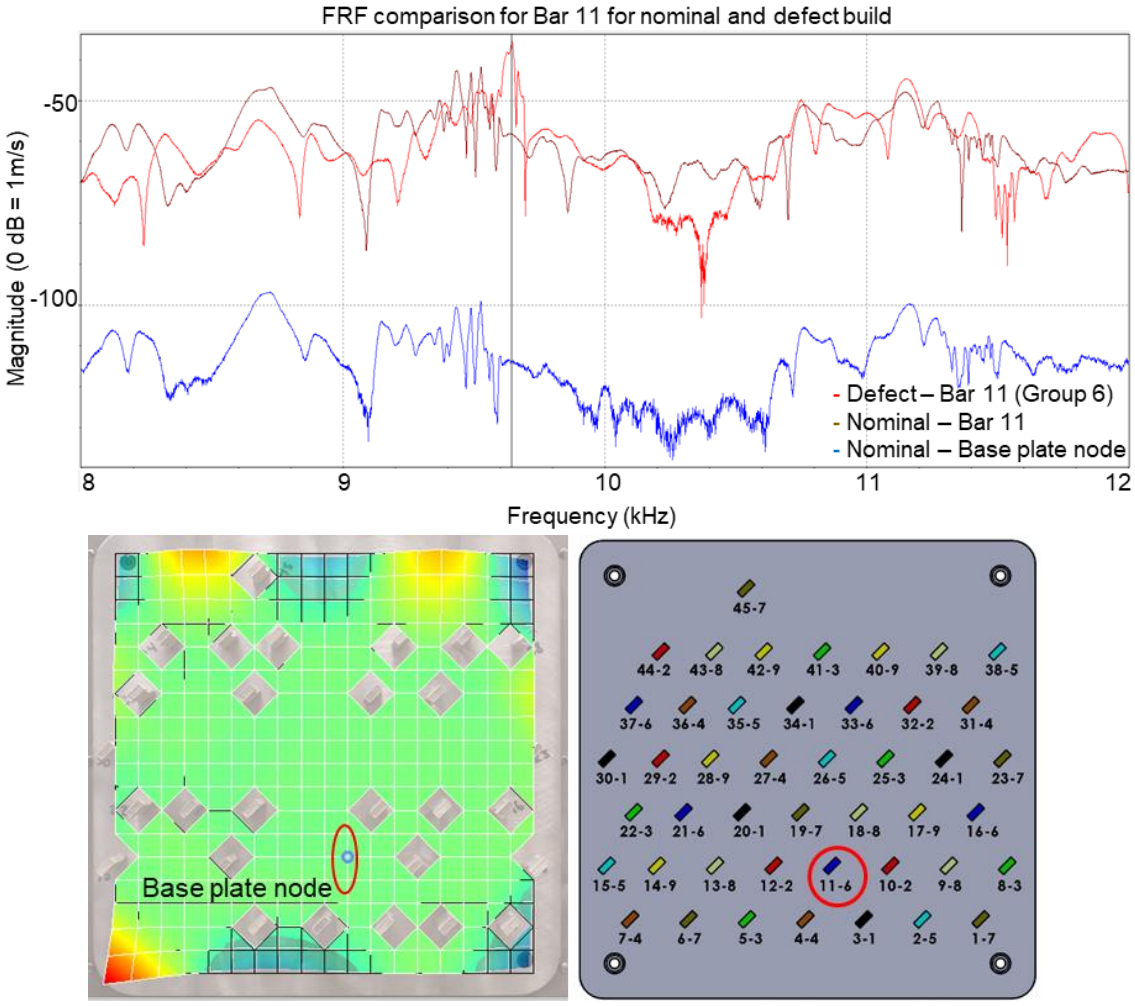

Fig. 51: FRFs from nominal and defect build (top), base plate node location (bottom left) and bar location (bottom right)

Investigating the groups on the defect build, there are no apparent differences between the groups (Fig. 52). Group 1 is nominal, Group 2 has the smallest defect (50 μm), and Group 9 has the largest defect (400 μm). The same span of peaks appears for each of the groups. The span is approximately 9400 to 9700 Hz. The groups do not appear to have any significant shifts as would be expected with different amounts of defect. There also appears to be multiple peaks around the axial mode frequency when there should be one distinct peak. Multiple peaks suggest plate mode interaction with the bar responses similar to what was seen on the nominal build.

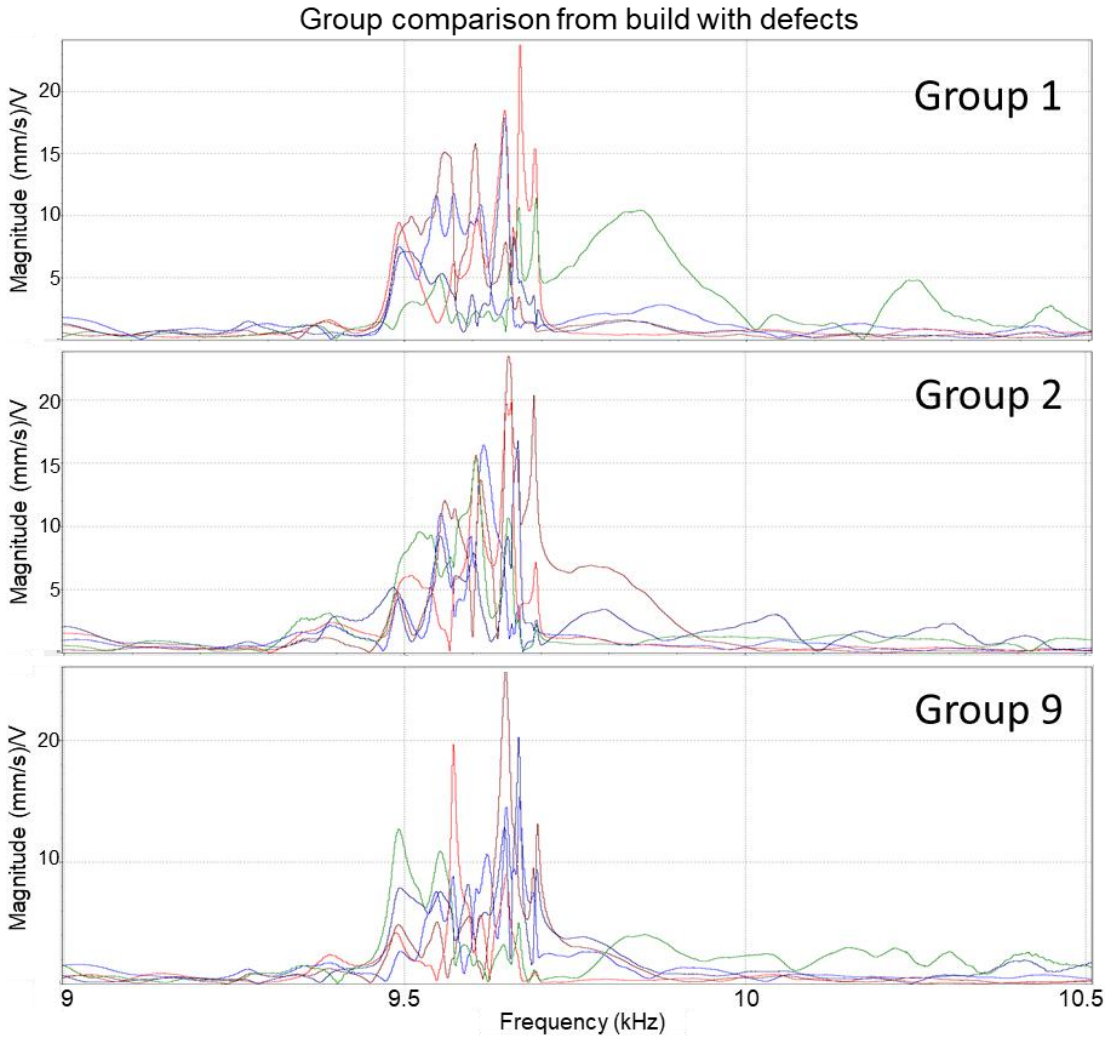

Fig. 52: FRFs for the defect build results for Groups 1, 2, & 9

Summarizing Acoustic Test 2, three results appeared. The first result is the plate modes drove the bar response. The second result is the FRFs did not have distinct peaks near the axial mode of frequency making it difficult to identify an individual mode. The third result is the defect build did not have any distinct shifts in frequency suggesting that the defects are still not being detected. The third acoustic test aims at reducing the plate mode response so the bar natural frequencies can be determined without build plate interaction.

3.1.6.3 Acoustic Test 3

The third acoustic test used the same adapter plate with two speakers as the second acoustic test, but the build was rotated from vertical to horizontal. Additionally, sand at 0.5-inches and 1.5-inches was added to the plate in an attempt to reduce the base plate modes.

The addition of sand reduced in amplitude some of the plate modes, but did not improve the quality of the FRFs. The FRFs continued to display indistinct peaks with some of the bars not displaying the 9755 Hz mode.

The response for all three testing conditions for Bar 1 (located at the bottom right edge of the plate) is shown in (Fig. 53). The sine sweep was from approximately 1000 to 12800 Hz. There are differences in amplitude on the FRF for the three testing conditions. As expected, the curve with no sand is largest in amplitude and the curve with 1.5-inches of sand is smallest in amplitude. The 9755 Hz axial mode is not immediately apparent while viewing the whole spectrum.

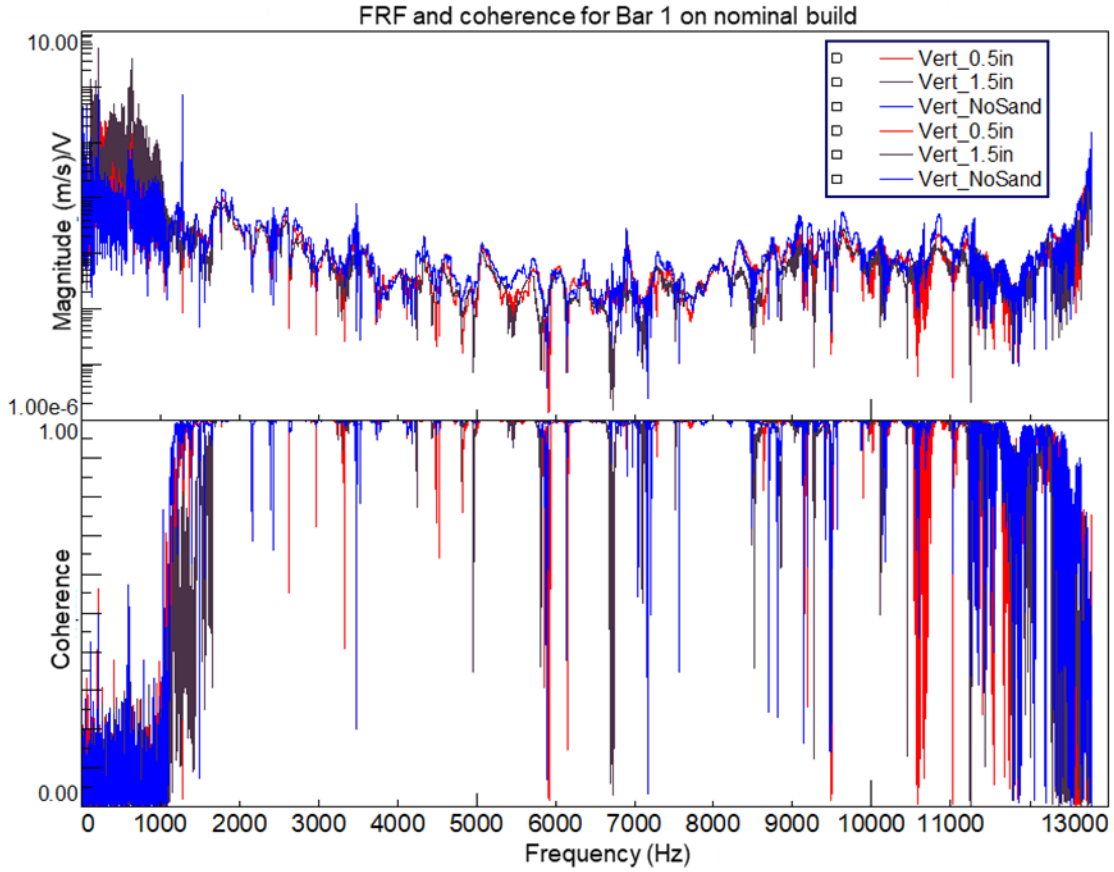

Fig. 53: FRF and coherence for nominal build Bar 1 from acoustic testing

Targeting the FRF and coherence between 8500 and 10500 Hz, the axial mode is more apparent for Bar 1 (Fig. 54). The FRF continues not to show a clear peak, but the axial mode could be at 9652 Hz or 9806 Hz. The shape of the FRF changes between no sand and 1.5-inches of sand effectively damping some of the plate mode response.

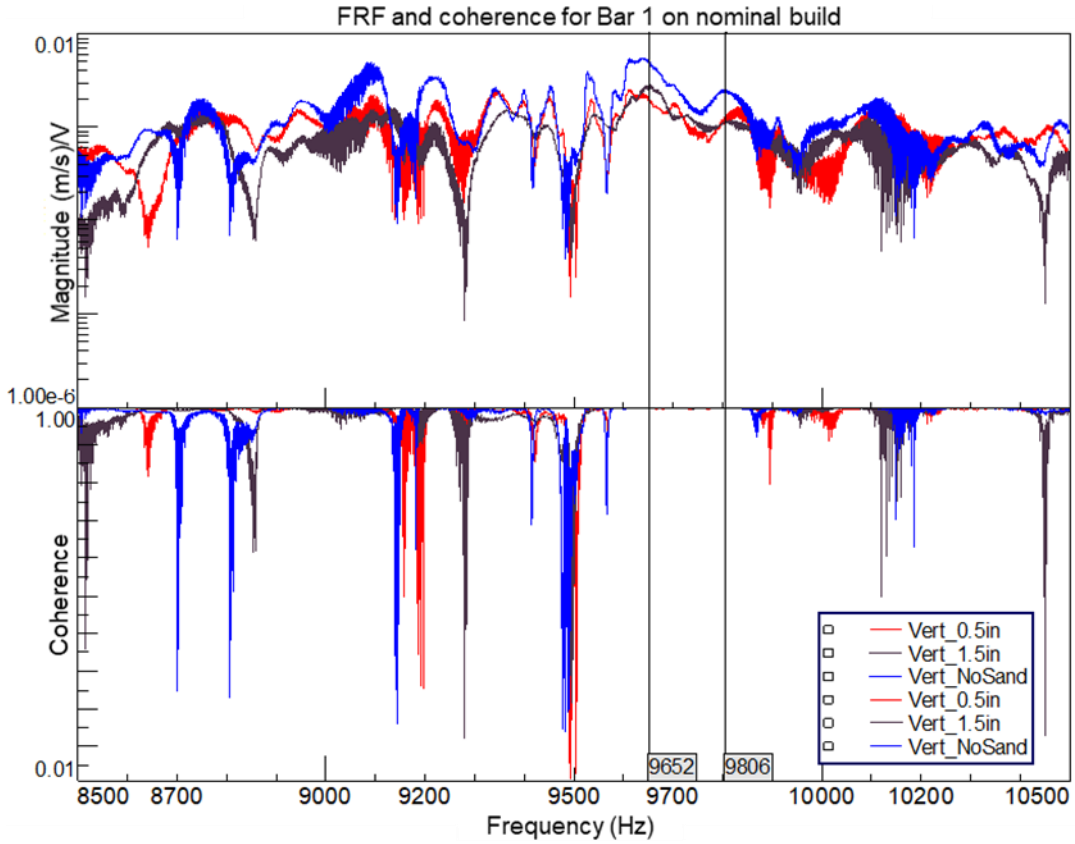

Fig. 54: FRF and coherence for Bar 1 from 8500 to 10500 Hz

Bar 1 may show the axial mode, but that condition does not hold true for all bars on the plate. The FRF for Bar 26, located in the middle of the plate, with no sand, 0.5 inches of sand, and 1.5 inches of sand is shown in (Fig. 55). The axial mode that is at 9,755 Hz does not appear in this FRF. The plate mode(s) near this frequency did not appear to provide excitation to this bar.

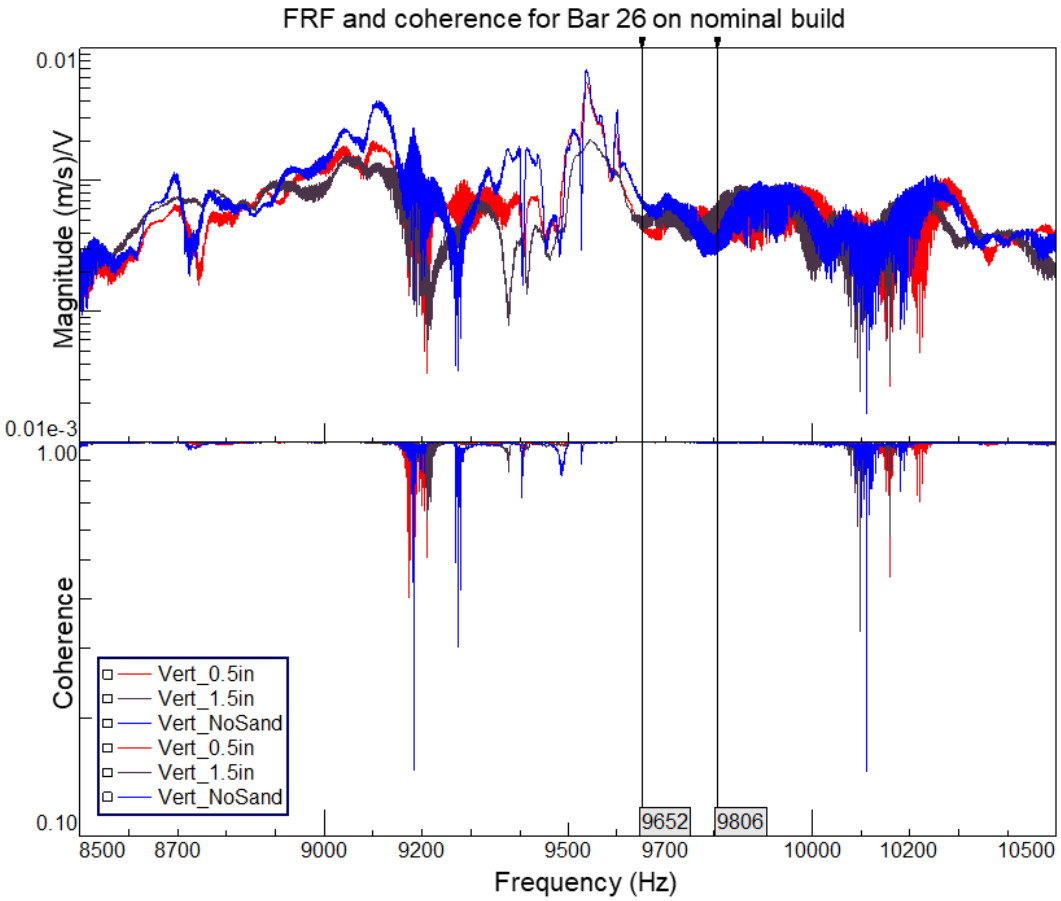

Fig. 55: FRF for Bar 26 on the nominal build with no sand, 0.5 inches of sand, and 1.5 inches of sand

Looking at the plate modes around 9755 Hz, the plate has little or no motion where Bar 26 is located (Fig. 56). This result suggests that the plate modes are affecting which bars receive excitation. Furthermore, the sand helps reduce some of the base plate mode response when a bar is receiving excitation from the plate. If the plate is not providing excitation to the bar, the bar response will not appear. If the bar does not receive excitation, the axial mode will not appear in the response.

Unfortunately, the plate modes caused some of the bars on the nominal plate to not show the axial mode for all bars. Without the axial mode appearing on the nominal plate, there was no reason to test the build with defects.

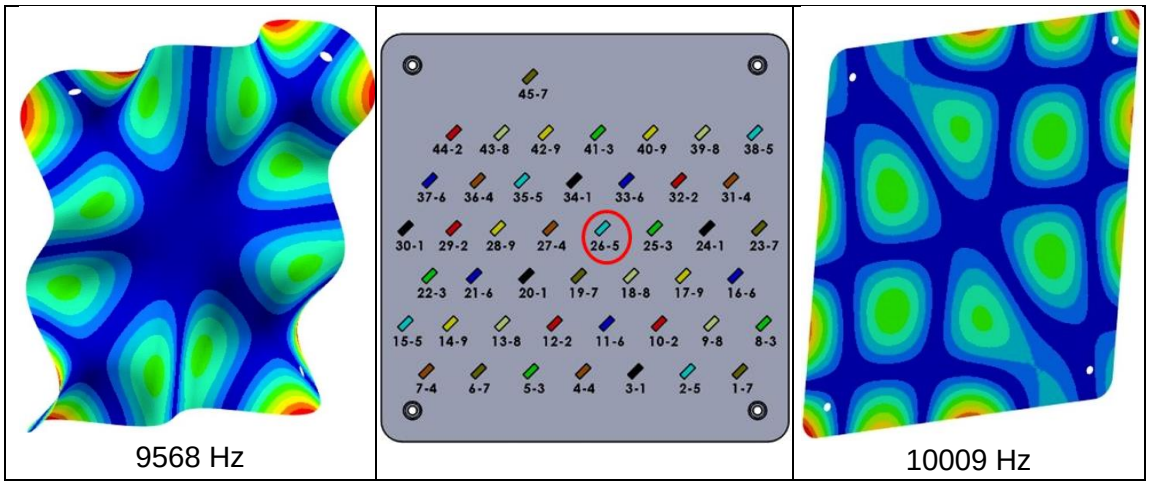

Fig. 56: Base plate mode at 9568 Hz (left), Bar 26 marked in red (middle), base plate mode at 10009 Hz (right)

3.1.6.4 Testing Issues

A signal problem arose under the third acoustic test. The problem was associated with three blown speaker diaphragms. Valuable testing time and additional cost was required to replace the diaphragms. The blown diaphragms were attributed to not using an amplitude ramp in the signal when starting and stopping. The signal with and without an amplitude ramp is shown in (Fig. 57). The speakers had an audible "popping" noise when starting and stopping without the amplitude ramp. The stereo speakers could not handle the jump in voltage which caused the speaker diaphragms to stop working. Future testing should use caution when using this type of excitation and use an amplitude ramp to eliminate the possibility of damaging equipment.

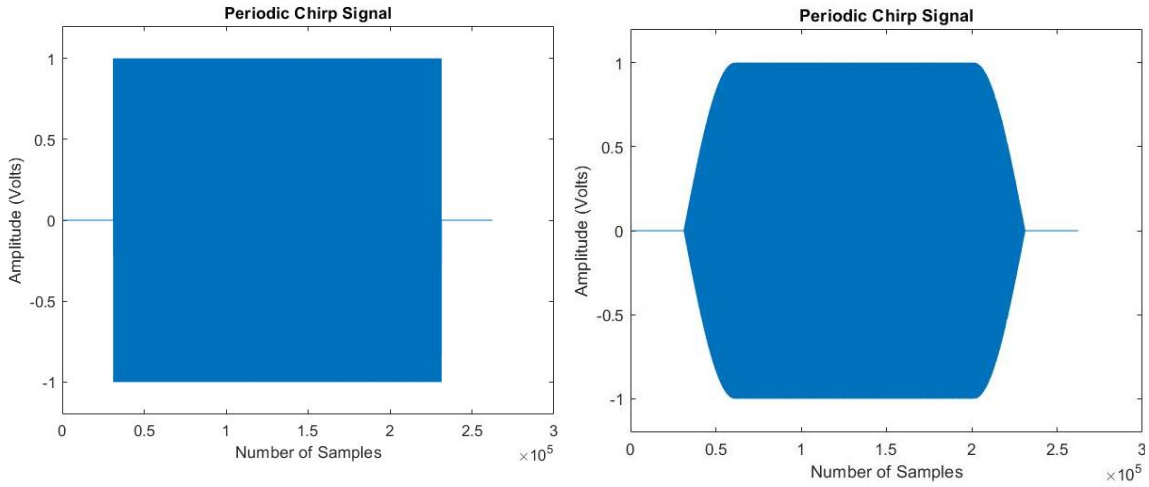

Fig. 57: Signal to speakers without amplitude ramp (left) and with amplitude ramp (right)

3.1.7 Piezoelectric Excitation

The PZT testing was performed to investigate if the plate could be excited in a better way than the acoustic tests to determine the axial mode. A PZT patch sent a periodic chirp signal from 5000 to 12800 Hz into the plate. The plate rested on a piece of foam with PZT superglued at the bottom of the plate (Fig. 58). The bars tested were selected from where the base plate shows excitation around 9755 Hz. Two lasers were used to measure the reference and response for this testing since, accelerometers would be difficult to attach between the bars.

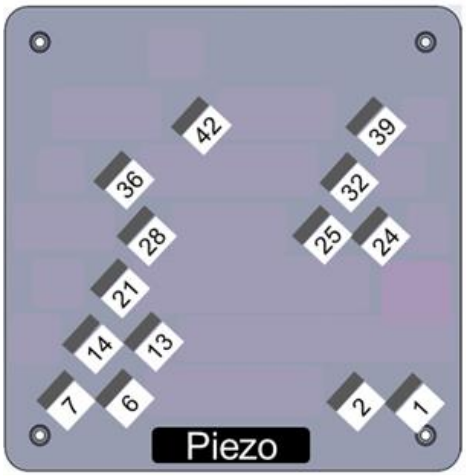

Fig. 58: Bars tested and piezo location on forest tensile build

The PZT excitation performed with the Leipei® amplifier did not provide improved results over the acoustic testing. The FRF and coherence for the bars tested are shown in (Fig. 59). The FRFs continue to appear noisy and there are large drops in coherence throughout the signal.

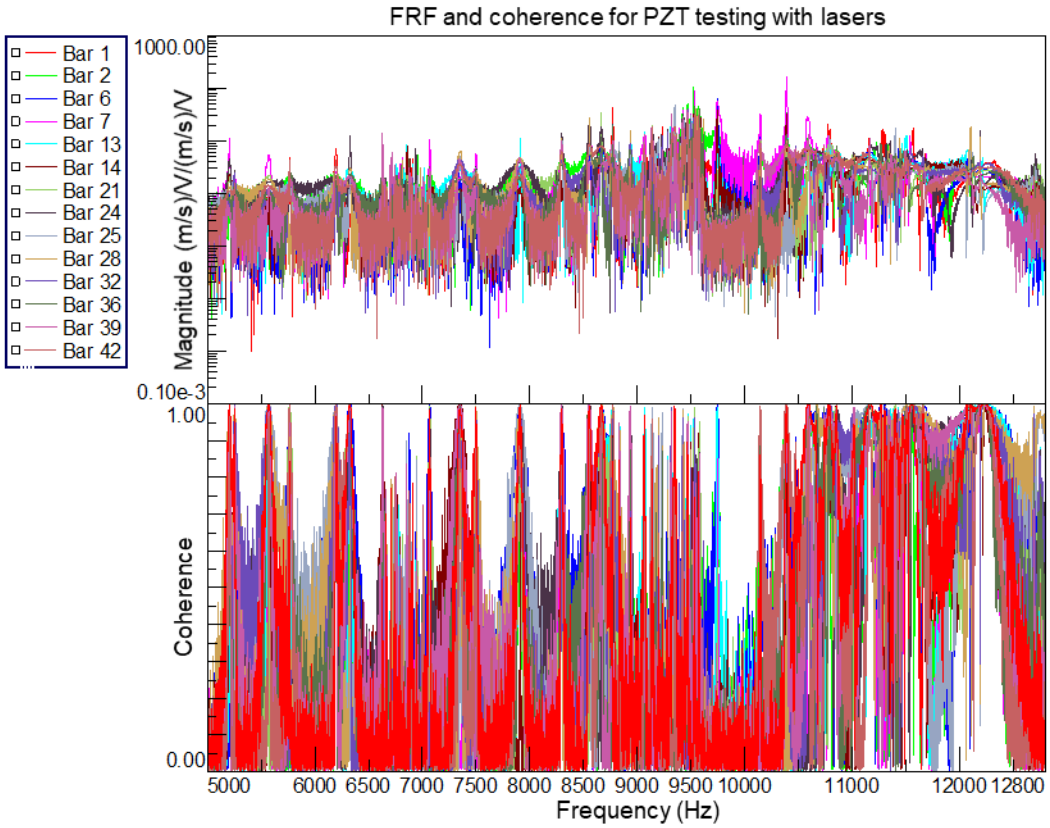

Fig. 59: FRF and coherence for PZT testing with Leipei® amplifier

Focusing the FRF from 9600 to 9900 Hz, the FRF is compared to the response power spectral density (PSD). The PSD shows where the bar is receiving a signal (Fig. 60). The PSD from the bar response was used to show which bars were receiving excitation. Analyzing the test results, only Bars 1, 2, 6, 7, 13, 14, 21, and 28 received excitation at the axial mode. The other bars did not show a peak at the axial mode. There were two hypotheses on why some of the bars were not receiving excitation. The first was that the plate modes could still be affecting the results. The second hypothesis was that the Leipei® stereo amplifier was not providing enough excitation to the plate as both lasers were on their most sensitive settings to record the response.

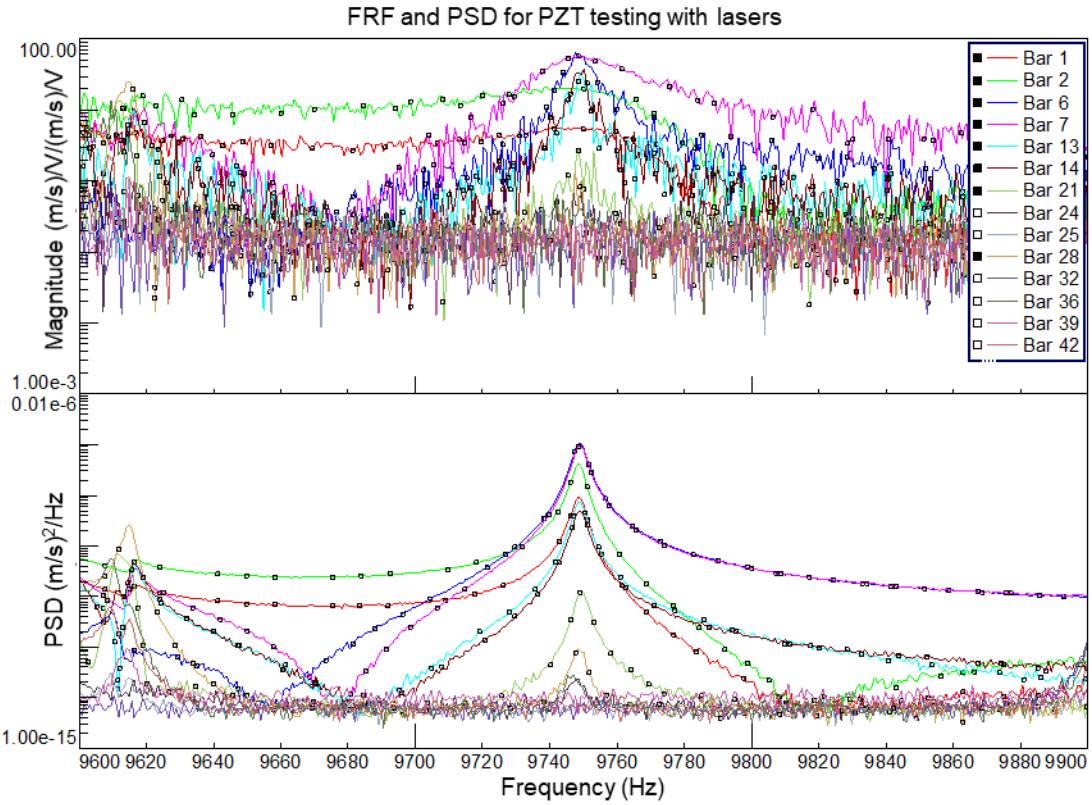

Fig. 60: FRF and PSD for PZT testing with Leipei® amplifier

The PZT amplifier was used to test whether the build was receiving enough excitation. The voltage into the plate was doubled from 5V peak to 10V peak for this testing. The other test parameters stayed the same as the previous test. Unfortunately, the Trek® amplifier yielded similar results to the Leipei® amplifier. The FRFs with the new amplifier gave similar curves except higher in amplitude (Fig. 61). The higher amplitude was expected since the signal is stronger to the plate. There did not appear to be any noticeable changes in the coherence.

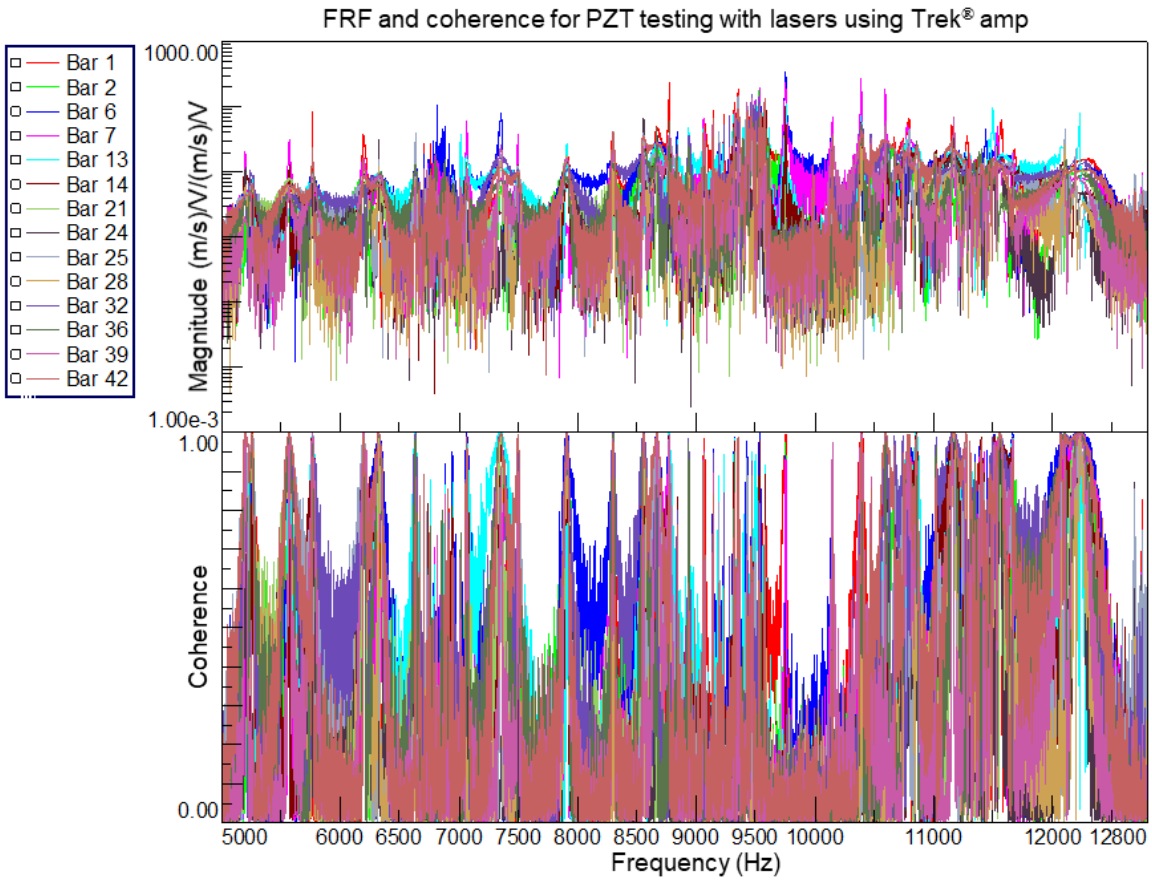

Fig. 61: FRF and coherence for PZT testing with Trek® amplifier

Comparing the FRF and PSDs for this test, the bars that received excitation were the same as the other amplifier with the exception of Bar 28. The FRF and PSD from 9600 to 9900 Hz are shown in (Fig. 62). The noise floor for the PSD appears to be higher for this testing in relation to the peak value than previous testing – indicating a difference between the two amplifiers.

Overall, this testing provided similar results to the acoustic testing. The axial mode of interest did not appear in all bars, suggesting that the plate modes are still affecting the results.

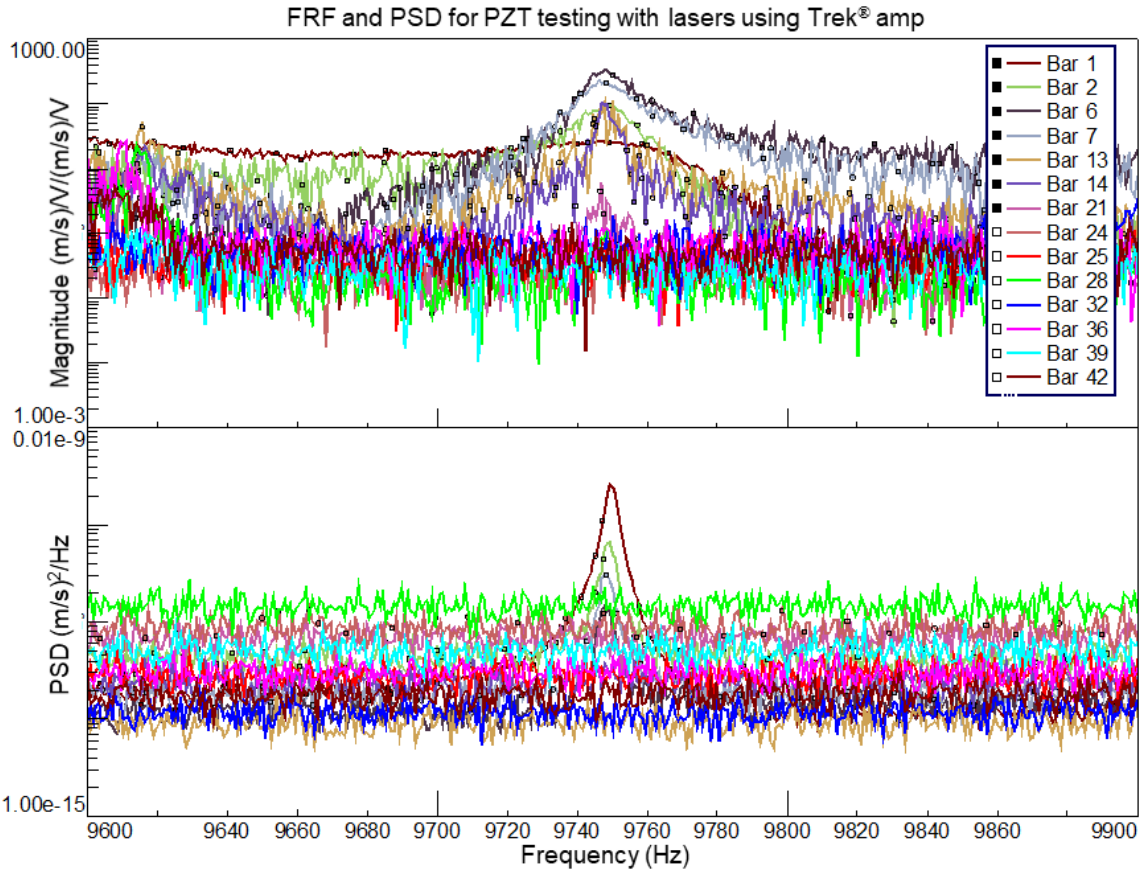

Fig. 62: FRF and PSD for PZT testing using the Trek amplifier

The results from the four tests performed on these builds propose that dynamic testing may be used as an indicator for build variation, but may not be sensitive enough to determine the defect groups in these bars. The build variation caused the bar location on the plate to have more of an effect on the results than the defects in the bars. Additionally, exciting the parts through the plate was not as effective, due to the presence of plate modes, as exciting each part individually.

3.2 Topology Optimized Brackets

3.2.1 Summary of Topology Optimized Brackets Results

The topology optimized brackets were tested two different ways. The impact testing performed on these parts did not provide enough dynamic range to determine the natural frequencies of the brackets. Providing higher frequencies than can be obtained with an impact hammer involved a new experimental test. The second test involved exciting the parts with a BB-gun to obtain the natural frequencies in these parts.

The BB-gun testing results obtained the natural frequencies and they were compared to FEA. The build plate was also tested fixed to how it affected the response. The bracket

modes moved up in frequency when fixed to the aluminum adapter plate. The results suggest this method has potential as a dynamic testing method, but would need to be refined for controlling/measuring the velocity of the BB.

3.2.2 Impact Testing

Impacting the ears of the brackets did not provide enough excitation for the natural frequencies of the brackets to be measured. The FRF and coherence for the larger impact hammer (PCB Model: 086C04) are shown in (Fig. 63). The coherence starts to drop off near where the first mode in FEA appears at 5536 Hz. Since the desired frequency was not achieved, the proposed testing points were not able to be tested.

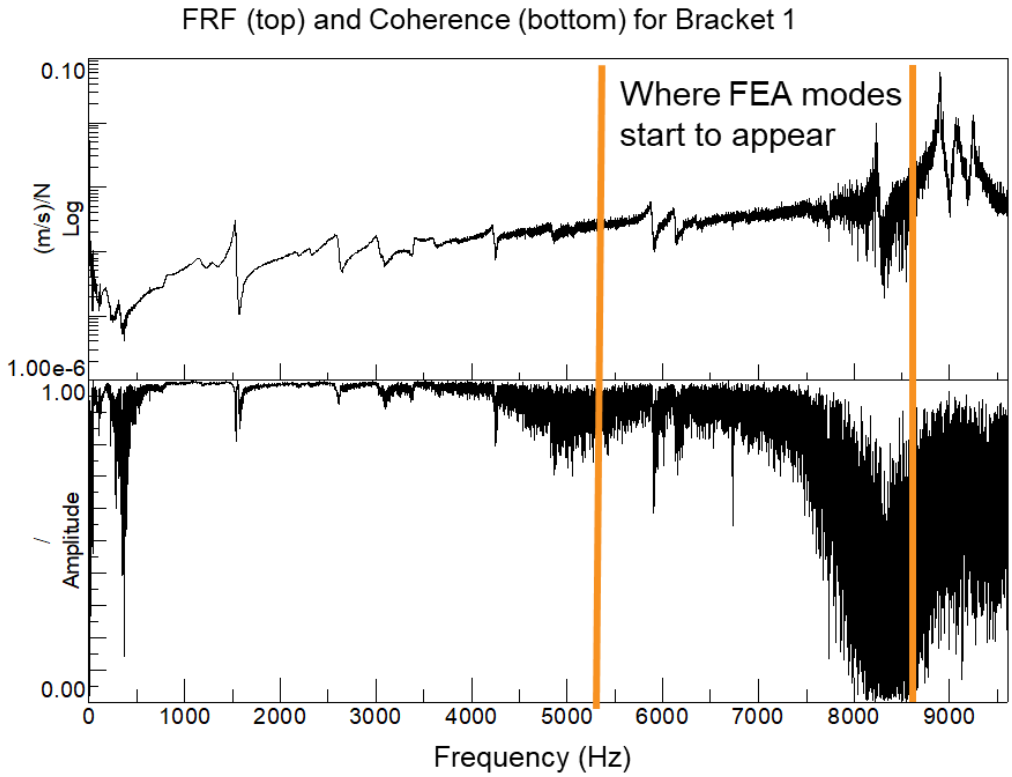

Fig. 63: FRF and coherence for Bracket 1 from impact testing

Since the highest mode is at 8324 Hz, the shaker testing would not provide all the frequencies of interest and was not performed on these parts. The Dongling shaker at MTU cannot reach this frequency and the build plate is too large (~20 lb.) to be tested on the smaller shakers. A creative way to excite the parts, involving the use of a BB-gun emerged after analyzing the impact results.

3.2.3 BB-gun Testing

The first testing performed on the brackets involved placing the build plate on a piece of foam inside a covered testing chamber. The testing chamber had holes for the microphone and BB-gun to impact the parts.

The first test overloaded the microphone measuring the response. The microphone could measure the response if the BB-gun was dry-fired outside of the chamber, but firing into the testing chamber caused the microphone to overload. A muffler adaptation on the BB-gun was proposed to reduce how much sound was transferred into the testing chamber. If the sound inside the testing chamber could be reduced, the microphone should be able to measure the response of the parts.

The addition of the muffler dropped the overall sound pressure level (SPL) in the chamber by approximately 16 dB (Fig. 64). A difference of ±6 dB is twice as loud or twice as soft. A person would perceive the difference in the test chamber as somewhere between a fourth to an eighth as loud as the testing without the muffler. This reduction in SPL caused the microphone to stop overloading so the response from the parts could be measured.

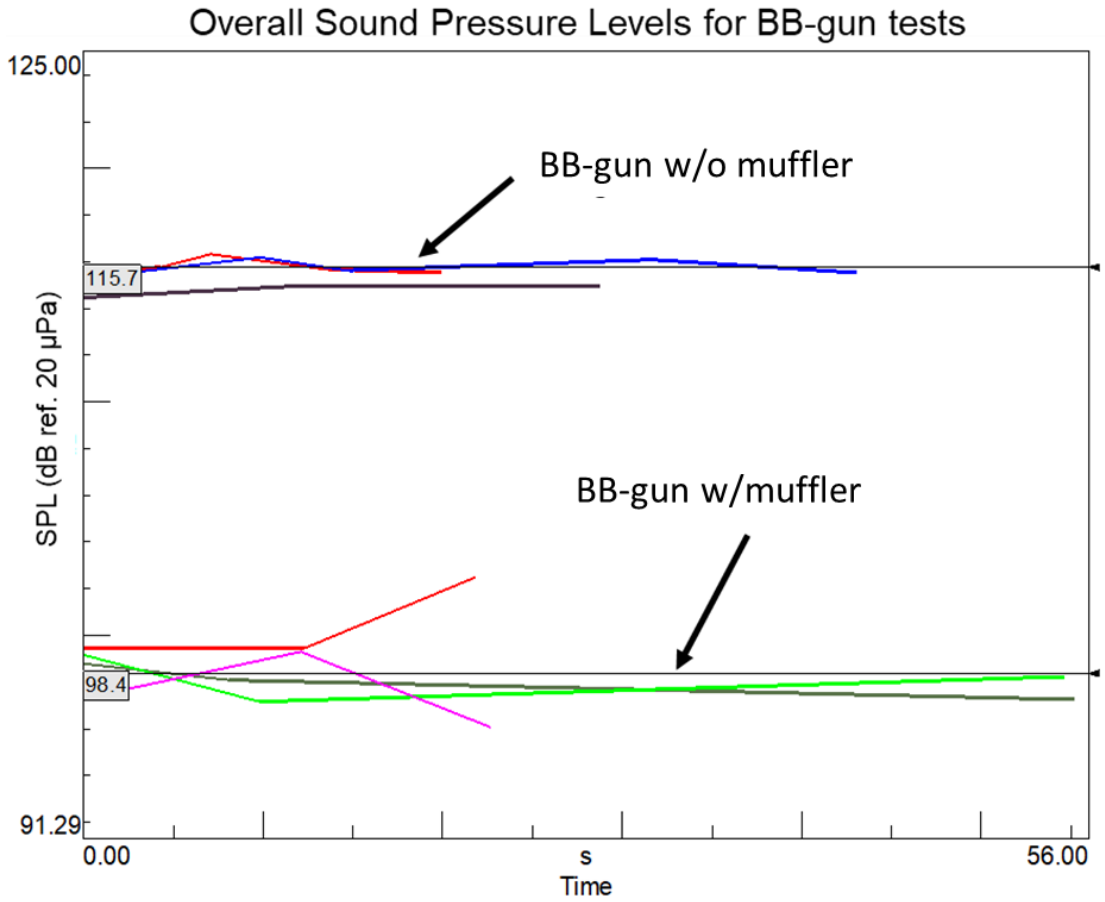

Fig. 64: Overall sound pressure levels for BB-gun testing with and without the muffler

The testing with the BB-gun extended the frequency range that was observed in impact testing from 5000 Hz to 10240 Hz (Fig. 65). As an excitation method, testing with a BB-gun could extend above 10240 Hz. Higher frequencies were not investigated in these parts since the highest FEA mode was at 8324 Hz.

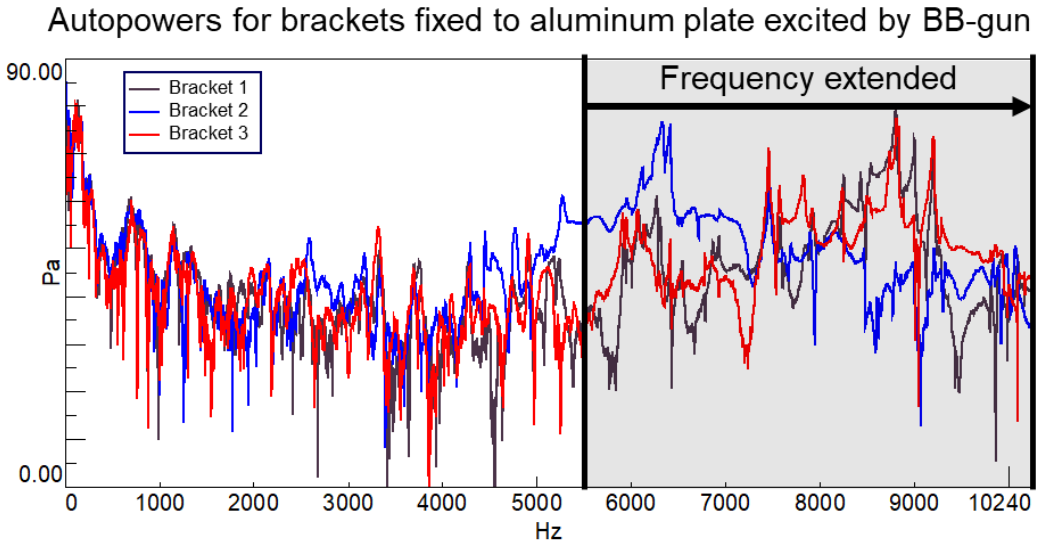

Fig. 65: Frequency range extended by using BB-gun to test brackets

The autopowers were able to be measured from this testing. The natural frequencies of the parts were obtained and are marked by black vertical lines in (Fig. 66). Tests performed on all three brackets are displayed.

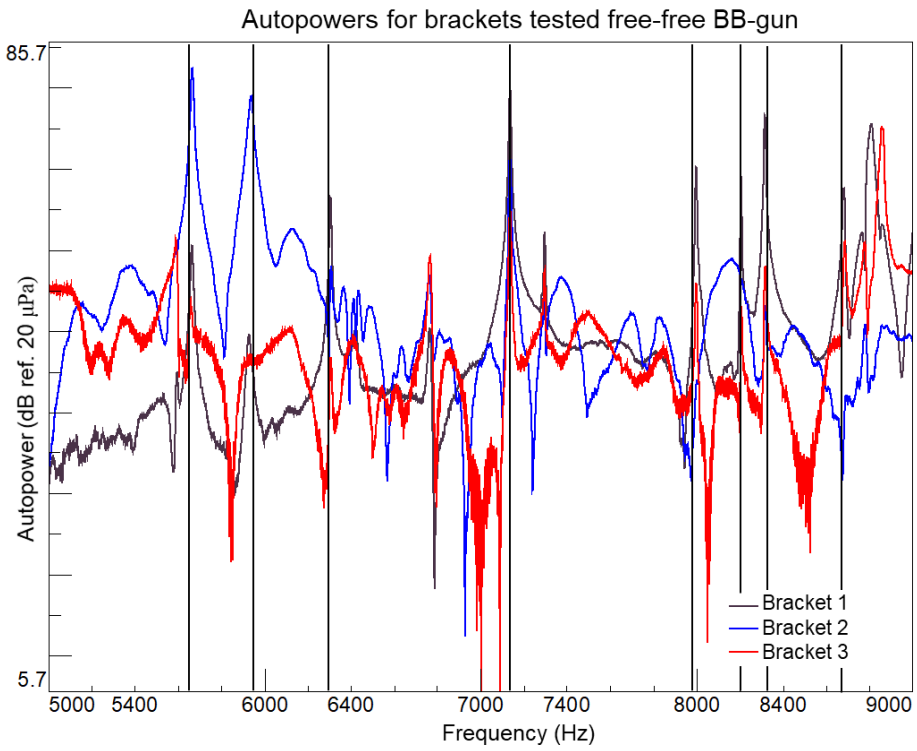

Fig. 66: Autopowers for brackets tested free with natural frequencies marked

Tabulating the natural frequencies obtained from experimental testing, the results were compared to FEA (Table 6). Since the FEA was modeled without the support material, there was some difference when compared to the experimental results. The largest difference is less than 4.5% for all modes. Without the support material being modeled, a 4.5% difference between the modes is considered acceptable.

Table 6: BB-gun natural frequencies compared to FEA

Mode No.	FEA (Hz)	BB-Gun Modes (Hz)	Difference (%)
1	5536	5663	2.29
2	5716	5913	3.45
3	6545	6303	3.70
4	7272	7135	1.88
5	7846	7995	1.90
6	8082	8204	1.51
7	8174	8313	1.70
8	8324	8680	4.28

The brackets tested fixed to the aluminum adapter plate display an upward shift in the natural frequencies found from free testing (Fig. 67). The natural frequencies should increase if the plate is fixed, since an increase in stiffness increases the natural frequency of a part. The FRF has more peaks than the first test, making some natural frequencies

difficult to determine. Mode 4 is shown by black lines in the figure. This mode shifted up in frequency from 7135 to 7451 Hz or approximately 320 Hz. Interestingly, both of the free and fixed tests at Mode 4 show all three brackets being excited. According to the FEA, only Bracket 1 should be excited at this frequency. This may indicate the presence of a plate mode instead of a bracket mode.

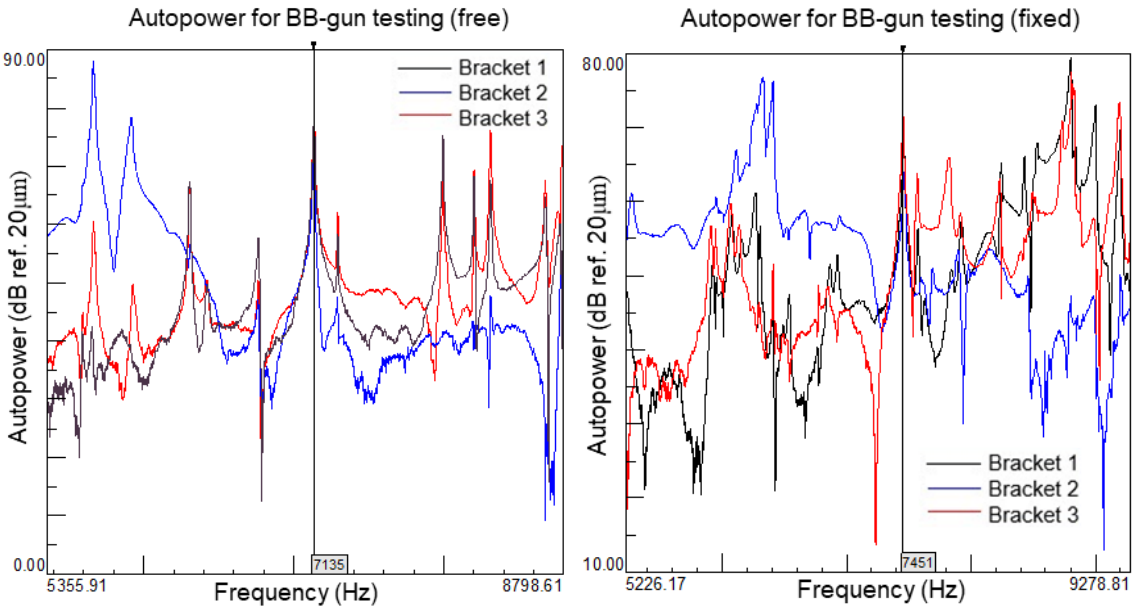

Fig. 67: BB-gun testing free (left) and fixed (right)

Overall, the fixed testing shifted the natural frequencies found in the free testing higher and indicated the presence of a plate mode. Using a BB-gun was successful in obtaining the natural frequencies of these parts. As a testing technique, exciting parts with a BB-gun is a viable option for obtaining natural frequencies above the dynamic range of the impact hammer(s).

3.2.4 Testing Considerations

The BB-gun testing was sufficient for determining the natural frequencies on the topology optimized build. This testing technique would need refinement before using in an industry setting. There currently is no way to measure coherence or the velocity at which the BB leaves the BB-gun. Implementing light sensors or imaging equipment that could detect how fast the BB leaves the gun could be used to measure the velocity/coherence.

The BB-gun testing technique was destructive as there was some damage to the parts (Fig. 68). The use of a regulated air supply such as an air hose instead of the CO_2 cartridges could reduce the damage to the parts.

Fig. 68: Damage to parts from BB-gun testing

3.3 Airbus Builds

3.3.1 Summary of Airbus Build Results

The Airbus builds were tested four different ways: shaker testing and impact tested semi-fixed, fixed, and free.

The shaker testing performed on these parts obtained the mode shapes to compare to FEA. The mode shapes were similar in shape and natural frequency. Modes 8-11 could not be found with this technique since their frequencies were above the maximum the shaker can provide. Impact testing was suggested to find these natural frequencies.

The impact testing on these builds had mixed results. The semi-fixed boundary condition had low confidence in the accuracy of the results since the results were not repeatable. The fixed boundary condition was better than the semi-fixed condition, but the FRFs still showed noise. The free testing gave the best results as the FRFs had distinct peaks.

Statistical analysis was performed on both the fixed and free testing results. The fixed results were only performed on the first five builds. All seven builds were used in the statistical analysis for the free testing.

After experimental testing was completed on these parts, they were tensile tested at MS&T. The tensile testing results indicated a porous layer defect in Build 7 that was not initially found in the experimental testing. The experimental results were re-evaluated to see if there were differences in this build. There were two differences appearing in Mode 6 and Mode 11.

Additionally, FRAC was performed on the FRFs from impact testing with the free boundary condition. The results from FRAC were not sensitive to the defect found in Build 7. The correlation values were high between this build and the rest of the builds.

3.3.2 Shaker Testing

The mode shapes acquired from shaker testing are comparable to FEA. The first three mode shapes from shaking in both the 90º and 45º directions compared to FEA are shown in (Fig. 69). The red areas from the shaker testing are locations that have the most motion while the green areas have the least motion.

The largest differences between the modes from shaker testing and FEA are in the first mode. The first mode from shaker testing is 6.5% higher in frequency than the FEA. The first mode being so much higher is interesting.

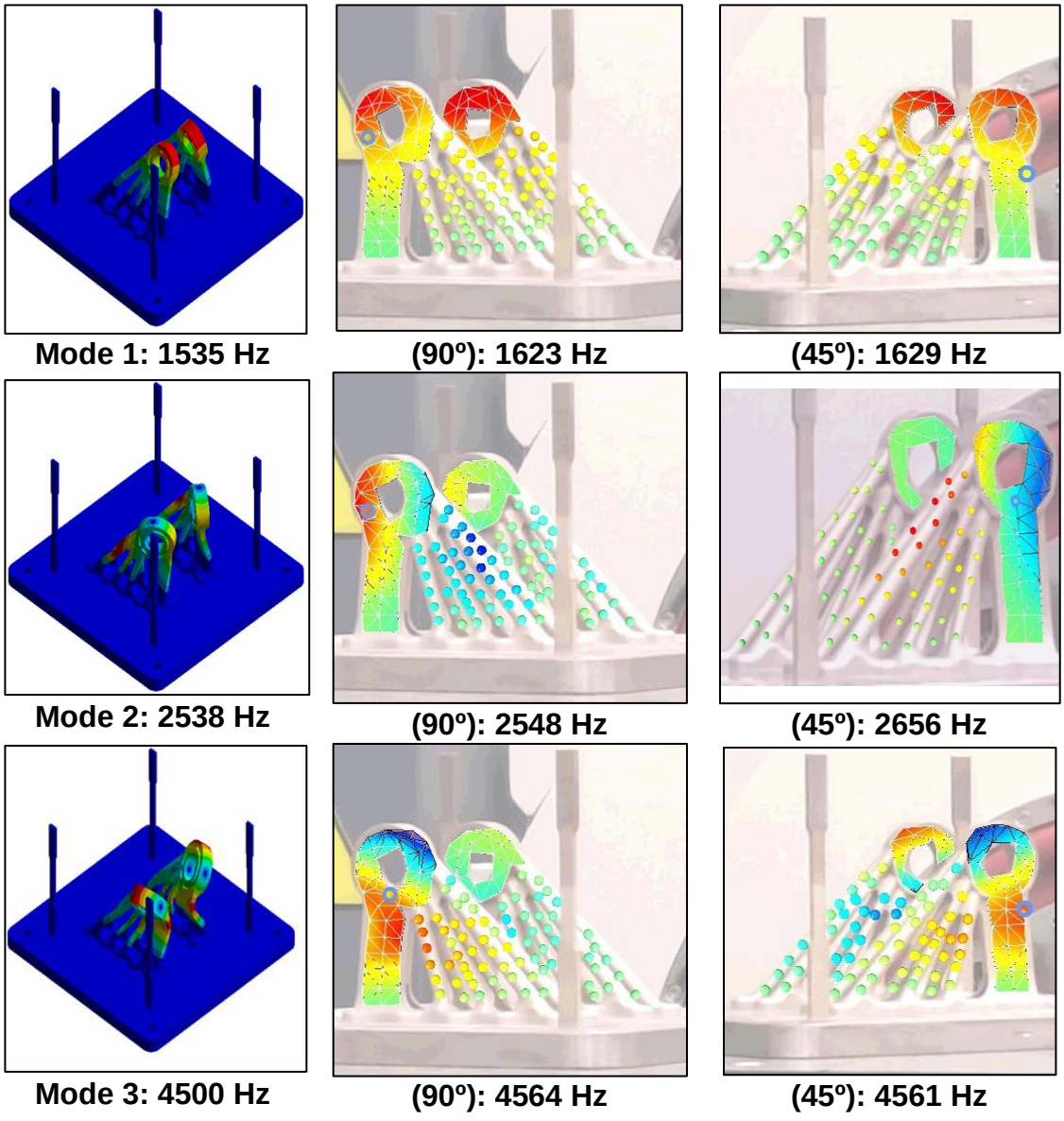

Fig. 69: Modes 1-4 from FEA (left) and shaker testing at 90º (middle) and 45º (right)

In addition to the first three modes, Modes 4, 6, and 7 were acquired from shaker testing the Airbus brackets. Mode 5 is a torsional mode, so it did not appear as a mode shape in the shaker results. The modes shapes for Modes 6 and 7 are shown in (Fig. 70). The motion for these modes is in the legs of the parts for both FEA and shaker testing.

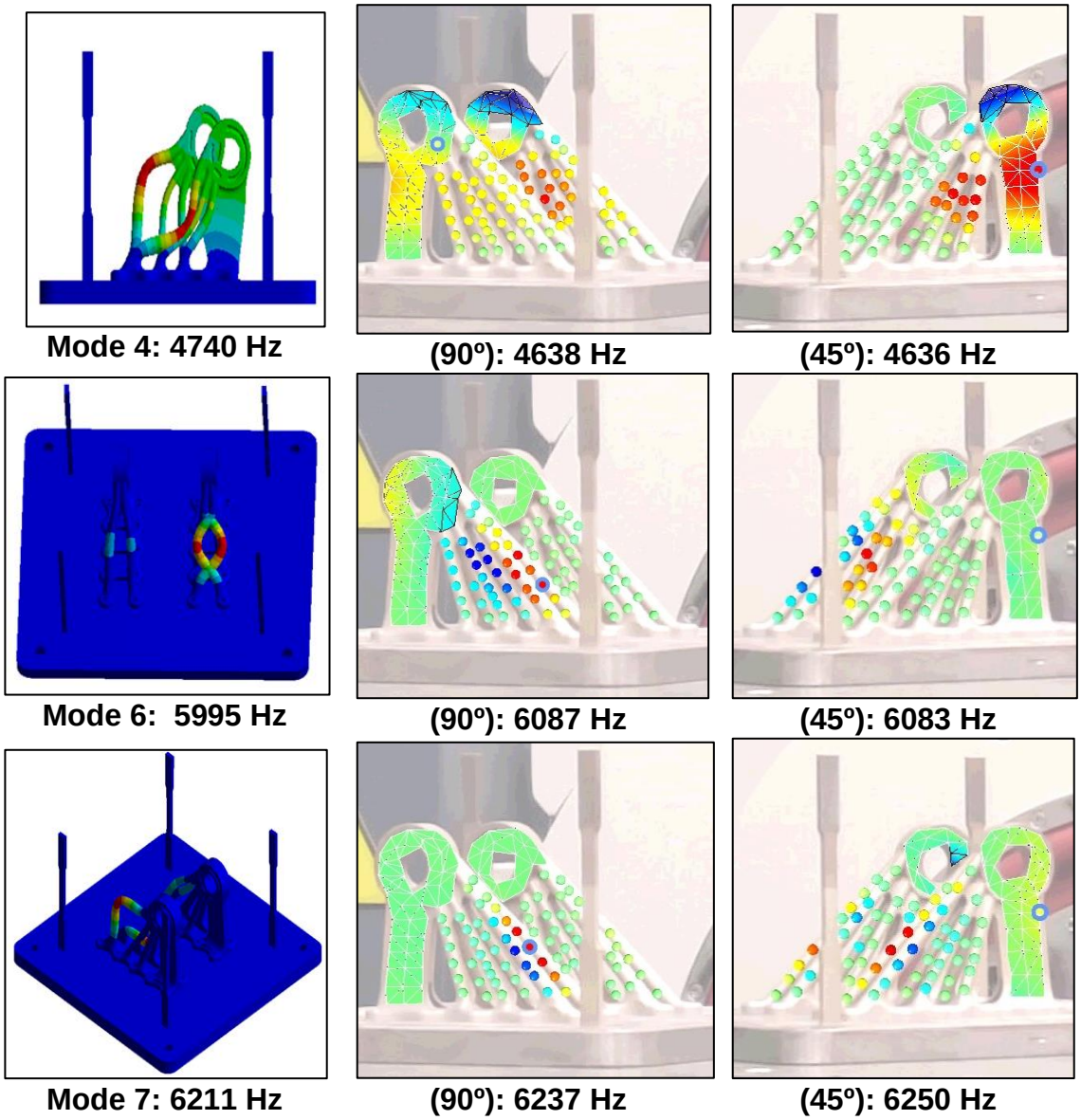

Fig. 70: Modes 6-7 from FEA (left) and shaker testing at 90º (middle) and 45º (right)

Shaker testing acquired Modes 1, 2, 3, 4, 6, and 7. Besides the frequency of Mode 1 being higher, the rest of the modes were comparable in shape and natural frequency to FEA. Impact testing the parts was performed, since the large shaker does not reach high enough in frequency for Modes 8-11 to be acquired.

3.3.3 Impact Testing

3.3.3.1 Semi-fixed boundary condition

The semi-fixed boundary condition consisted of the build plate attached to the adapter plate placed on a table. The SLDV recorded the response for all the points tested. This boundary condition gave the least consistent results out of the three boundary conditions.

The FRF and coherence for the first five points on Bracket 2 are shown in (Fig. 71). The FRFs have differences in amplitudes for some modes (marked on the figure). There appears to be some noise or unaccounted input in Point 1 of Build 1 between the second and third natural frequency as the coherence drops and the FRF changes. The difference in FRF shapes occurs in the outermost legs at high frequency. Compared with the FEA, only the legs were excited at the higher modes, which explains why Points 4 and 5 are different.

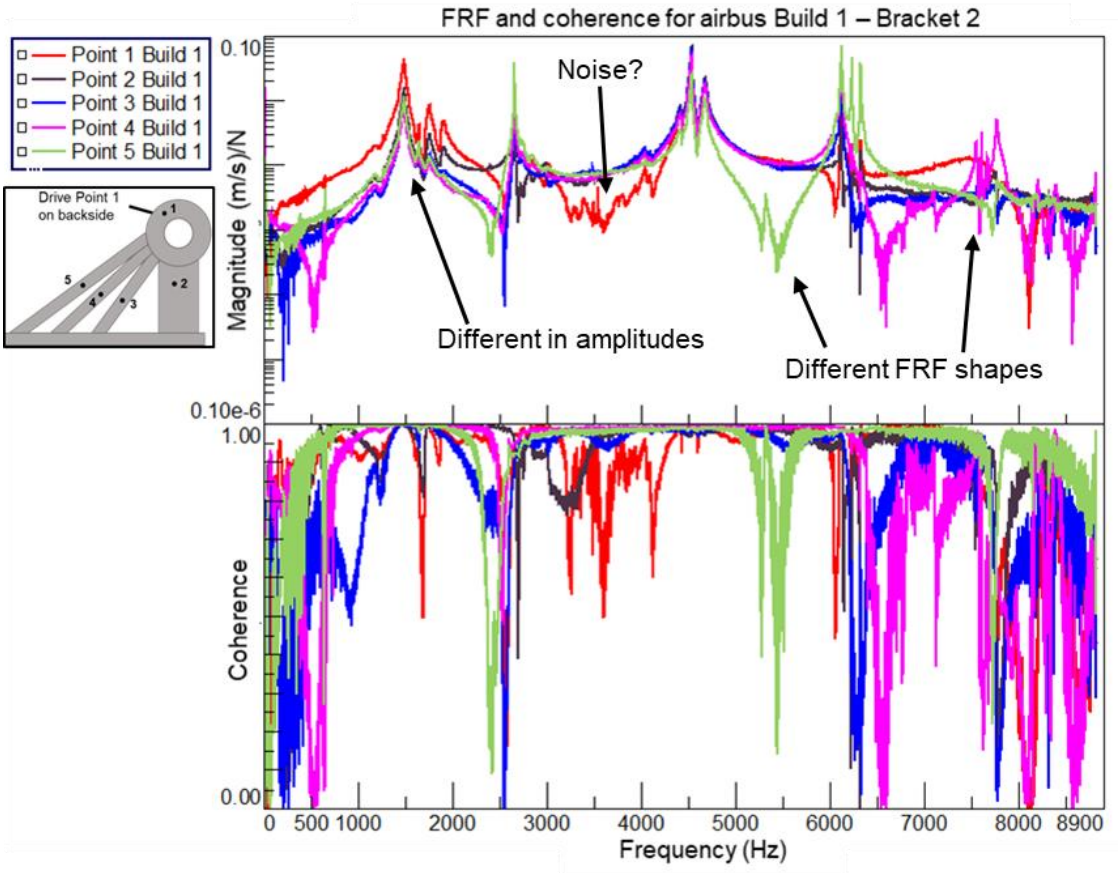

Fig. 71: FRF and coherence for Airbus Build 1 – Bracket 2

The FRF and coherence for Bracket 1 on Build 1 are displayed in (Fig. 72). The results are the same as Bracket 2 when comparing similar locations. The same areas that were marked for Bracket 2 were marked for Bracket 1. Overall, this means that the brackets

appear to show little variation and should be very similar. Since both parts were created nominal, they should be the same.

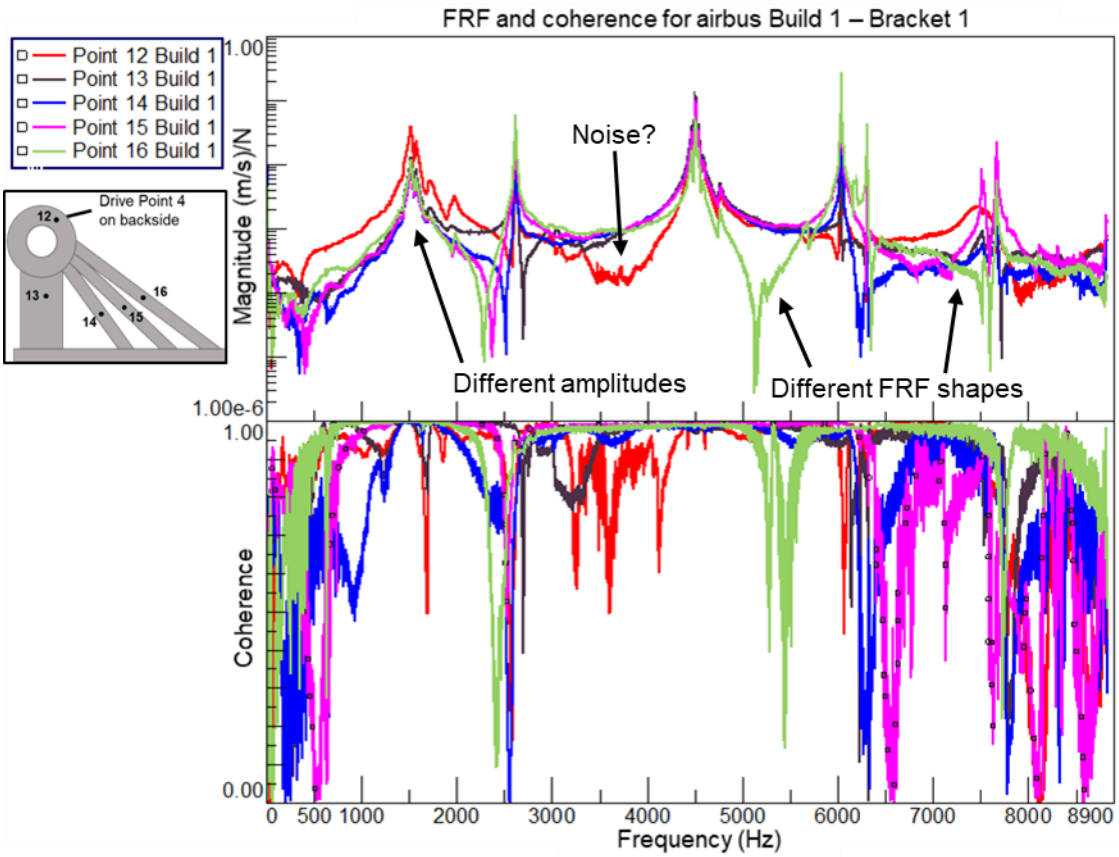

Fig. 72: FRF and coherence for Airbus Build 1 – Bracket 1

The remaining points, Points 6-11, are in the legs of the bracket (Fig. 73). The FRFs from testing these points are displayed in (Fig. 73). The FRFs appear to have many peaks suggesting a complex response from the drivepoint through the part. Multiple peaks make finding the natural frequencies difficult to determine. Additionally, impacting on the curved part of the bracket is not ideal, as there is no way to get a flat impact location. Since these points were both difficult to test and interpret, these points were not tested for the fixed and free boundary conditions.

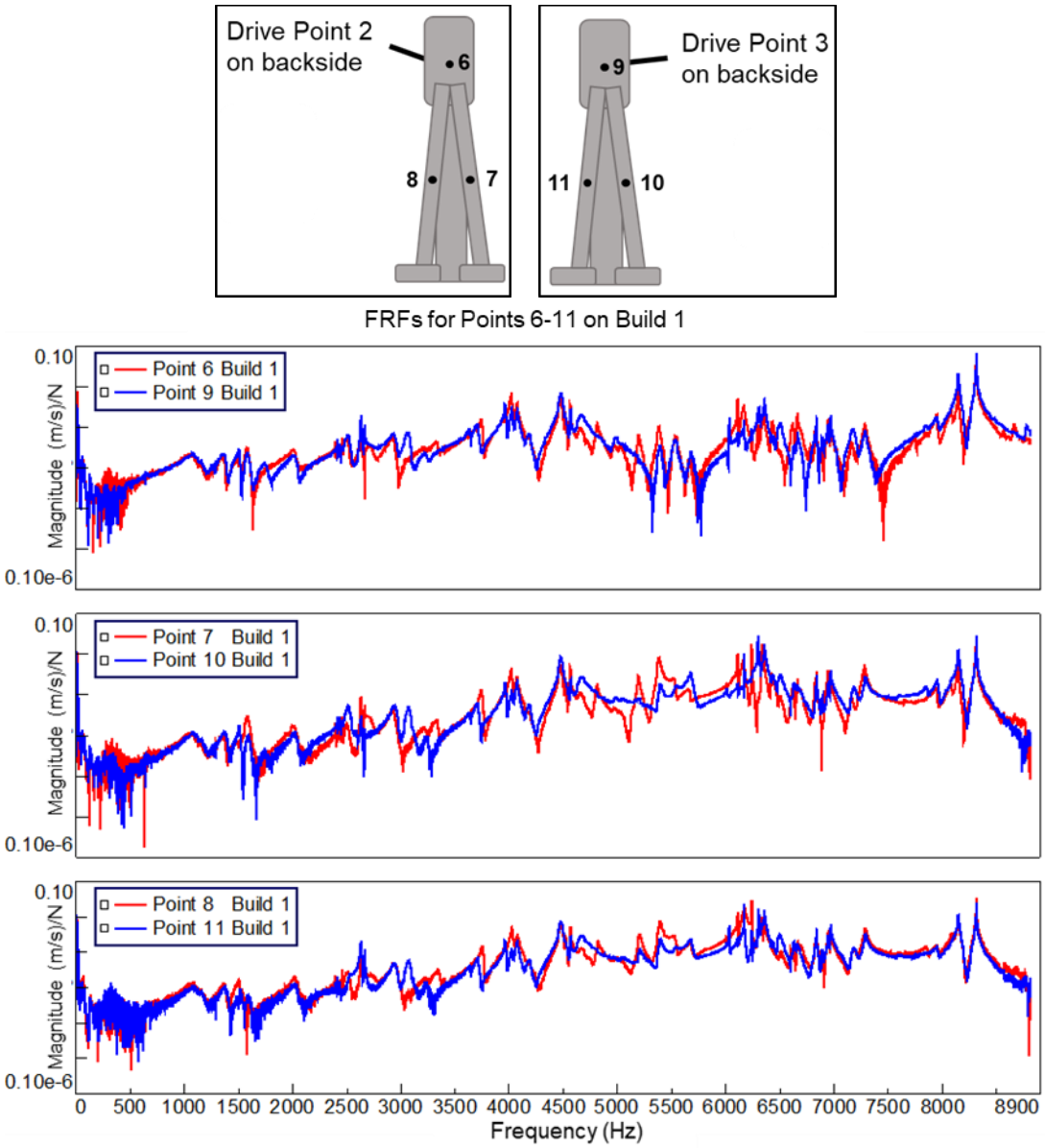

Fig. 73: Point locations (top) and FRFs for Points 6-11 on Build 1 (bottom)

The FRFs for Point 1 on the first five builds are compared in (Fig. 74). A clean FRF measurement should have smooth curves around peak values. The FRFs for the first five builds do not appear to be smooth, indicating there is some noise or structure characteristics in the FRFs. At around 7700 Hz, the FRFs are not very similar, as some builds show a natural frequency peak and some do not. The differences in the FRF led to a repeatability test on Builds 1 and 2.

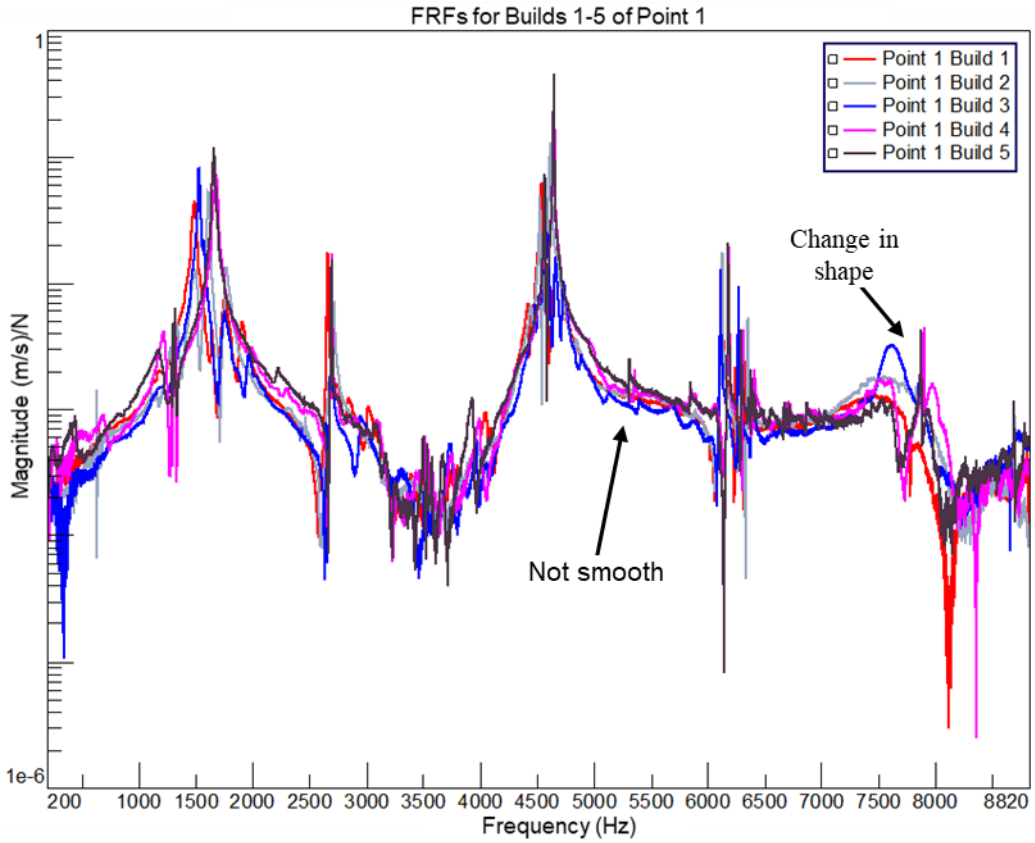

Fig. 74: FRFs for builds 1-5 of Point 1 from 200 to 8820 Hz

Build 1 and Build 2 were tested to check repeatability of the test setup. The FRFs between the first and second tests displayed differences (Fig. 75). The number of peaks surrounding the first modes changed between tests. The first mode shifted higher in frequency by 4.5% for Build 1 and 4.3% for Build 2. The shift in the first mode suggests that the boundary condition changed between tests. The boundary condition changing lends low confidence in the accuracy of the results from the semi-fixed boundary condition. The change in boundary condition could be due to the differences in bolting torque as the bolts were hand-tightened.

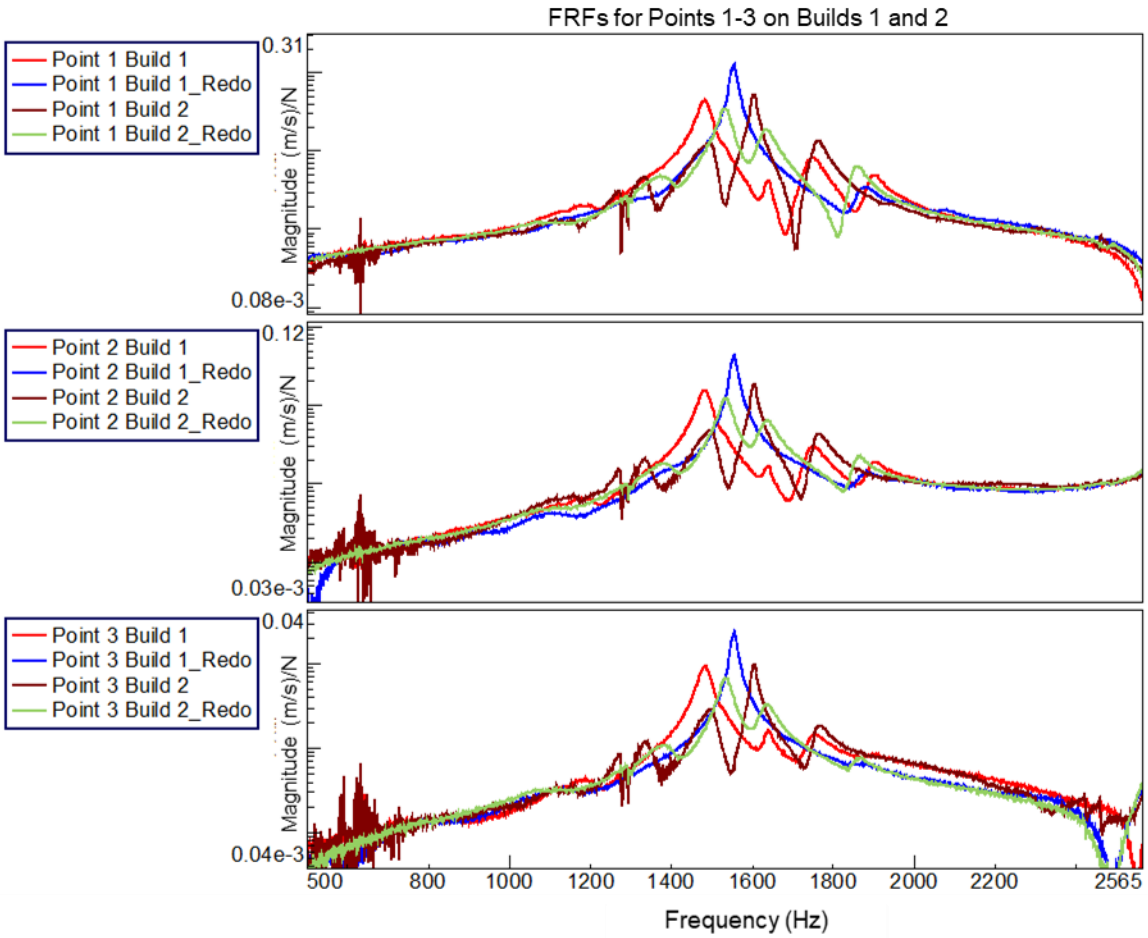

Fig. 75: FRFs for Points 1-3 on Builds 1 and 2 tested for repeatability

3.3.3.2 Fixed boundary condition

Testing the fixed boundary condition consisted of bolting the build plate onto the test frame used in the acoustic testing. The fixed boundary condition displayed similar FRFs to the semi-fixed boundary condition (Fig. 76). Comparing Point 1 on Bracket 2 to Point 12 on Bracket 1, there appears to be more noise in Point 1 below 1500 Hz. Point 1 also does not show separation between two peaks at 6000 to 6500 Hz.

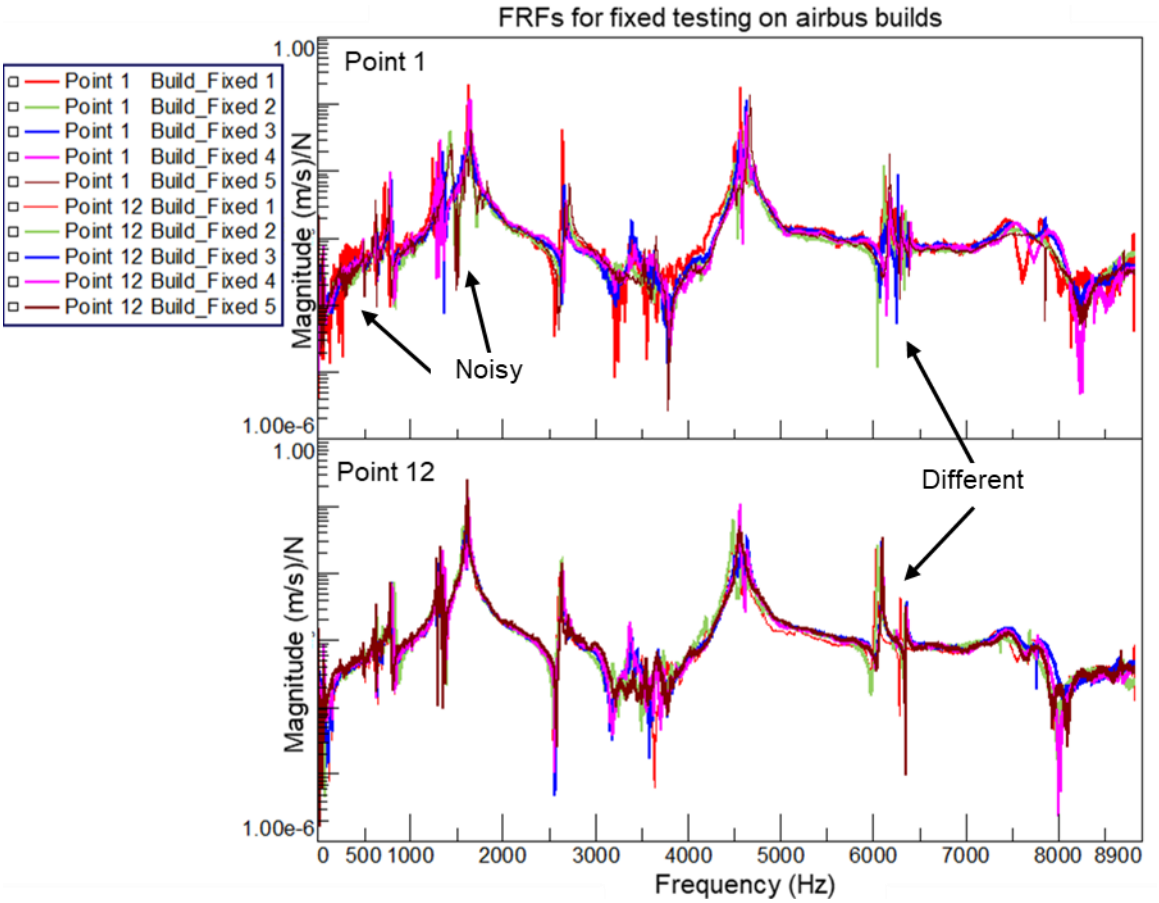

Fig. 76: FRFs for fixed testing on Airbus builds

The FRFs are zoomed in to analyze Mode 6 and Mode 7 which appeared to be different between Points 1 and 12 when looking at the full bandwidth (Fig. 77). These points are at the same location on both brackets – Point 1 is on Bracket 2 and Point 12 is on Bracket 1. The zoomed in view of Point 1 confirms that there is not separation between these modes. There is no apparent reason why one bracket shows separation between the modes and the other bracket does not.

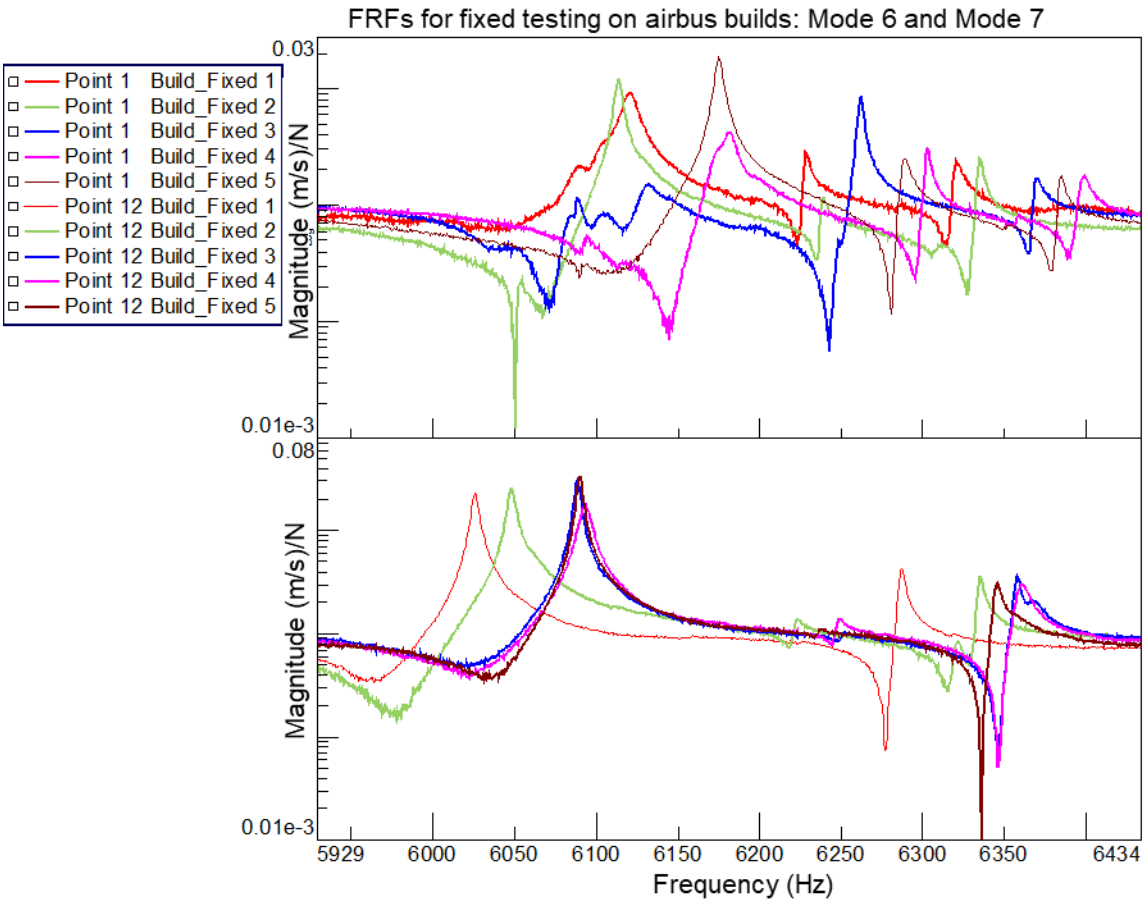

Fig. 77: FRFs for fixed testing on Airbus builds at Mode 1

The build mean values, percent change from FEA, range, and standard deviation were analyzed for the fixed testing (Table 8). Points that did not show a natural frequency peak were removed from the analysis, such as some of the points for Modes 6 and 7. Mode 5 and 9 are bending in the legs of the parts and did not show up in the points tested. From FEA, the builds were 6% or less different. The standard deviation ranges from Mode 1 at 8.4 Hz to Mode 11 at 36.9 Hz. The last two builds were not tested fixed, as the results between fixed and free were similar enough to only need to test the last builds free.

Table 7: Statistics on fixed Airbus build testing

FEA (all modes)		All Builds		Build 1	Build 2	Build 3	Build 4	Build 5	Stats	
Mode	Freq. (Hz)	Mean (Hz)	% change from FEA	Mean (Hz)	Mean (Hz)	Mean (Hz)	Mean (Hz)	Mean (Hz)	Range (Hz)	S.D. (Hz)
1	1535	1628	6.0	1621	1616	1632	1640	1628	24.0	8.4
2	2538	2654	4.6	2625	2663	2650	2661	2671	46.1	16.0
3	4500	4535	0.8	4535	4504	4539	4559	4536	54.5	17.5
4	4740	4608	-2.8	4591	4596	4627	4605	4620	36.6	13.9
5	5883	-	-	-	-	-	-	-	-	-
6	5995	6109	1.9	6094	6081	6100	6137	6132	56.3	22.1
7	6211	6254	0.7	6258	6231	6254	6272	6256	41.0	13.2
8	6254	6356	1.6	6340	6335	6363	6379	6363	44.1	16.2
9	7340	-	-	-	-	-	-	-	-	-
10	7495	7591	1.3	7586	7606	7576	7604	7580	30.5	12.5
11	8068	7776	-3.6	7736	7738	7809	7828	7769	91.4	36.9

3.3.3.3 Free-Free boundary condition

The Airbus build was tested free by placing the plate on a piece of foam. All seven Airbus builds were tested in this configuration. FRFs from the free testing provided the "cleanest" measurement out of the three tests (Fig. 78). Cleanest is defined in this case to be the least noisy. The results are better for Point 1 than with fixed testing, as there was separation between Modes 6 and 7. The two brackets on each build display similar frequencies and FRFs. Since the full bandwidth is difficult to analyze, some of the modes are analyzed in more detail over sections of the bandwidth.

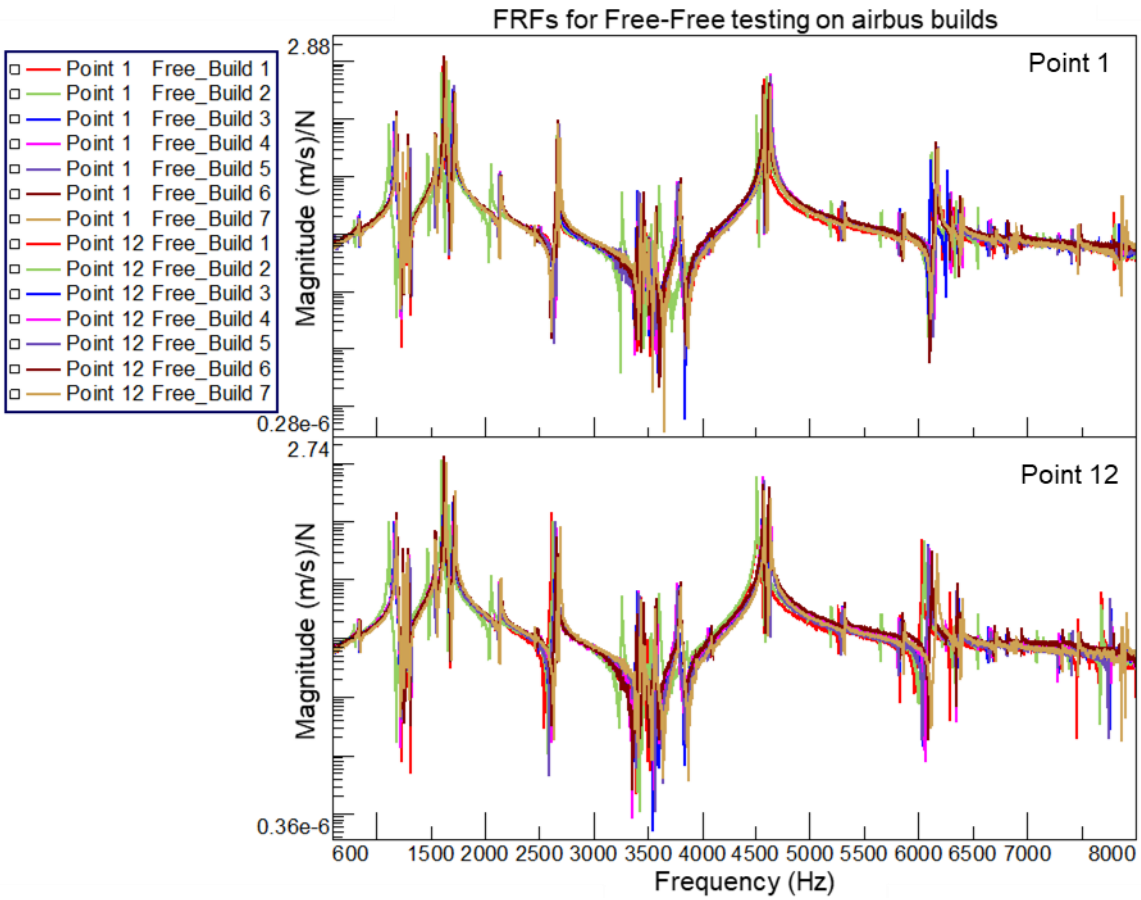

Fig. 78: FRFs from Free-Free testing on Airbus builds

The FRFs from Mode 1 show low variation between brackets on the same plate (Fig. 79). An interesting observation is that Build 2 appears shifted farthest to the left while Build 7 is shifted farthest to the right. The rest of the builds appear closer in natural frequency. The trends observed in this mode are further investigated by the statistical analysis on these parts.

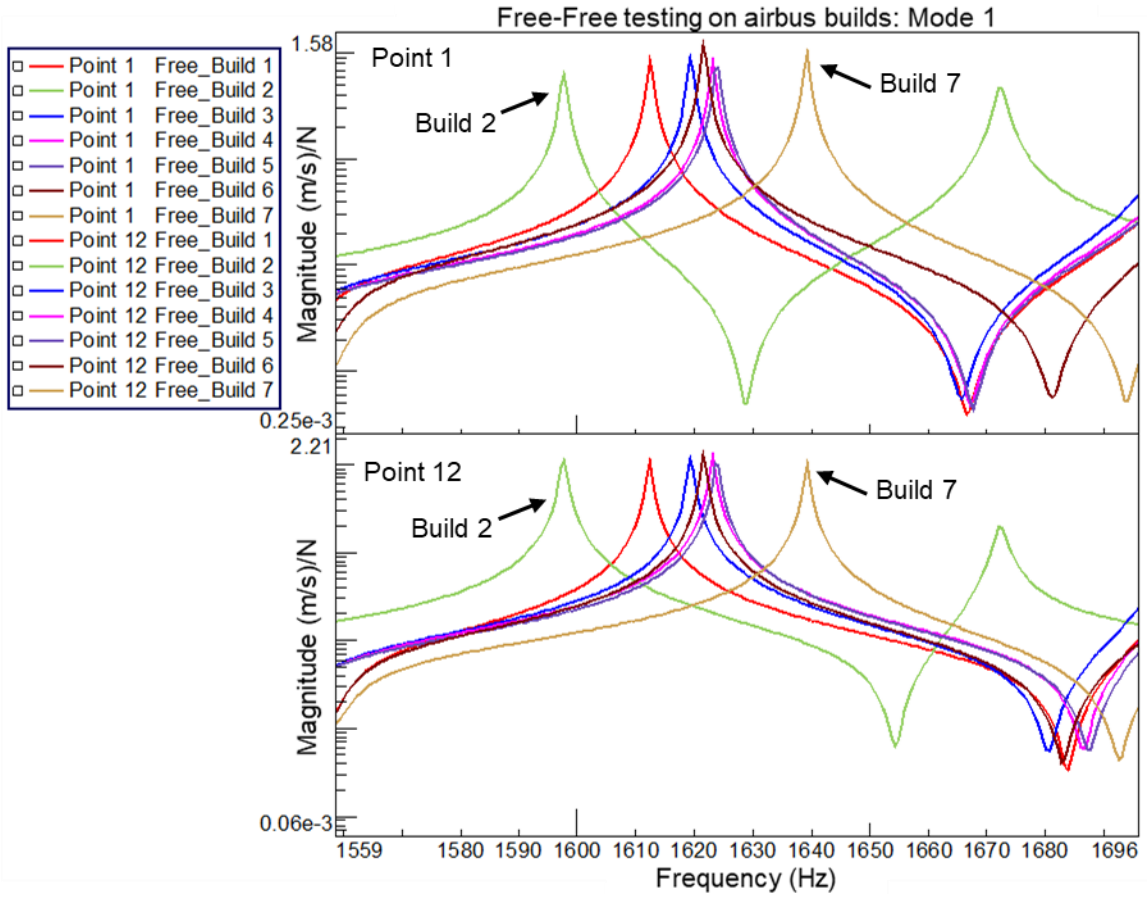

Fig. 79: Mode 1 from Airbus free-free testing

Mode 2 from the free testing displayed a double peak around the natural frequency (Fig. 80). Presumably, both brackets are showing up in the response. The frequency of one bracket is shifted from the other bracket, but without knowing which response is which, it is difficult to determine which peak is from which bracket.

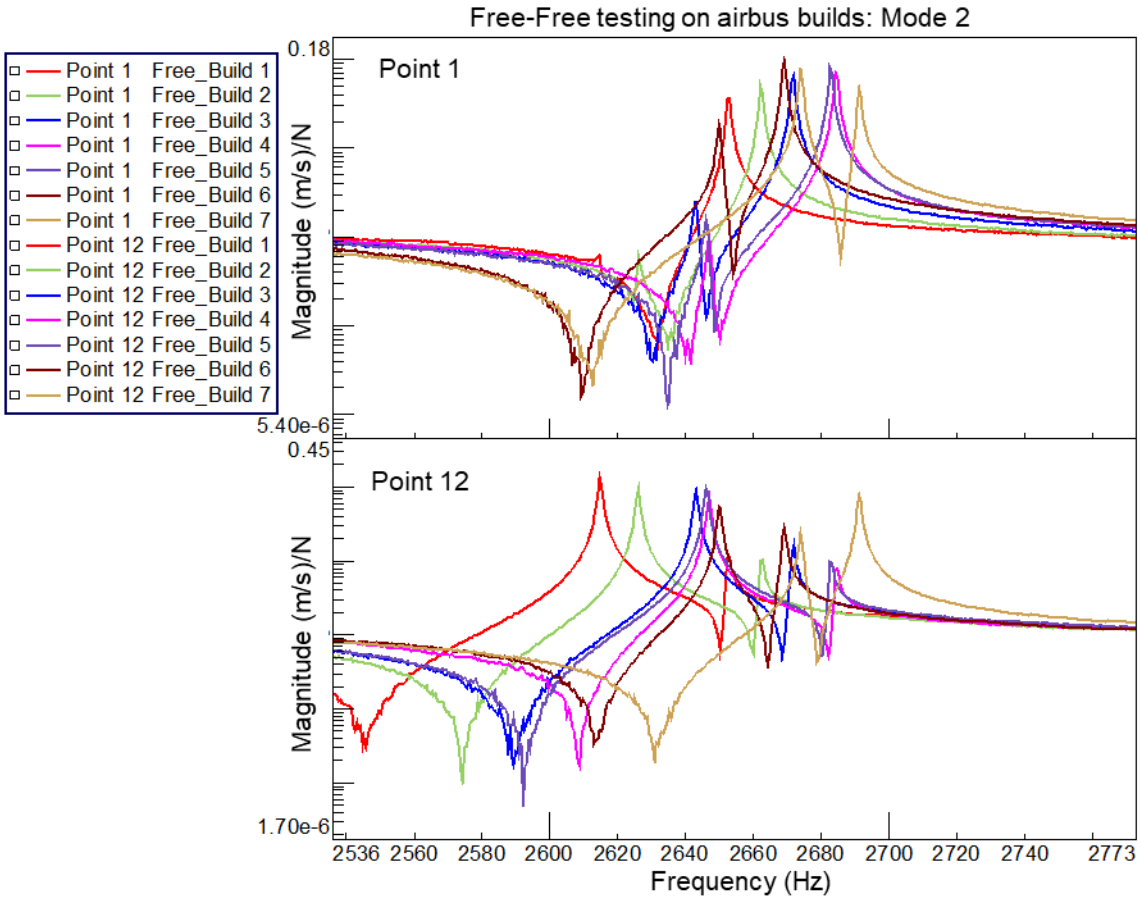

Fig. 80: Mode 2 from Airbus free-free testing

The build mean values, percent change from FEA, range, and standard deviation are shown in (Table 8). Mode 2 is not shown since there were multiple peaks around this natural frequency. Mode 5 and 9 are bending in the legs of the parts and did not show up because the bending direction was not the direction in which the points were tested. From FEA, the builds were 5.5% or less different. The standard deviation ranges from Mode 1 at 11.6 Hz to Mode 11 at 40.7 Hz.

Looking back at Mode 1, Build 2 is 22 Hz below the average and Build 7 is 19 Hz above the average. With the exception of Mode 4, Build 7 was highest in frequency for all modes by approximately 0.93%. Build 2 is only lowest in frequency for Mode 1, and there is no apparent reason why this occurred.

Table 8: Statistics on Free-Free Airbus build testing

FEA (all modes)		All Builds		Build 1	Build 2	Build 3	Build 4	Build 5	Build 6	Build 7	Stats	
Mode	Freq. (Hz)	Mean (Hz)	% change from FEA	Mean (Hz)	Mean (Hz)	Mean (Hz)	Mean (Hz)	Mean (Hz)	Mean (Hz)	Mean (Hz)	Range (Hz)	S.D. (Hz)
1	1535	1620	5.5	1612	1598	1619	1623	1624	1621	1639	41.5	11.6
2	2538	-	-	-	-	-	-	-	-	-	-	-
3	4500	4546	1.0	4504	4506	4556	4559	4562	4558	4575	71.0	26.3
4	4740	4616	-2.6	4574	4596	4624	4638	4637	4613	4632	64.1	22.0
5	5883	-	-	-	-	-	-	-	-	-	-	-
6	5995	6116	2.0	6069	6080	6098	6135	6131	6133	6169	99.6	32.6
7	6211	6252	0.7	6249	6222	6236	6240	6229	6274	6310	88.3	28.5
8	6254	6363	1.7	6338	6336	6363	6379	6365	6366	6394	58.2	19.2
9	7340	-	-	-	-	-	-	-	-	-	-	-
10	7495	7685	2.5	7682	7682	7711	7670	7673	7651	7724	73.3	23.1
11	8068	7796	-3.4	7788	7788	7772	7774	7760	7798	7892	131.2	40.7

As a production run, the Airbus builds displayed an average of 1.5% difference in the range of natural frequencies. The standard deviation was an average of 0.5% of the mean value.

3.3.4 Tensile Specimens

After impact testing was completed, the tensile specimens were sent to MS&T to be tensile tested. From the tensile specimens, MS&T discovered there was a porous layer defect in Build 7 that was not initially detected with impact/shaker testing performed on this build. This porous layer caused the tensile specimen to fail prematurely, resulting in a lower yield strength.

Re-evaluating Airbus Build 7, there were two noticeable differences between this build and the other six builds. The first difference was a double peak present on Mode 6 of Build 7 that was not present in any other builds (Fig. 81). Only Point 1 from Bracket 2 and Point 12 from Bracket 1 are shown, but the double peak appears in all points from Build 7.

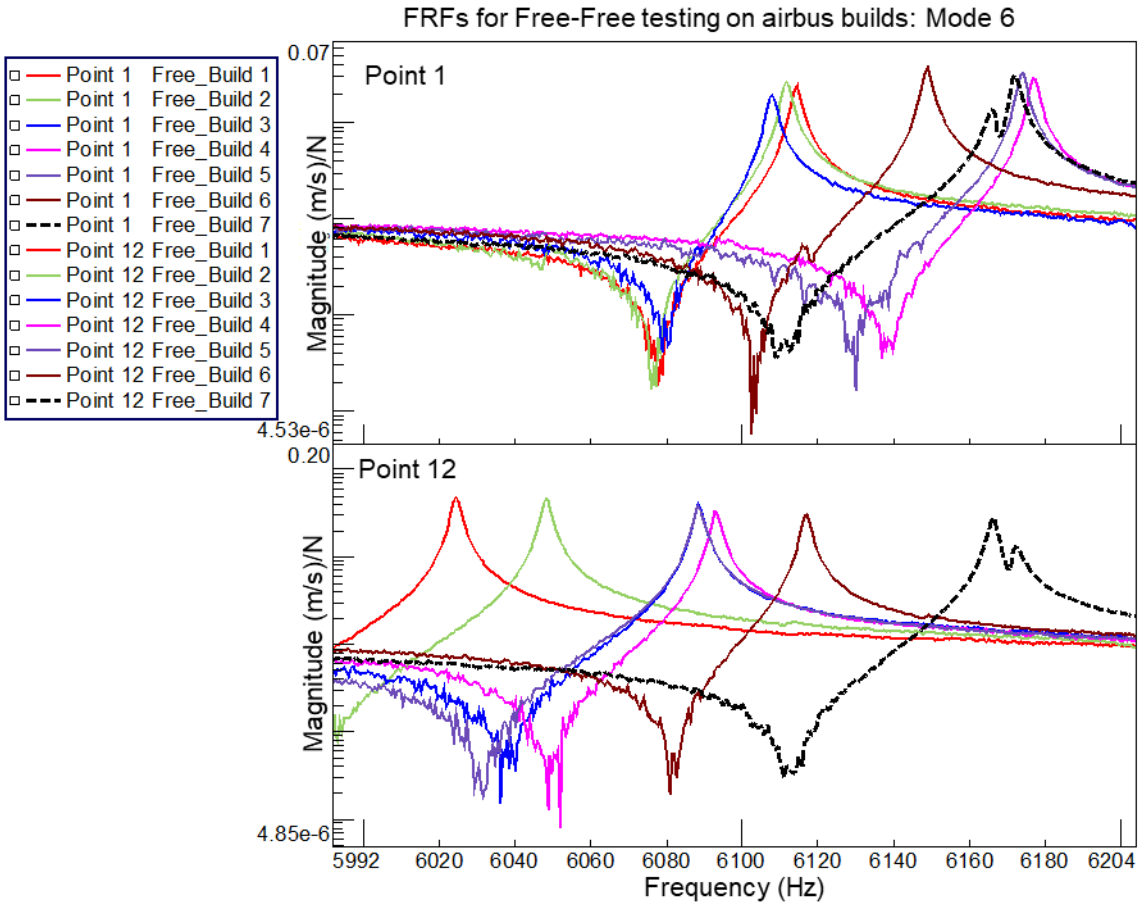

Fig. 81: FRF of Mode 6 from Build 7 tested free-free

The second difference is in Mode 11. The mean value for Build 7 is 100 Hz (1.4%) higher for this mode in comparison to all other builds. Excluding Build 7 from the statistical analysis, the mean value drops 0.2%, the range drops 71%, and the S.D. drops 69% (Table 9). This would place Build 7 more than 6 standard deviations above the mean value, indicating that Build 7 is significantly higher in frequency than the other builds.

Table 9: Statistical analysis into Mode 11 for Airbus builds

	FEA (all modes)		Build 7	All Builds	Stats			
	Mode	Freq. (Hz)	Mean (Hz)	Mean (Hz)	Range (Hz)	S.D. (Hz)	3 S.D. (Hz)	6 S.D. (Hz)
Including Build 7	11	8068	7892	7796	131.2	40.7	122.1	244.2
Excluding Build 7	11	8068	7892	7780	37.9	12.6	37.8	75.6
Difference (Hz)	-	-	-	16	93.3	28.1	84.3	168.6
Difference (%)	-	-	-	0.2	71.1	69.0	69.0	69.0

3.3.5 FRAC

FRAC analysis compares a simulated FRF to any number of experimental FRFs and provides a correlation value between 0 and 1. Build 7 was first used as the simulated data. After the tensile testing showed a defect in this build, Build 4 was used as the simulated data. Build 4 was selected since most of its natural frequencies were nearest the mean value for all the modes tested.

The average correlation for each build from calculating FRAC is shown in (Table 10). Build 4 as the reference shows better correlation at 0.23 on average than Build 7 with 0.07 on average. Interestingly, this does show that Build 2 and Build 7 are the least correlated with Build 4. As mentioned earlier, Build 2 was lowest in frequency on some modes and Build 7 was highest in frequency.

Table 10: FRAC for Airbus builds referenced to Build 7 and Build 1

Frequency Range: 1050-7979 Hz							
	Build 1	Build 2	Build 3	Build 4	Build 5	Build 6	Build 7
Ref. Build 7	0.07	0.03	0.11	0.06	0.06	0.08	1
Ref. Build 4	0.12	0.04	0.25	1	0.65	0.27	0.06

The low correlations were due to drops in coherence between natural frequency peaks (Fig. 82). FRAC was re-evaluated to take bands around natural frequency peaks to determine if that would increase the correlation between FRFs.

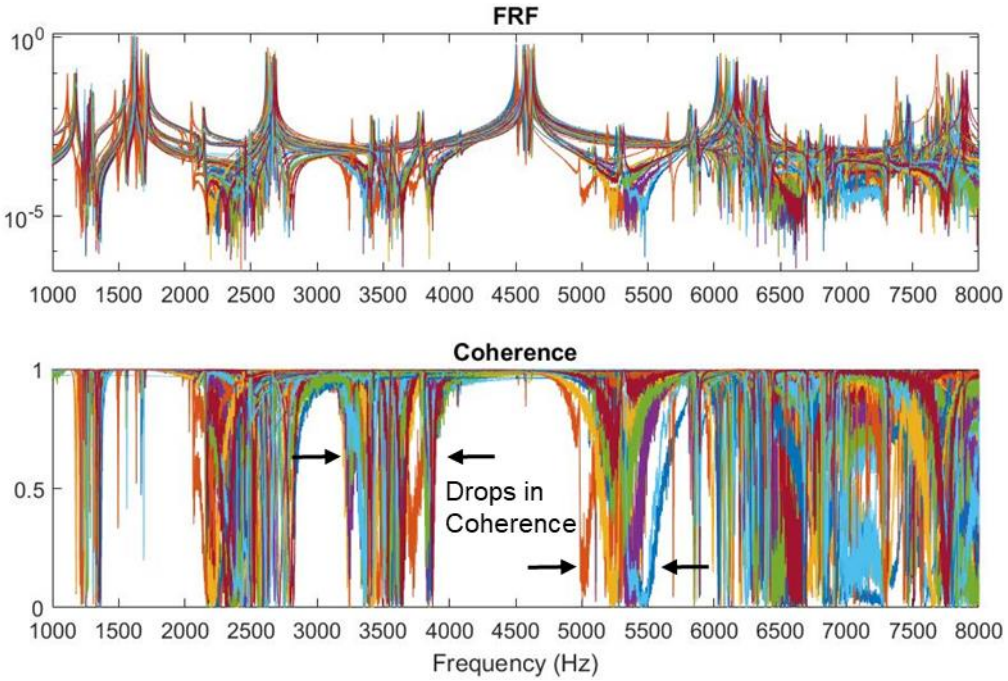

Fig. 82: FRF and Coherence for Points 1-5 and 12-16 on all Airbus builds

When FRAC was analyzed in sections where natural frequencies occur, the correlation between FRFs increases (Table 11). The average correlation between builds was 0.90 for using Build 7 as the reference and 0.89 for using Build 4 as the reference. Interestingly, Build 7 does not drop in correlation when Build 4 is the simulated data. This indicates that the FRAC analysis on these builds is not sensitive to the porous layer defect found from tensile testing. If Build 7 was very different from the rest of the builds, the correlation should be lower.

Table 11: FRAC over bands where natural frequencies occur

Frequency Ranges: 1026-1909, 2532-2707, 4374-4754, 5931-7974 Hz							
	Build 1	Build 2	Build 3	Build 4	Build 5	Build 6	Build 7
Ref. Build 7	0.97	0.88	0.86	0.87	0.87	0.97	1
Ref. Build 4	0.86	0.89	0.88	1	0.92	0.86	0.86

Caution should be taken when evaluating FRAC on experimental data, since the results are dependent on multiple variables such as which frequency bands are selected, which FRF is chosen as the simulated data, and which points on the structure are selected for comparison. FRAC results may also show low correlation due to leakage or windowing effects in the experimental data.

4 Summary and Recommendations

This section summarizes the testing and offers recommendations in two categories: the printing process and the dynamic testing methods performed on the builds.

4.1 Printing Process and Part Orientation

When testing the forest build plates, the cover gas flow in the printing chamber caused more variation than the defects placed in the parts. Unfortunately, the printer that printed all of these parts has little user control over the gas flow from right to left in the chamber. Unless this variability can be reduced, finding defects in parts such as were placed in the tensile bar builds will continue to be difficult. The dynamic testing method must be sensitive to the defect to be able to detect it. In the case of the forest builds, the testing methods were more sensitive to the plate variation than the defects themselves.

It is further recommended that part orientation be taken into account before printing the parts if they are to be dynamically tested. Printing the parts with the end testing in mind would greatly reduce testing time. For example, if one of the brackets on the Airbus builds could have been flipped, testing with the SLDV would have been much faster as both brackets could have been tested at once. The SLDV cannot see through the part and the build had to be turned to test the other bracket. Every time the build is moved, the SLDV has to be recalibrated to the new orientation which costs additional time.

4.2 Dynamic Testing Methods

There were five methods used to dynamically test these parts: acoustic, shaker, PZT, impact, and BB-gun testing. The following summaries and recommendations on these testing methods are separated into two categories: Plate excitation and Part excitation.

4.2.1 Plate Excitation

The methods that excited the parts through the build plate – acoustic, shaker, and PZT – were the least effective testing methods for two reasons. The first reason is that the excitation to the part is dependent on the build plate modes. The forest plates exemplified this, as some bars were not excited through the plate, because the plate did not have excitation at the location of the bar.

The second reason is that even if the part receives excitation through the plate, extracting the individual part response from the build plate response is difficult. Reducing the build plate response in the parts is possible, but would need more analysis to determine the effectiveness of this method. One attempt was made at reducing the build plate response by adding sand to the plate. The addition of sand assisted with reducing the build plate response, but the quality of the FRFs was not sufficient to determine the effectiveness of this method.

4.2.1.1 Acoustic testing

The acoustic testing assisted in determining base plate mode response, but was not an effective method for determining individual part responses. Using the speakers to excite through the build plate created responses that were difficult to interpret due to the lack of distinct peaks.

4.2.1.2 Shaker testing

Shaker testing can be an effective method for some parts, but may not be suited to test all types of parts. An advantage of this type of testing is that it is typically the fastest to perform. This was why it was often performed as the first dynamic test. This method can be effective in finding mode shapes and natural frequencies, but has a limited dynamic testing range. This was true with the Airbus builds, as the high frequency modes needed additional testing since the shaker could not reach these frequencies. The "may not be suited to all parts" is exemplified by the shaker testing on the forest tensile builds. The natural frequency peaks from this testing were not distinct enough to be determined.

4.2.1.3 PZT testing

The PZT testing was performed near the end of this research, and there are more opportunities with this testing. The testing performed was not effective at exciting through the plate, but the PZT can be cut to any size and could be attached to individual parts to excite them. The greatest advantage of PZT testing is that very high frequencies can be tested – up to 50-60 kHz or more – depending on the type of PZT. This method has potential for testing parts with natural frequencies above the excitation range of impact hammers and shakers. Although, more research would need to be performed before evaluating the effectiveness of PZT as a dynamic excitation method.

4.2.2 Part Excitation

The methods that were most effective in determining natural frequencies in the builds tested each part individually. These methods included impact testing and BB-gun testing.

4.2.2.1 Impact Testing

Impact testing was the most effective dynamic test from this research. The results from impact testing provided the best FRF and coherence measurements. Statistical analysis was able to be performed on the results of this testing as well. The effectiveness of this test is dependent on the size of the part and the ability to impact a flat surface repeatedly. The topology optimized brackets were very rigidly connected and impact testing was not very effective in finding the natural frequencies. The surfaces of both these parts and the Airbus parts were difficult to test, as the topology optimization does not provide many flat surfaces to test.

4.2.2.2 BB-gun Testing

As an excitation method, BB-gun testing shows potential as it can provide higher frequencies than an impact hammer. This test method would need refinement to be commercially adapted for a few reasons. The first reason was only the autopowers can currently be obtained. The second reason was the BB's impacted the parts too hard, causing surface damage. The third reason is there was no measure on how fast the BB was moving.

5 Conclusions and Future Work

Dynamic testing to find defects in AM parts was met with mixed success. The defects printed in previously tested parts were able to be determined. The defects in the parts researched were unable to be determined due to printing process variation. Cover gas flow in the printing process is causing part variation across the build to have a larger effect on the response than defects in the parts. Additionally, one of the biggest barriers in testing these parts is separating the part response from the build plate response.

Overall, the most effective testing method was impact testing each part individually. As a way to measure part integrity, dynamic testing has the potential to be an effective method for testing AM parts. But the results suggest more research needs to be conducted into the printing process and build plate response before this method can be considered successful and commercially adapted.

The work on this project is on-going and the future testing continues to examine defect size and part integrity. The future work is focused on determining the critical defect size. Critical defect size is associated with answering the question: What size and at what location do we need to find a defect to ensure a part will not fail? To answer this question, future parts could be printed with a use case in mind, as critical size is dependent on the loading conditions for the part. Future work will also experiment further PZT and impedance testing.

6 Reference List

[1] A. Allen, K. Johnson, J. Blough and A. Barnard, "Frequency Inspection of Additively Manufactured Parts for Layer Defect Identification," in *Annual International Solid Freeform Fabrication Symposium*, Austin, TX, 2019.

[2] A. Allen, K. Johnson, J. Blough and A. Barnard, "Using BB-gun or Acoustic Excitation to Find High Frequency Modes in Additively Manufactured Parts," in *International Modal Analysis Conference*, Houston, TX, Feb. 2020.

[3] Jabil, "Current State of Additive Materials and 3D Printing," Jabil, Jan. 2019.

[4] A. Bandyopadhyay and S. Bose, Additive manufacturing, Boca Raton, FL: CRC Press, 2016, pp. 1-16, 66.

[5] G. Bingham, "The History and Application of Additive Manufacturing for Design Personalisation," *Design for Personalisation*, no. 1, pp. 113-130, 2017.

[6] A. Davis, "Layer-by-Layer The Evolution of 3-D Printing," *IEEE Spectrum*, 04 Nov 2014.

[7] T. Wohler and T. Gornet, "History of additive manufacturing," Wohlers Associates Inc., Fort Collins, CO, 2014.

[8] M. Mani, S. Feng, B. Lane, A. Donmez, S. Moylan and R. Fesperman, "Measurement Science Needs for Real-time Control of Additive Manufacturing Powder Bed Fusion Process," 2015. [Online]. Available: https://nvlpubs.nist.gov/nistpubs/ir/2015/NIST.IR.8036.pdf. [Accessed 02 Feb. 2020].

[9] G. Davis, R. Nagarajah, S. Palanisamy, R. Rashid, P. Rajagopal and K. Balasubramaniam, "Laser ultrasonic inspection of additive manufactured components," *The International Journal of Advanced Manufacturing Technology*, vol. 102, no. 5-8, pp. 2571-2579, Feb. 2019.

[10] A. Karme, A. Kallonen, V. P. Matilainen, H. Piili and A. Salminen, "Possibilities of CT Scanning as Analysis Method in Laser Additive Manufacturing," *Physics Procedia*, vol. 78, pp. 347-356, 2015.

[11] J. Waller, B. Parker, K. Hodges, E. Burke and J. Walker, "Nondestructive Evaluation of Additive Manufacturing," NASA, Hampton, VA, 2014.

[12] W. Du, Q. Bai, Y. Wang and B. Zhang, "Eddy current detection of subsurface defects for additive/subtractive hybrid manufacturing," *The International Journal of Advanced Manufacturing Technology*, vol. 95, no. 9-12, pp. 3185-3195, Aug. 2017.

[13] N. Knezovic and B. Dolsak, "In-process non-destructive ultrasonic testing application during wire plus arc additive manufacturing," *Advances in Production Engineering & Management*, vol. 13, no. 2, pp. 158-168, 2018.

[14] W. Na and J. Baek, "Impedance-Based Non-Destructive Testing Method Combined with Unmanned Aerial Vehicle For Structural Health Monitoring of Civil Infrastructures," *Applied Sciences*, vol. 7, no. 1, p. 15, 2016.

[15] M. I. Albakri, L. Sturm, C. B. Williams and P. A. Tarazaga, "Impedance-based non-destructive evaluation of additively manufactured parts," *Rapid Prototyping Journal*, vol. 23, no. 3, pp. 589-601, 2017.

[16] B. Schwarz, "Experimental Modal Analysis," CSI Reliability Week, Oct. 1999.

[17] S. Bremen, W. Meiners and A. Diatlov, "Selective Laser Melting," *Laser Technik Journal*, vol. 9, no. 2, pp. 33-38, 2012.

[18] B. Zhang, Y. Li and Q. Bai, "Defect Formation of Mechanisms in Selective Laser Melting: A Review," *Chinese Journal of Mechanical Engineering*, vol. 30, no. 6, p. 515–527, Mar. 2017.

[19] Vibration Research, "Model VR5200-HF," VR5200-HF datasheet, Aug. 2018.

[20] The Modal Shop MTS Systems Corporation, "Model Number 2004E Electrodynamic Exciter," PS-0056 datasheet, Apr. 2003.

[21] D. Domme, *Introduction to Laser Doppler Vibrometry*, Houghton, MI: Polytec, Michigan Technological University, Sept. 27, 2018.

[22] A. Chen, "Frequency Response Assurance Criterion and Applications to Model Correlation of Body Structures," in *Noise & Vibration Conference and Exhibition*, Traverse City, MI, May 5-8, 2003.

[23] K. Johnson, J. Blough and A. Barnard, "Frequency Response Identification of Additively Manufactured Parts for Defect Identification," in *Annual International Solid Freeform Fabrication Symposium*, Austin, TX, Aug. 2018.

[24] P. Avitabile, "Modal Testing A Practitioner's Guide," in *General Theory of Experimental Modal Analysis*, The Society of Experimental Mechanics and John Wiley & Sons Ltd, 2018, pp. 42-43.

[25] H. Lord, G. William and H. Evensen, "Noise Control For Engineers," Malabar, FL, Robert E. Kreiger Publishing Company, Inc., 1987, pp. 13-14.

A FRAC MATLAB Code

The following is the code used to calculate FRAC for the Airbus builds. The code inputs the FRF and coherence data exported from LMS. The code outputs a table of FRAC values for the points and builds selected.

Contents


```
% FRAC_updated
% Aimee Allen
% 01/14/2019
clear
clear vars
clc
```

Load Data

```
%data exported from LMS Test.Lab
data = load('airbus_free_allpoints');
coh = load('airbus_free_allpoints_coherence');
```

User inputs

```
%%%%%%%%%%%%%%%%%%%%%%%%%%%%%%%%%%%%%%%%%%%%%%%%%%%%%%%%%%%%%%%%%%%%%%%
%ONLY CHANGE THE FOLLOWING INPUTS%
frf_sim = 1; %choose which FRF(s) you want to be the simulated data
num_part = 7; %number of parts
num_point = 10; %number of points

pointbegin = 1; %Choose where the points begin
pointend = 70; %Choose where the points end
xlimit = [1000 8000]; %Frequency start and end
xlabels = [1000:500:8000]; %how many xlabels you want on plot

%Choose number of frequency bands for computing FRAC over
numberofbands = 1;

%Create Row (number of points) and Column (number of Builds) names for...
%output table
rownames = table({'1';'2';'3';'4';'5';'12';'13';'14';'15';'16';'Avg'});
colnames = {'Point_No','Part_1','Part_2','Part_3','Part_4',...
    'Part_5','Part_6','Part_7'};
%%%%%%%%%%%%%%%%%%%%%%%%%%%%%%%%%%%%%%%%%%%%%%%%%%%%%%%%%%%%%%%%%%%%%%%
```

Create frequency vector and select frequency bands

```
%Find df and create frequency vector
df = data.FRF.x_values.increment;
freq = (0:df:length(data.FRF.y_values.values(:,1))*df-df);

%Select only number of FRFs and coherence values you want to evaluate
y_part1 = data.FRF.y_values.values(:,pointbegin:pointend);
y_coh = coh.Coherence.y_values.values(:,pointbegin:pointend);

%Find the total number of points
tot_points = num_part*num_point; %total number of points

%Plot the FRF/Coherence
figure('units','normalized','outerposition',[0 0 1 1])
subplot(2,1,1)
semilogy(freq,abs(y_part1))
set(gca,'XTick',xlabels) %set x-axis labels
xlim(xlimit)
title('FRF')

subplot(2,1,2)
plot(freq,y_coh)
set(gca,'XTick',xlabels) %set x-axis labels
xlim(xlimit)
xlabel('Frequency (Hz)')
title('Coherence')
%Select the frequency bands you want to evaluate on plot
[x,y] = ginput(numberofbands*2);
```

Setup FRAC calculation

```
%Cut off poor coherence
start = round(x(1:2:end)); %start of each frequency band
last = round(x(2:2:end)); %end of each frequency band

%Create index for pulling the correct points out of the y_value matrix
%Points are organized [1,1,...1,2,2,...2...n1,n2,...n]
indexy = [frf_sim:num_part:tot_points];

%This loop organizes the FRFs for the simulated data (xa) and the
%experimental data for the frequency bands you select (xe)
for hh = 1:length(start)
    for ii = 1:length(indexy)
        temp(:,ii) = y_part1(start(hh):last(hh),indexy(ii));
    end
    temp2 = data.FRF.y_values.values(start(hh):last(hh),1:tot_points);
    if hh == 1
        %xa is the simulated data in this case
        xa = temp;
        xe = temp2;
    else
        xa = [xa;temp];
        xe = [xe;temp2];
    end
```

```
    clear temp
    clear temp2
end

%xe is reshaped to run through the rows and columns in the matrix
xe = reshape(xe,length(xe(:,1,1)),num_part,num_point);
```

Compute Frequency Response Assurance Criteria

```
for kk = 1:length(xe(1,:,1)) %loop through parts
    for jj = 1:length(xa(1,:)) %loop through points
        %Frac will be organized (row,col) as (point #,build #)
        Frac(jj,kk) = abs(xa(:,jj)'*xe(:,kk,jj)./(sqrt(xa(:,jj)'*xa(:,jj))*sqrt(xe(:,kk,jj)'*
xe(:,kk,jj))));
    end
end

%The average was taken for each Build and added as the last row in Frac
%vector
average = mean(Frac,1);
Frac = [Frac;average];
```

Create table for outputting FRAC results

```
rounded = round(Frac,2); %round values to 2 decimal places
Frac_table = array2table(rounded); %create table
big_table = [rownames,Frac_table]; %table with rows labeled
big_table.Properties.VariableNames = colnames %apply column names
```

Published with MATLAB® R2018a

B Additional Figures

The following figures may be of interest.

B.1 Frequency vs Bar Number for 2nd- 4th x-bending

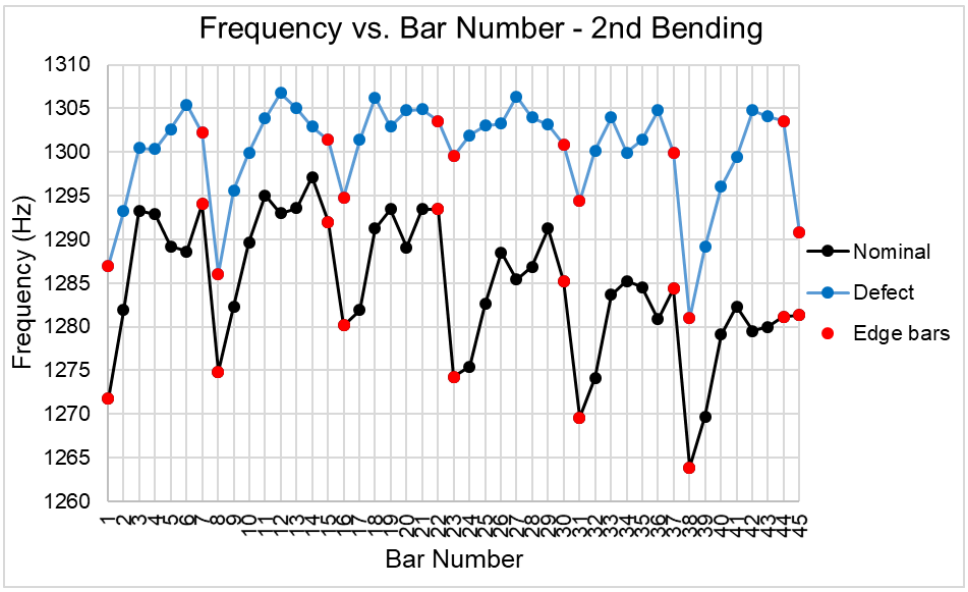

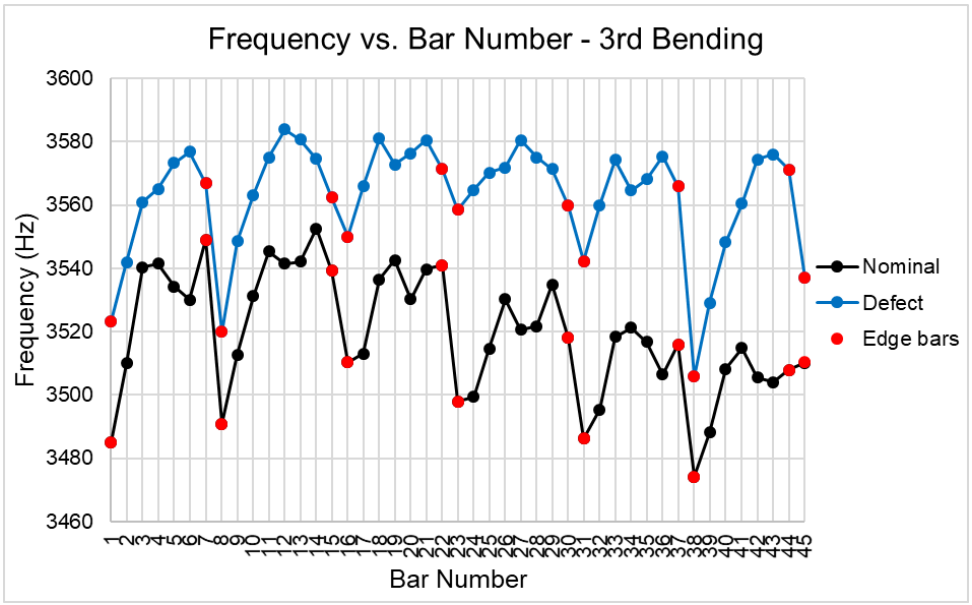

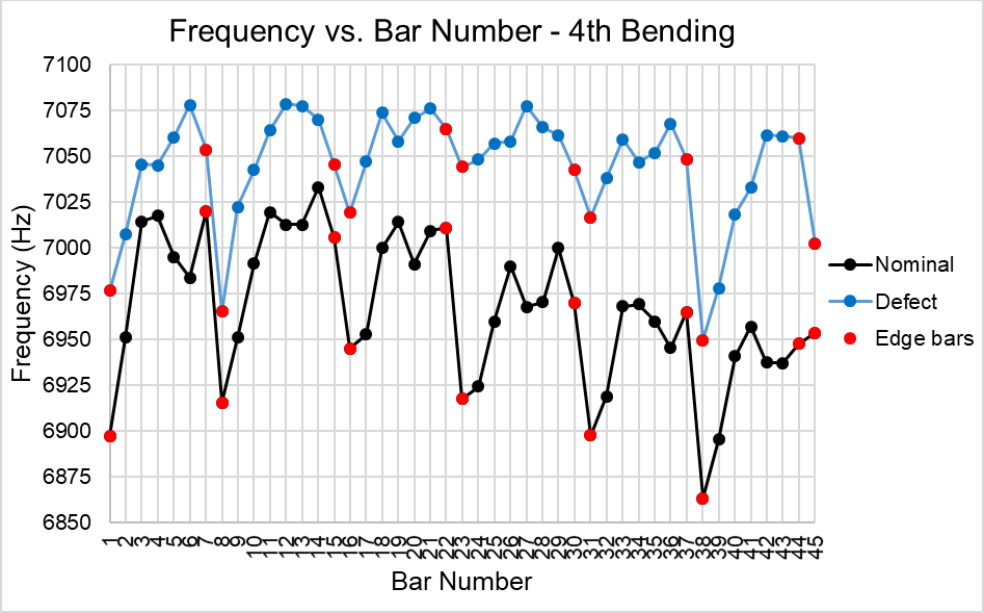

B.2 Frequency vs Column Number for 2nd- 4th x-bending